NTNU

Norwegian University of
Science and Technology

Automatic model identification of high-speed autonomous surface vehicles

Torstein Myrene Kvalvaag

Master of Science in Cybernetics and Robotics
Submission date: June 2018
Supervisor: Morten Breivik, ITK
Co-supervisor: Bjørn-Olav Holtung Eriksen, ITK
Mikkel Eske Nørgaard Sørensen, ITK

Norwegian University of Science and Technology
Department of Engineering Cybernetics

Preface

This thesis concludes what has been an educational semester and covers some of my findings. However, the sum of what I have learned these past months goes beyond the contents of this document. For that I would like to take this opportunity to thank some of the people that contributed to the process. First off, I owe a big thank you to my supervisors Morten Breivik, Bjørn-Olav Holtung Eriksen, and Mikkel Eske Nørgaard Sørensen. The discussions I have had with them during our meetings have been important in giving me confidence as a newbie about to embark upon a new journey filled with challenges. I would also like to thank the people at Maritime Robotics for supplying a test platform and the support they provided during my experiments.

The work covered in this thesis is based on the article [7] written by my supervisors Bjørn-Olav and Morten. The article formulates a control-oriented model and a method for manual model identification. As I was tasked with extending this existing modelling framework I have benefited from some of the resources made available to me from work with [7]. A list of these resources is provided below:

- Access to sensor data gathered through experiments performed by the authors of the article. This has allowed me to test my own method in a realistic environment.
- Parameters of the control-oriented model identified in the article. This has aided me in creating simulation environments based on the control oriented model.
- Access to the Telemetron surface vessel was provided by Maritime Robotics. That includes sensor equipment for measuring heading, rate of turn, and speed over ground.
- A python script for interfacing with the vessel used in full scale experiments was provided. Besides from saving me the trouble of creating one, it also aided me in creating a realistic simulation environment to test my implementation.

– As co-supervisor Bjørn-Olav had experience with the vessel I used in my full scale experiments, and accompanied me as a certified vessel operator, he played an important part in troubleshooting the vessel's onboard systems.

Besides from the elements of the list above, my work with this project has been independent in its nature. My supervisors have primarily assisted me through challenging my ideas and providing feedback on my thesis.

Abstract

This thesis investigates a method for identification of a non-first principle control-oriented model for autonomous surface vehicles (ASVs) suggested in [7]. The goal is to develop an automatic substitute for the identification procedure. The identification is divided into three steps: steady state identification (SSID), data extraction, and a parameter identification with linear regression. Automatic solutions are developed for each step, implemented, and tested in full-scale.

The identification procedure is based on analysis of data collected from experiments performed by executing input step sequences. To automate the experiments a method for online SSID in noisy processes suggested in [5] is adapted and applied. The method is based on the behavior of a ratio between two variance estimates and performs well given reasonable sea conditions.

Measurements of damping and inertia are extracted from each step response performed in the experiment. Damping is read directly from steady state behavior, while inertia is obtain by curve fitting the transient response. The curve fitting is solved using numerical optimization, more specifically through application of Broyden, Fletcher, Goldfarb, and Shanno's method (BFGS).

The measurements of damping and inertia are gathered in data sets and linear regression is applied to identify models describing the data in each set. An automatic weighting scheme is formulated to be used in the regression, and ridge regression is applied for regularization.

The developed method is implemented as a real time system using the Robot Operating System (ROS). Then, full-scale experiments are performed using a surface vessel supplied by Maritime Robotics called Telemetron.

Results from the experiment emphasizes the need for better experiment designs and strategies to combat the effects of the high signal-to-noise ratio present in some parts of the state space. Methods for identifying and repeating step responses heavily influenced by disturbances, and for detecting and removing outliers in the data sets are considered necessary if the method

is to be used without human supervision. That being said, given that the vessel behaves within reason during the experiments the method represents a powerful and easily accessible modelling tool.

Sammendrag

Denne oppgaven undersøker en metode for identifisering av en ikke-første prinsipp kontrollorientert modell for autonome overflatekjøretøyer (ASVs) som foreslås i [7]. Målet er å utvikle en automatisk erstatning for identifikasjonsprosedyren. Identifikasjonen er delt inn i tre trinn: steady state identifikasjon (SSID), generering av målepunkter og en parameteridentifikasjon gjor med bruk av lineær regresjon. Automatiske løsninger utvikles for hvert trinn, implementeres og testes i fullskala.

Identifikasjonsprosedyren er basert på analyse av data samlet fra eksperimenter utført som en sekvens av steg i inngangssignalet. For å automatisere eksperimentene blir en metode for online SSID i støyete prosesser, foreslått i [5], tilpasset og anvendt. Metoden er basert på oppførselen til et forhold mellom to variansestimater og ser ut til å fungere bra gitt rimelige sjøforhold.

Målinger av dempning og treghet utvinnes fra hver steg respons i forsøket. Målinger av dempning kan leses direkte fra steady state, mens treghetmålinger finnes ved å tilpasse en kurve til transientene. Kurvetilpassningen gjøres ved hjelp av numerisk optimalisering, nærmere bestemt ved anvendelse av Broyden, Fletcher, Goldfarb og Shanno's metode (BFGS).

Målingene av demping og treghet samles i datasett, og lineær regresjon brukes for å identifisere modeller som beskriver dataene i hvert sett. En automatisk vektingsmetode formuleres og annvendes i regresjonen, og ridge regresjon brukes for regularisering.

Den utviklede metoden implementeres som et sanntidssystem ved bruk av Robot Operating System (ROS). Deretter utføres fullskala eksperimenter ved bruk av et overflatefartøy som tilhører Maritime Robotics, kalt Telemetron.

Resultater fra eksperimentene legger vekt på behovet for bedre planlegging av eksperimenter og strategier for å bekjempe effektene av det høye signal-til-støy forholdet som er tilstede i enkelte deler av tilstandsrommet. Metoder for å identifisere og gjenta trinnresponser som er sterkt påvirket av forstyrrelser, og for å detektere og fjerne avvikere i datasettene anses nødvendig hvis metoden skal brukes uten menneskelig tilsyn. Når det er sagt, gitt at fartøyet

oppfører seg innenfor fornuftens grenser under forsøkene, representerer metoden et kraftig og lett tilgjengelig modelleringsverktøy.

Contents

List of tables

List of figures

List of acronyms

ASV autonomous surface vehicles. xi, 1, 2, 5, 8, 85

BFGS Broyden, Fletcher, Goldfarb, and Shanno's method. 58, 59, 61

CV cross validation. 15, 16

DOF degrees of freedom. xi, 6, 8

LTI linear time-invariant. 26, 27, 29, 31, 41, 56, 67, 73

PDF probability density function. 43, 44

ROS the Robot Operating System. 4, 75, 85

ROT rate of turn. 8, 19, 25, 31, 33, 34, 36, 41, 50, 52, 56, 68, 69, 72, 80

SOG speed over ground. 8, 19, 21–23, 27, 30, 31, 33, 34, 36, 47, 50, 52, 54, 64, 78, 80

SSID steady state identification. xii, xiii, 3, 37, 38, 41–43, 47, 50–52, 55, 56, 62, 71, 72, 78, 80–82, 85

Chapter 1

Introduction

1.1 Motivation

There are many possible applications of ASVs. Currently, they are centered around military and scientific operations at sea. As with other automated solutions, ASVs are well suited for dirty, dull and dangerous tasks, as they remove the need for a human operator. This frees an important resource and offers potential improvements in cost, safety, availability and more. Compared to other small-sized autonomous vehicles suited for operations at sea, like the aerial and submerged alternatives, ASVs offer greater capabilities in terms of payload capacity and persistence [18]. This means that they can make an important contribution to a heterogeneous network of autonomous vehicles operating at sea. They can provide support in terms of service as a potential base station and as a communication interface between units below and above the water surface. Examples of application areas for ASVs include military intelligence and surveillance, mine countermeasures, oil and gas exploration, and hydrographic, oceanographic and environmental surveillance. A historical perspective of the evolution of unmanned surface vehicles is presented in [2], and a look at the more recent development is given in [12].

A beneficial element to have in any application of surface vessels is the option to maneuver at high speeds without significant loss in operational capabilities. To achieve this, it is advantageous for path planning and trajectory tracking methods to increase the feasibility of their output by consulting an accurate model. More specifically, a model that is representative of the vessel's dynamics in all modes of operation, whether it be in displacement, semi-displacement or planning. Such a model also allows for improvements in control objectives where a model-based approach is a feasible solution, possibly in combination with feedback to correct for eventual unmodelled disturbances. Work with this kind of control-oriented modelling is done in [17] and [18] where a selection of models are compared and applied in control designs.

Figure 1.1: The Telemetron ASV. Photo courtesy of Maritime Robotics.

Another article that investigates the topic of control-oriented modelling of small, agile ASVs capable of aggressive maneuvering at high speeds is [7]. The article is based on further development of a modelling and control approach suggested in [4] and [3]. It proposes the use of a non-first principle model and an empirical identification procedure. The method was tested in a full-scale identification experiment using an ASV provided by Maritime Robotics. The vessel, named Telemetron, is shown in Figure 1.1. The identified model and its application in various control schemes showed promising results in a variety of performance metrics presented in [7]. Due to the vessel having continuously changing dynamics as a result of factors like wear and tear of the engine, as well as algae growth on the hull, the model has to be updated every so often in order to facilitate reliable results in further research done with the vessel. The implications of an automatic modelling method go beyond the salvation of future researchers who are forced to revisit the modelling procedure. It also means that any research or other application requiring that a model is in place becomes more accessible as researcher will not have to spend time on learning about modelling.

1.2 Problem description

To avoid having to manually carry out the modelling procedure every time, a time consuming process, the call for a fully automatic implementation is issued. That is essentially what the work covered in this thesis has aimed to accomplish. The modelling method as it is presented in [7] can be described as consisting of three separable steps. Therefore the objective of this thesis is to *automate, or provide automatic substitutes, for each of these three steps and tie them together in such a way that the entire procedure can be initiated and completed with the push of a button.* It is of course important that the automation does not come at the cost of a loss in performance.

1.3 Contributions

Before specifying the contributions of this work, contributions from previous work with the method is described. A brief description of the three steps that outline the modelling method as it is described in [7] goes as follows. The first step is an online steady state identification performed by the operator of the vessel. The second step is the extraction of data from the identified transient and steady state regions. The extracted data is measurements of inertia and damping from throughout the state space. The third and final step is to use linear regression to generate statistical models of damping and inertia which can be used to parameterize the kinetic model equations describing the vessel dynamics. Now, the results from work done during the autumn of 2017. For the first step, an investigation of steady state identification methods that are capable of handling noisy signals lead to the method suggested by [5]. For step two, numerical optimization was applied to extract measurements of inertia. The linear regression of the third step was left unchanged in practice as tools such as regularization and weighting served little purpose in the simplistic simulation environment.

With previous contributions in place the contributions of the work done for this thesis can be made clear. The first part of the work was concerned with adapting the method for use on real data and the following contributions were made.

1. Analysis of the performance of the original method when applied to data from real experiments.
2. Adapted the SSID method suggested in [5] to handle the signal complexity of surface vessel applications, and formulated guidelines for identification of method parameters.
3. Modification of the linear regression step including:
   (a) altered damping and inertia models (basis functions) suggested in [7],
   (b) applied new regularization technique, and
   (c) formulated fully automatic weighting scheme for use in identification of inertia models.
4. Proposed model extensions for inclusion and identification of propagation delay and second order terms.

The second part of the work was concerned with testing the method in full-scale and the contributions were as follows.

1. Automated solutions for rudder bias identification were proposed and set up for comparison. The following two methods were implemented.

   (a) Use of rudder bias as hyperparameter in identification of rate of turn damping model.
   (b) Using motion control to measure rudder input at constant heading as part of preliminary rudder bias identification experiment. A PID-controller with state feedback linearization was implemented.

2. The model identification method was implemented as a real time solution using the Robot Operating System (ROS). Some features of the implementation were:
   (a) Framework for user interaction during experiment including commands for
      i. lossless navigation to any part of the experimental procedure,
      ii. pausing and stopping without loosing progress in ongoing experiment, and
      iii. loading backup to resume from any prior point of an experiment.
   (b) Simulation environment.
3. Full-scale experiments were performed using the Telemetron.

Due to poor time management on my part neither the rudder bias identification nor any details of the implementation are covered in this thesis.

1.4 Outline

This report is organized as follows. Chapter 2 describes the model and identification method suggested in [7]. The description of each step is followed by a discussion of weaknesses that one should be aware of when attempting to automate the step. Chapter 3 describes the automated solutions to each step described in Chapter 2, and shows results from each step of the method when applied to data gathered by the authors of [7]. Weaknesses of the automatic solutions are highlighted in discussions at the end of each section. The last section of the chapter covers proposed model extensions that were not implemented but that are considered important when moving forward with development of the method. Chapter 4 covers results obtained from application of the automated method in full-scale using the Telemetron vessel. Rounding it off is the conclusions in Chapter 5, giving a retrospective assessment of what has been done, including suggestions of what should be done in future work to improve the solution. Throughout Chapter 2 and Chapter 3 topics that might be unfamiliar but essential for understanding will be introduced as they become relevant.

Chapter 2

An approach to modelling and identification of high-speed vessels

This chapter will provide some background for vessel modelling and cover the approach to modelling and identification of high-speed ASVs suggested in [7]. More specifically, this article suggests the use of a non first principle model and the empirical identification method. Extra care is put into discussion of the method because the intention of this work is to automatize the modelling procedure which means that one can not rely on human intervention to correct or suppress the unforeseen. Once the method has been described and discussed, the next chapter will describe the proposed automatic solution.

Note that throughout the chapter, figures with data from experiments performed by the authors of [7] is shown. However, all the figures were created using the automated method developed in Chapter 3. The results should still be representative of what is achievable with the method developed in [7] as the two methods have comparable performance.

2.1 Vessel modelling

This section will first provide some background to vessel modelling by covering a more traditional vessel model and approach. The limitations of the traditional approach will serve as motivation for the new approach and model which will be introduced at the end of the section.

2.1.1 Traditional vessel modelling

In order to describe the complete motion of a surface vessel in 3D-space 6DOF are needed, 3DOF for translation and 3DOF for rotation; see Figure 2.1. However, most surface vessel control applications are restricted to the horizontal plane, thus a formulation with 3DOF is often sufficient. The 3DOF needed to describe horizontal motion are surge, sway and yaw.

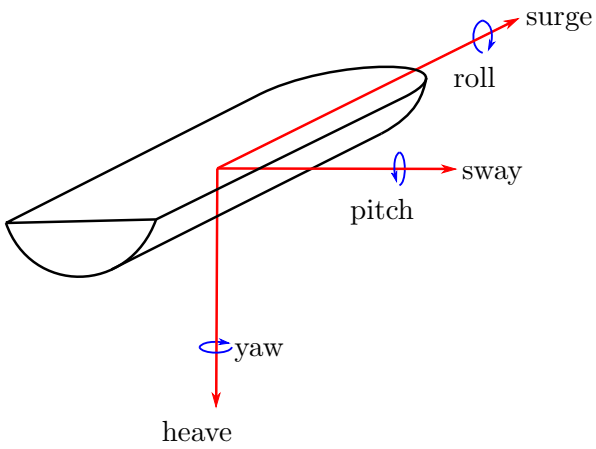

Figure 2.1: Description of surface vessel with 6 DOF.

When tasked with designing a control oriented model of a surface vessel operating in the horizontal plane, a reasonable starting point is the 3DOF maneuvering model described in [9]. The model is formulated as

$$\dot{\boldsymbol{\eta}} = \boldsymbol{R}(\psi)\nu \tag{2.1a}$$

$$\boldsymbol{M}\dot{\boldsymbol{\nu}} + \boldsymbol{C}(\boldsymbol{\nu})\boldsymbol{\nu} + \boldsymbol{D}(\boldsymbol{\nu})\boldsymbol{\nu} = \boldsymbol{\tau} + \boldsymbol{\tau}_{wind} + \boldsymbol{\tau}_{wave}, \tag{2.1b}$$

where $\boldsymbol{\eta} = \begin{bmatrix} N & E & \psi \end{bmatrix}^\top \in \mathbb{R}^2 \times \mathbb{S}$ describes the vessel position and heading in a North-East reference frame; $\boldsymbol{\nu} = \begin{bmatrix} u & v & r \end{bmatrix}^\top \in \mathbb{R}^3$ describes the vessel velocity in the body frame; and $\boldsymbol{\tau}, \boldsymbol{\tau}_{wind}, \boldsymbol{\tau}_{wave} \in \mathbb{R}^3$ describes the forces and moments generated by actuators, wind and waves acting on the vessel. As for the matrices, $\boldsymbol{R}(\psi)$ is the rotation matrix about the z-axis, $\boldsymbol{M}$ is the inertia matrix, $\boldsymbol{C}(\boldsymbol{\nu})$ represents the Coriolis and centripetal effects, and $\boldsymbol{D}(\nu)$ contains the hydrodynamic damping forces. Obtaining accurate values for the model parameters of (2.1b) is generally not an easy task in practice. Furthermore, the result is a model designed for a category of surface vessels known as displacement vessels. Displacement vessels are described by [8] in a classification of surface vessels based on the dimensionless Froude number

$$Fn = \frac{U_r}{\sqrt{Lg}}. \tag{2.2}$$

Here U_r is the vessel velocity relative to the water, L is the overall submerged length of the vessel, and g is the gravitational acceleration. Displacement vessels are those that operate in the approximate region $Fn < 0.4$. They are objects of study in [9] and are accurately described by (2.1).

The kinetics of displacement vessels are characterized by dominant hydrostatic terms. For vessels that are faster and/or smaller, the effects of hydrostatics decrease relative to hydrodynamic effects as we move through the region of semi-displacement vessels which operate at higher Froude numbers. High-speed vessels with $Fn > 1.0 - 1.2$, such as the Telemetron studied in this thesis, can enter the region of planning vessels where aerodynamic forces start to become significant and should be included in the model in some way. This means that using (2.1) is not be a good option for accurate control of high-speed surface vessels. An in depth description of some considerations and methods for modelling the kinetics of these kinds of vessels can be found in [8]. However, in this thesis a more empirically focused modelling method is put in focus. This is a method described by [7] where a non-first principle model is formulated, and a parameter identification process using linear regression is suggested. The model suggested by [7] will be closer reviewed in the next section, and the identification method will be described and discussed in section 2.3.

2.1.2 Empirical modelling

As mentioned in the previous section, the author of [8] provides a variety of tools for describing vessels operating at high speeds. The models covered in both [8] and [9] belong to the class of first principle models. These models rely on breaking down the system into subsystems that can be described by the laws of physics, the first principles. Consequently the model complexity, as well as the complexity of the modelling procedure, is dependent on how many subsystems or how many elements of physics have to be included in order to get an accurate representation of the real system. As illustrated by the variety of physical phenomena considered in [8], high-speed vessels can be regarded as complicated systems.

This is where non first principle modelling can become relevant. Starting with a set of differential equations,

$$\dot{\boldsymbol{x}}(t) = \boldsymbol{f}(\boldsymbol{x}(t), \boldsymbol{\tau}(t)), \tag{2.3}$$

where $\boldsymbol{x}(t)$ is the state and $\boldsymbol{\tau}(t)$ the input vector, the properties of the model can be identified using observations of system behavior. This comes with a shift in focus from physics to statistics. There has not been done as much work with non first principle models of marine vessels compared to work

with first principles; but, as mentioned earlier, one article that covers the subject is [7].

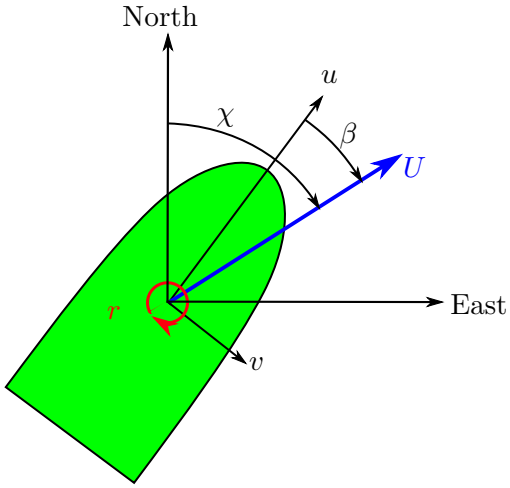

Figure 2.2: The vessel states, $\boldsymbol{x} = [U \quad r]^\top$, described in a North-East reference frame and the body frame.

The article, [7], describes a 2DOF control-oriented model. 2DOF are chosen due to the fact that ASVs are generally underactuated, unable of independent control of surge, sway, and yaw. The states of the 2DOF model are the vessel's speed over ground (SOG), $U = \sqrt{u^2 + v^2}$, where u and v are surge and sway; and the vessel's rate of turn (ROT), or yaw rate, r. The kinematic equations are found as a modification of (2.1a) and given by

$$\dot{\boldsymbol{\eta}} = \begin{bmatrix} cos(\chi) & 0 \\ sin(\chi) & 0 \\ 0 & 1 \end{bmatrix} \begin{bmatrix} U \\ r \end{bmatrix}, \tag{2.4a}$$

$$\dot{\chi} = r + \dot{\beta}, \tag{2.4b}$$

where $\chi = \psi + \beta$ is the course angle, and β the sideslip angle. As SOG can only have positive values $U \geq 0$ an assumption of positive surge speed $u > 0$ is made to remove ambiguity from the model. Consequently, the system's valid configuration space becomes limited. But, the limitation is reasonable when considering that the typical control application involves vessels in forward motion.

As mentioned in section 2.1.1, the kinetics of a marine vessel can be challenging to model if the vessel is allowed to operate at high speeds. Therefore [7] proposes the use of a simple non first-principle model on the form

$$\boldsymbol{M}(\boldsymbol{x})\dot{\boldsymbol{x}} + \boldsymbol{\sigma}(\boldsymbol{x}) = \boldsymbol{\tau}, \tag{2.5}$$

to make modelling more approachable. The terms of the model are unitless; $\boldsymbol{x} = [U \;\; r]^\top$ is the state vector, $\boldsymbol{M} = \text{diag}(m_U(\boldsymbol{x}), m_r(\boldsymbol{x}))$ is the inertia matrix, $\boldsymbol{\sigma}(\boldsymbol{x}) = [\sigma_U(\boldsymbol{x}) \;\; \sigma_r(\boldsymbol{x})]^\top$ is a damping term, and $\boldsymbol{\tau} = [\tau_m \;\; \tau_\delta]^\top$ is the control input where $\tau_m \in [0, 1]$ and $\tau_\delta \in [-1, 1]$ describes the motor throttle and rudder angle respectively. The elements of $\boldsymbol{M}(\boldsymbol{x})$ and $\boldsymbol{\sigma}(\boldsymbol{x})$ are chosen to have a polynomial basis and will be identified using linear regression. This process will be described in section 2.3.3, and linear regression will be introduced in section 2.2.

When working with empirical models such as this one, it's important to be aware of the fact that the model is only valid within the region of the state space in which the system explored during the experiments used for parameter identification. The behavior of the identified model outside of this region is unpredictable and often quite dramatic. That is because good extrapolation is not a general property of functions used in curve fitting.

2.2 Linear regression

The model presented in the previous section represents a general structure. As mentioned, the elements of $\boldsymbol{M}(\boldsymbol{x})$ and $\boldsymbol{\sigma}(\boldsymbol{x})$ have a polynomial basis. This means that a they are assumed to have a structure which can be represented by polynomials. Measurements of the elements will be obtained during the identification process described in section 2.3 and these will be used to identify the parameter of the polynomial structures used to describe the terms of the model. An introduction to linear regression will be given here. And then its application in the model identification process will be described in section 2.3.3. For details on the subject of linear regression and statistical learning, literature such as [10] is highly recommended.

Linear regression is a method used to model the relationship between a dependent variable y and some independent variables $\boldsymbol{x}$. At the core of this relationship lies a linear combination of a vector of basis functions $\boldsymbol{\phi}(\boldsymbol{x})$, describing the underlying structure of the model; and a parameter vector $\boldsymbol{\beta}$, instantiating the structure. The first step of the regression is to identify some $\boldsymbol{\phi}(\boldsymbol{x})$ able to represent the most relevant behavior of our system based on knowledge about its nature. Then, given a $\boldsymbol{\phi}(\boldsymbol{x})$, measurements from experimentation are used to determine the value of $\boldsymbol{\beta}$ that minimizes an error term, ε, which represents the unmodelled system dynamics, disturbances and noise.

From the description above, the measurement and estimate of y can be

formulated as

$$y(\boldsymbol{x}, \boldsymbol{\beta}) = \boldsymbol{\phi}(\boldsymbol{x})^\top \boldsymbol{\beta} + \varepsilon, \text{ and} \tag{2.6a}$$

$$\hat{y}(\boldsymbol{x}, \boldsymbol{\beta}) = \boldsymbol{\phi}(\boldsymbol{x})^\top \boldsymbol{\beta}. \tag{2.6b}$$

Using the fact that $y(\boldsymbol{x}, \boldsymbol{\beta})$ is linear in terms of $\boldsymbol{\beta}$, the regression looks for the $\boldsymbol{\beta}$ that minimizes the least square error, ε_{LS}, between measurement and estimate. The least square error is given by

$$\varepsilon_{LS} = \frac{1}{N} \sum_{i=1}^{N} (y_i - \boldsymbol{\phi}(\boldsymbol{x}_i)^\top \boldsymbol{\beta})^2, \tag{2.7}$$

where N is the total number of measurements, and y_i and $\boldsymbol{x}_i$ is the i'th pair of measurements in the data set $\big\{\{\boldsymbol{x}_1, \boldsymbol{x}_2, \ldots, \boldsymbol{x}_N\}, \{y_1, y_2, \ldots, y_N\}\big\}$. The minimization of (2.7) has the analytic solution

$$\boldsymbol{\beta} = (\boldsymbol{X}^\top \boldsymbol{X})^{-1} \boldsymbol{X}^\top \boldsymbol{Y}, \tag{2.8}$$

where $\boldsymbol{X} = \begin{bmatrix} \boldsymbol{\phi}(\boldsymbol{x}_1)^\top & \boldsymbol{\phi}(\boldsymbol{x}_2)^\top & \ldots & \boldsymbol{\phi}(\boldsymbol{x}_N)^\top \end{bmatrix}^\top$ and $\boldsymbol{Y} = \begin{bmatrix} y_1 & y_2 & \ldots & y_N \end{bmatrix}^\top$.

At this point all the terms necessary to evaluate the estimated model, (2.6), are available. Performance of the model in real world applications depends on the various limitations encountered, and decisions made, throughout the regression process. For example; the choice of which measurements of y to include, which is relevant if outliers are a threat; the choice of which $\boldsymbol{\phi}(\boldsymbol{x})$ to base the model on, a high degree of non-linearity increases the risk of overfitting while a simple basis might be unable to capture essential dynamics; the quantity and quality of measurements, elements that determine the amount of noise that slips through as well as its impact; etc. There is a variety of countermeasures available to limit the impact of some of these shortcomings. Three of them are described below and will be taken advantage of later on. These are weighted linear least squares, regularization, and cross-validation.

2.2.1 Weighted linear least squares

The nature of a system can be such that the reliability of measurements is correlated with the system state. This happens when the variance of the error term, ε, in our model (2.6) is not constant, but dependent on $\boldsymbol{x}$. That is, in general:

$$\mathrm{Var}(\varepsilon_i | \boldsymbol{x}_i) = g(\boldsymbol{x}_i) \neq \text{constant}, \tag{2.9}$$

where $g(\boldsymbol{x}_i)$ is some unknown function. The effect is illustrated in Figure 2.3. Looking at Figure 2.3 it is fair to say that a measurement at a high x-value is more likely an accurate representation of the true function value than a measurement with a lower x-value. If this is the case and it is not accounted for, the model may suffer as imprecise data points will have

the same influence as precise data points. This is especially concerning as the regression considers the quadratic error, meaning large errors, such as the ones generally found in high variance regions, have considerable more impact.

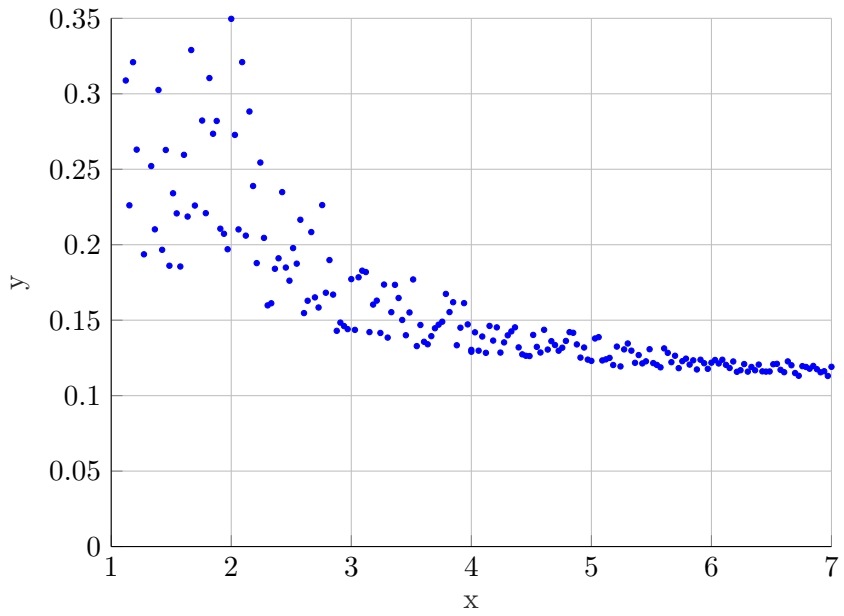

Figure 2.3: Samples from a system where the variance of y is clearly dependent on x.

In the context of modelling marine vessels the phenomenon is expected to be encountered when applying regression to identify model parameters due to multiple causes. When a surface vessel operates at speeds close to zero, effects on the system state caused by disturbances, such as waves, current and wind, will be quite large relative to the state value. This means that it becomes difficult to get a good representation of the actual vessel dynamics at low speed, separated from the dynamics of the sea. Furthermore effects of control input are hard to identify in this region as well. The inertia of surface vessels at speeds close to zero can be many times greater than inertia experienced at higher speeds, which in combination with the high damping of the low speed region, means that environmental effects will dominate. Perhaps most importantly is how inertia influences the acceleration of a system at different values, but this discussion will be picked up later on.

The idea behind weighted least squares is that a weight is assigned to each point in the data set which indicates how reliable this measurement is rela-

tive to the others. The new least square error can be formulated as

$$\varepsilon_{LS} = \frac{1}{N}\sum_{i=1}^{N} w_i^2 (y_i - \boldsymbol{\phi}(\boldsymbol{x}_i)^\top \boldsymbol{\beta})^2, \tag{2.10}$$

where $w_i > 0$ are weight coefficients. This way the regression makes the most out of measurements from trusted regions of the state space, while also evaluating measurements from regions of the state space troubled by uncertainty more skeptically. Weighted least squares is therefore advantageous to use when evaluating small data sets where there might not be enough data points to guarantee a proper representation of the underlying dynamics. If the weights are wrongfully determined, weighted least squares can serve against its purpose by giving uncertain regions a high influence. Another important issue is the effect of outliers in weighted least squares. As with other types of regression they are troublesome, but an outliers negative influence can be significantly multiplied if it appears in a highly trusted/weighted region.

The challenging part of weighted least squares is that (2.9) is difficult to determine, so it must be estimated in some manner, or weights must be determined with a heuristic approach. For estimation of the functional form of (2.9), one can use techniques such as feasible generalized least square estimation, but the quality of the estimation will be dependent on the data set. The estimator is biased, and in order to minimize the bias, a large data set is required. Consequently, estimating the functional form of (2.9) is not a good option for the purpose of this thesis because measurements are extracted in a way that generates relatively few data points. Therefore, a priori knowledge of the measurement dynamics will be used to formulate a weighting scheme later on. For more information about weighted linear regression [13] is recommended, in addition to [10].

2.2.2 Regularization

A central problem in statistical modelling is overfitting. Overfitting is what happens when a model starts to describe the behavior of noise in the data and loses sight of the relationship between dependent and independent variables. It occurs when the ratio between data points and model parameters becomes too small. This allows the model to specialize on the data set used in the regression and thus losing generality. The phenomenon is illustrated in Figure 2.4. Overfitting is an element of concern in the identification process described in this report as it aims to use a relatively sparse data set.

One of many techniques to counteract the regression's desire to overfit is regularization. With regularization, a term is added to the least square

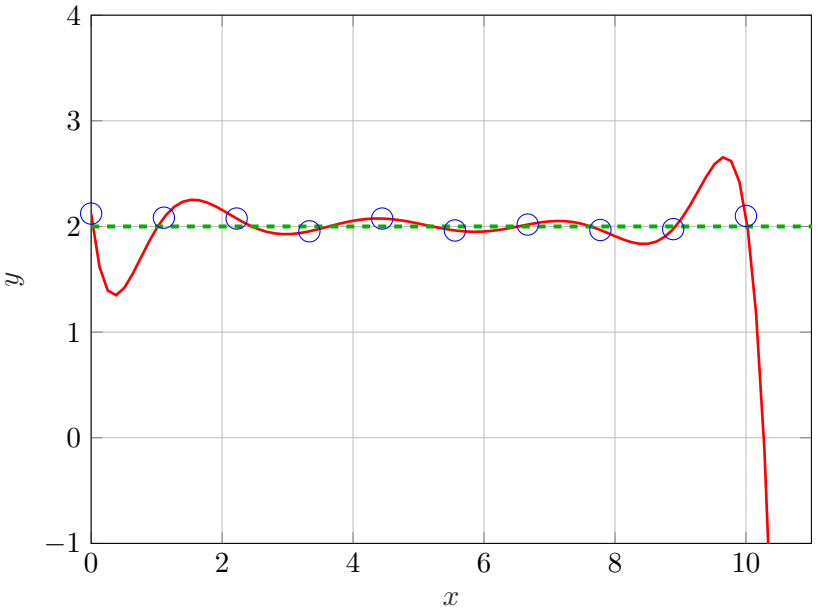

Figure 2.4: Overfitting due to insufficient ratio between model complexity and number of data points. The identified model, red line, is too focused on minimizing the error to measurements, blue marks, to successfully capture the dynamics of the true signal, green line.

error (2.7) whose purpose is to reduce model complexity, for example by penalizing large parameter values. Equation (2.7) becomes

$$\varepsilon_{LS} = \frac{1}{N}\sum_{i=1}^{N}(y_i - \boldsymbol{\phi}(\boldsymbol{x}_i)^\top \boldsymbol{\beta})^2 + \lambda R(\boldsymbol{\beta}), \tag{2.11}$$

where $\lambda > 0$ is a parameter determining the weight of the regularization term relative to that of the sum-of-squares error term, and $R(\boldsymbol{\beta})$ is a penalty function chosen to have the desirable impact on $\boldsymbol{\beta}$.

A class of penalty functions that has seen wide use is

$$R(\boldsymbol{\beta}) = \sum_{j=1}^{M} |\beta_j|^q, \tag{2.12}$$

where M is the number of model parameters in $\boldsymbol{\beta}$, and $q \in \mathbb{R}_{>0}$. By adding the regularization term to the least square error as in (2.11) it generally does not have a closed form solution anymore. Instead the overall problem can be formulated as a quadratic problem with (2.7) acting as the objective

function, subject to the constraint given by (2.12) as

$$\boldsymbol{\beta}^*_{reg} = \underset{\boldsymbol{\beta}}{\operatorname{argmin}} \frac{1}{N}\sum_{i=1}^{N}(y_i - \boldsymbol{\phi}(\boldsymbol{x}_i)^\top \boldsymbol{\beta})^2 \tag{2.13a}$$

$$\text{subject to } \sum_{j=1}^{M} |\beta_j|^q \leq \eta \tag{2.13b}$$

where there is a one-to-one correspondence between η and λ; see [10] for further details.

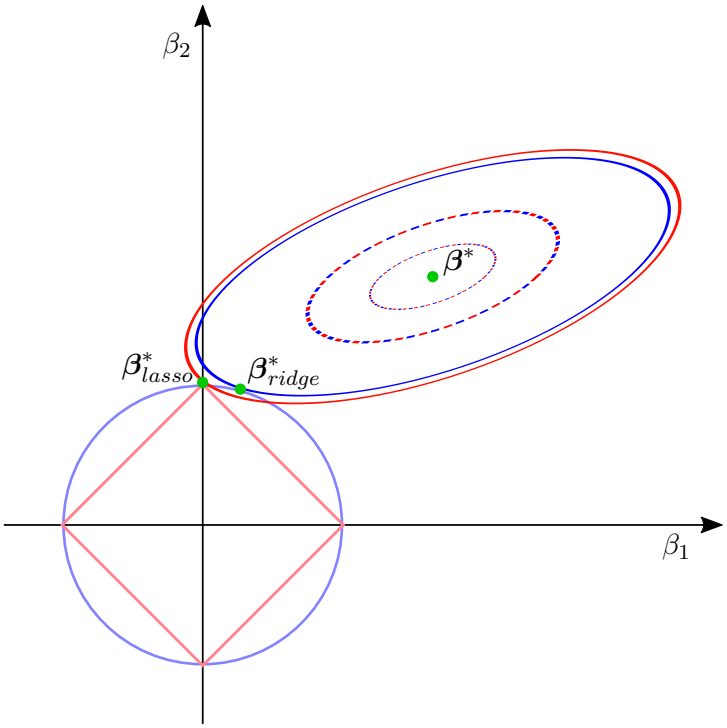

Figure 2.5: Regularization example. Solutions to lasso, $\boldsymbol{\beta}^*_{lasso}$; ridge regression, $\boldsymbol{\beta}^*_{ridge}$; and standard linear regression, $\boldsymbol{\beta}^*$, are plotted. With them, visualizations of the lasso constraint, red square; ridge constraint, blue circle; and contours of the least square error function, blue and red ellipses. Figure adapted from [10].

In this thesis the two cases $q = 1$ and $q = 2$ will become relevant. These are also the most widely used, and they are known as *lasso* and *ridge regression* respectively. The difference in functionality between the two is illustrated in Figure 2.5. The figure shows a case where the parameter vector has

two variables, β_1 and β_2, and minimizer of (2.7) is the green dot labeled $\boldsymbol{\beta}^*$. When a regularization term is added as in equation (2.11) the problem becomes constrained as mentioned earlier. The constraint in the cases of lasso and ridge regression has the form of shown in (2.13b) and its outer boundary is visualized as the red square, $|\beta_1| + |\beta_2| \leq \eta_{lasso}$, and blue circle, $\beta_1^2 + \beta_2^2 \leq \eta_{ridge}$, respectively. The ellipses centered at $\boldsymbol{\beta}^*$ represent the contours of the objective function, which is the equivalent of the least square error (2.7). At the point where the outer red ellipse intersects with the red square, or rather the point with the lowest least square error satisfying the lasso constraint, lies the solution, $\boldsymbol{\beta}^*_{lasso}$, to the lasso method. Likewise, $\boldsymbol{\beta}^*_{ridge}$ is the solution to the ridge regression.

Figure 2.5 displays some of the properties of lasso and ridge regression. Lasso tends to drive some elements of $\boldsymbol{\beta}$ to zero, working somewhat like a feature selection method, selecting a subset of the available parameters; and generally restricts the size of the elements. Ridge regression on the other hand, does not exclude any elements of $\boldsymbol{\beta}$. It generally keeps them all and shrinks together correlated elements of $\boldsymbol{\beta}$. The discussion of when to use which of the two will be picked up in section 3.3.2. For more details about lasso and ridge regression, as well as other regularization methods the insightful discussion of the topic in [10] is recommended.

2.2.3 Cross validation

Cross validation (CV) is a technique that can be used to determine hyperparameters, meaning parameters that has to be set before the regression is performed, such as the regularization weight λ. The method has multiple variations. A commonly used, and rather intuitive, variant is K-fold CV. The workings of the method is illustrated in Figure 2.6. In K-fold CV the data set is divided into K subsets, or *folds*. Iterating through the folds, each fold takes a turn serving as validation data while the other $K - 1$ folds are used for training. Performing a regression on the training folds and validating the resulting model using the validation fold produces a validation error, denoted e_i in the figure. After going through each fold, a validation score, E_{val}, is obtained by averaging the validation errors from each iteration.

Provided a set of possible hyperparameter values, for example a range between an upper and lower bound, K-fold CV can be performed for each value. Once the whole set has been evaluated, the hyperparameter value with the best E_{val} is chosen. As the use of CV in hyperparameter identification is an optimization problem, there are more sophisticated methods for obtaining a solution. However, linear regression is a post processing step in the method covered in this thesis. As such, there are no strict time

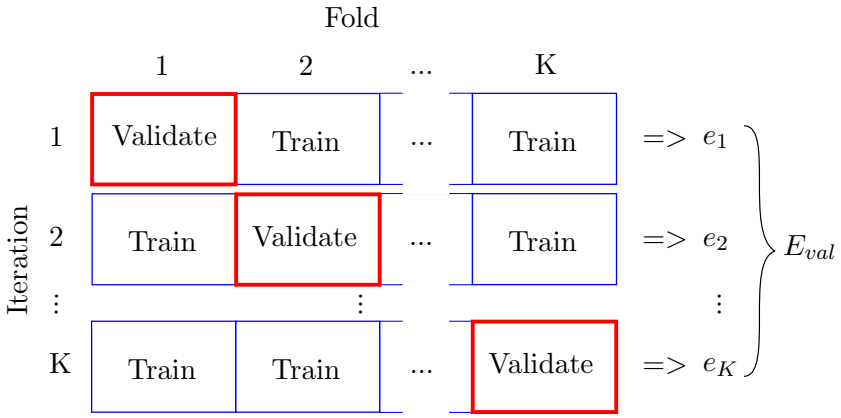

Figure 2.6: K-Fold cross validation. One fold of samples is excluded from training and used to validate at each iteration. The average validation error, E_{val}, of all iterations can be used to score hyperparameter values.

constraints; additionally, boundaries of the hyperparameter ranges that are suitable for the system studied here have been determined in earlier work.

The choice of how many folds, K, to use in CV comes down to multiple factors. In general it is recommended to use $K = 10$. Increasing the number of folds means that the validation error, E_{val}, will have a higher variance as the training data becomes similar for each iteration. Decreasing the number of folds means, E_{val}, will be more biased as it becomes an overestimate. The deciding factor in context of this thesis is the small size of the data set compared to the complexity of the model. By choosing $K = N$, which is called leave-one-out, the regression can make the most of each data point. Normally, computation time is a considerable factor as well. But as a relatively small data set is being used, and there are no strict time constraints, it is a feasible option.

2.3 Model identification

The model identification procedure can be thought of as a five step process. A rough sketch of it is shown in Figure 2.7 where some intermediate results are shown. The details of the figure are not essential at this point as similar results will be presented and discussed later on. For now the contents of the figure will serve as a visual reference for the purpose of each step in the modelling procedure as they are described later in this section.

Now a brief description of each step in the method is given and then each step will be expanded upon in the sections that follow.

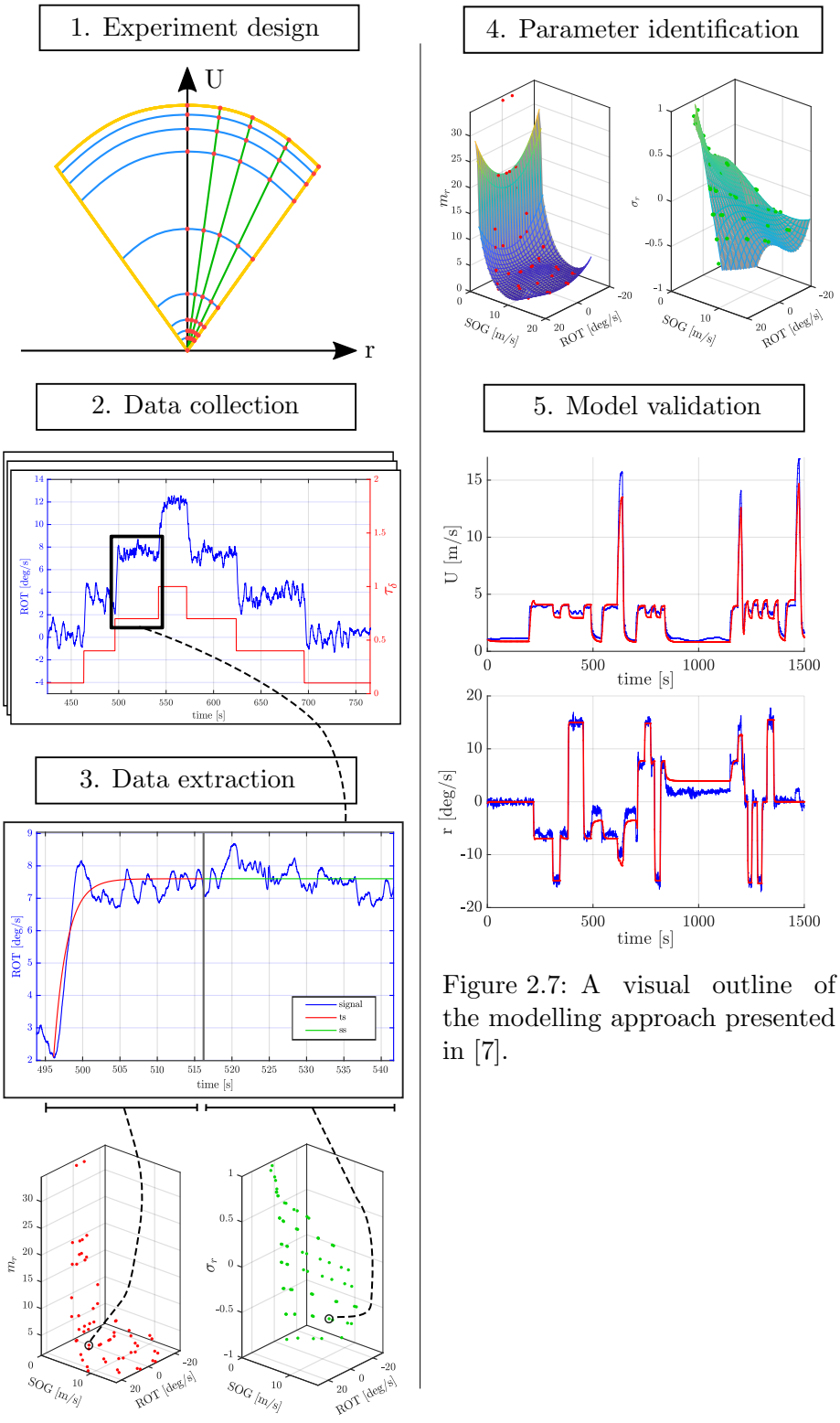

Figure 2.7: A visual outline of the modelling approach presented in [7].

1, 2 The first and second step of the method are experiment design and data collection. The modelling method is based on collecting data from the vessel's step response; more specifically, recording transient and steady state responses. Therefore, the experiments are performed by executing a sequence of steps in input $\boldsymbol{\tau}$. To achieve a satisfactory sampling of the vessel's dynamics throughout the state space some thought has to be put into design of the step sequence.

3 The third step is to analyze the data collected in step two, and extract measurements that are descriptive in a modelling context. Measurements of the vessel's transient behavior is used to identify the parameters of the inertia term $\boldsymbol{M}(\boldsymbol{x})$, while measurements of the steady state behavior is used to identify the parameters of the damping vector $\boldsymbol{\sigma}(\boldsymbol{x})$.

4 The fourth step is to feed the measurements extracted in step two into a parameter identification tool such as linear regression. Given that the measurements are well distributed in the vessel's state space, the linear regression should provide sufficiently accurate estimates of $\boldsymbol{M}(\boldsymbol{x})$ and $\boldsymbol{\sigma}(\boldsymbol{x})$.

5 The fifth and final step is to ensure that the newly identified model performs adequately. This is done by comparing the models simulated response to the vessel's actual response in a validation experiment.

2.3.1 Experiment design and data collection

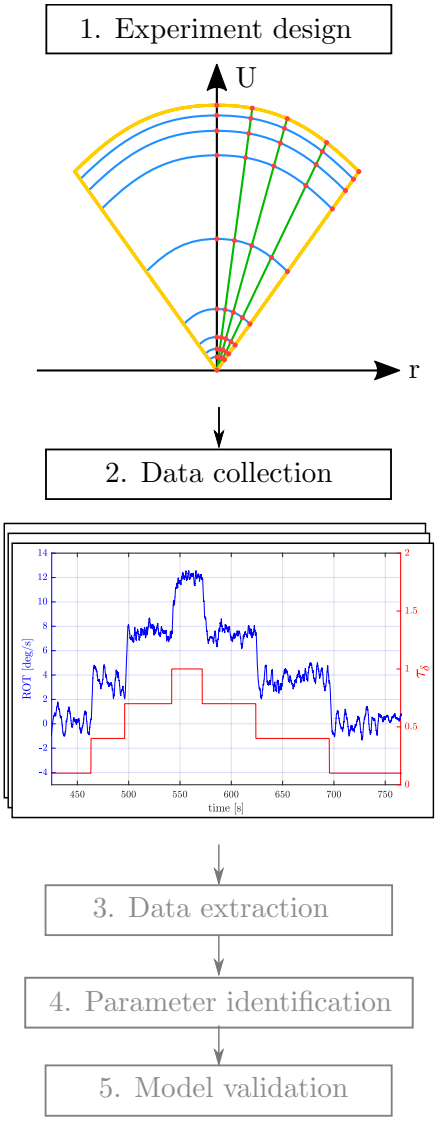

Figure 2.8: The intention of the two first steps is to provided data well distributed in the state space.

To gather data for the model identification, [7] describes experiments consisting of a sequence of step responses. The step responses are recorded, then data from the transient is used to describe the vessel's inertia, and steady state data is used to describe the damping. The experimental procedure described in [7] for gathering data to estimate SOG parameters, $m_U(\boldsymbol{x})$ and $\sigma_U(\boldsymbol{x})$, is formulated as follows. *Note: The notation has been slightly modified in order to increase generality.*

Experimental procedure

1. Start at $\tau_m = \tau_{m,min}$. Select $\tau_\delta = \tau_{\delta,min}$
2. Step τ_m stepwise from $\tau_{m,min}$ to $\tau_{m,max}$ in steps of $\tau_{m,\Delta}$, letting the vessel SOG and ROT reach steady state before the next step is applied. Let the vessel do at least on full turn after reaching steady state, to be able to minimize the effect of external disturbances through averaging.
3. Step τ_m stepwise from $\tau_{m,max}$ to $\tau_{m,min}$, in the same fashion as in step 2.
4. Repeat step 2 and 3 with the next rudder setting.

As noted in [7], the experimental procedure for identification of ROT parameters, $m_r(\boldsymbol{x})$ and $\sigma_r(\boldsymbol{x})$, is the same, except the roles of τ_m and τ_δ are switched. Figure 2.8, under "Data collection", shows the ROT response of one iteration from identification of ROT parameters. Both increasing and decreasing input steps are performed to include the effects of rate dependent hysteresis. The experimental procedure is also designed with an assumption of symmetric rudder response in mind.

This means that samples from the region of state space where $r < 0$ can be obtained by mirroring data sets obtained later on.

The use of step responses to model surface vessel dynamics is discussed in [4]. In this article the concept of maneuverability, which is a central concept in studies of aircraft [1], is adapted to a marine setting. As described in [1] maneuverability is 'a measure of the ability to achieve and transition between steady maneuvers.' In the context of maneuverability, data from the steady state achieved in a step response can be used to describe the vessel's *maneuver performance*, which in our case is closely related to the damping term of the model (2.5), $\boldsymbol{\sigma}(\boldsymbol{x})$. This is easily seen by evaluating the equation (2.5) in steady state, where $\dot{\boldsymbol{x}}$ is zero. The transient of the step response can be used to describe the vessel's *agility*. And, if maneuver performance is evaluated first, this means that the recorded transient can be used to estimate the inertia of the model (2.5), $\boldsymbol{M}(\boldsymbol{x})$. This process will be expanded upon in section 2.3.2.

Parameters of the experimental procedure

The input bound parameters, $\tau_{m,min}$, $\tau_{m,max}$, $\tau_{\delta,min}$, and $\tau_{\delta,max}$, decide the size of the region in state space where the model is valid. Extrapolation is generally not considered in empirical model identification so the model has to be saturated when operation takes place outside the valid region. Therefore, operation should be restricted to be within this region in state space as there are no promises of accuracy when operating outside of it.

Even though maximizing the valid region of the model is desirable, there are some considerations that should done before setting the input bounds. These consideration are usually case specific. In [4] a similar experimental procedure is described where $\tau_{m,min}$ is chosen to be

$$\tau_{m,min} = 0.4. \tag{2.14}$$

This was done because "a throttle input of less than [0.4] was barely recognizable on the surge speed output, which means that the range [0 0.4] in practice constitutes a dead band." The authors of [7] chose $\tau_{m,max}$ to be

$$\tau_{m,max} = 0.6, \tag{2.15}$$

because "[they] observed that the motor response [was] greatly reduced for $\tau_m > 0.6$ [...]." As the vessel studied in this report is the same as the one studied in [7] the same bound will be used here. Additionally, since the experiments are going to be done automatically in the work covered by this

thesis, the bound defined by $\tau_{\delta,max}$ will be tightened when combined with large values of τ_m; more specifically,

$$\tau_{\delta,max} = \begin{cases} 0.4, \text{ if } \tau_m > \tau_{m,max} - \tau_{m,\Delta} \\ 1.0, \text{ else.} \end{cases} \tag{2.16}$$

This is a safety/comfort measure as aborting a potentially dangerous maneuver, like a sharp turn at high speed, has the added delay of a manual takeover. When it comes to $\tau_{\delta,min}$, it can be favourable to select a nonzero value small enough to ensure proper sampling near $r = 0$, but large enough for it to be reasonable to complete a circle in steady state, as suggested in step 2 of the "Experimental procedure." Failing to complete a circle will result in a current induced bias, this is primarily a threat in low SOG regions where the signal-to-noise ratio is low. An exaggerated illustration of the valid model regions belonging to the three cases presented here is shown in Figure 2.9.

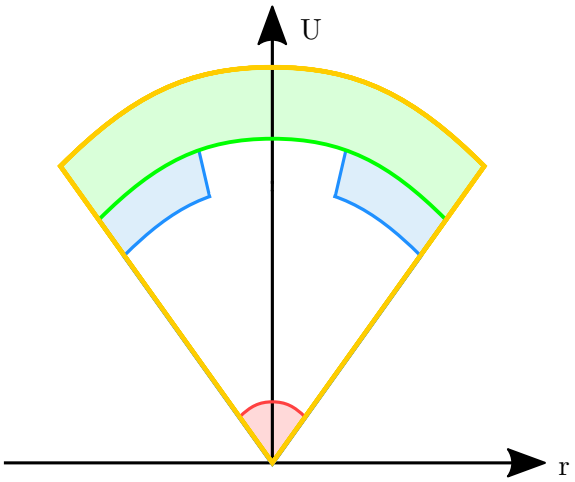

Figure 2.9: An exaggerated example of how different input boundaries might translate into the state space. The red region and the green region could be from restrictions in motor input with the purpose of removing dead bands in opposite end of the input range. The blue region could be from a wish to avoid sharp turns at high speed for safety reasons.

In addition to the input bound parameters, the step sizes, $\tau_{m,\Delta}$ and $\tau_{\delta,\Delta}$, are also important for the outcome of the modelling procedure. As just mentioned, the input bounds could be tightened to leave out input intervals with negligible effect. The input steps' varying effect throughout the state space is important to be aware of when formulating the experimental procedure also. A visualization of how uniform steps might translate to the state space is shown in Figure 2.10. As seen in the figure, steps in throttle tend to have

a large effect in the middle of the input range but it decreases in direction of either boundary. The effect of rudder steps is also dependent on U. However, the effect of rudder steps is closer to being uniformly distributed in the direction of r.

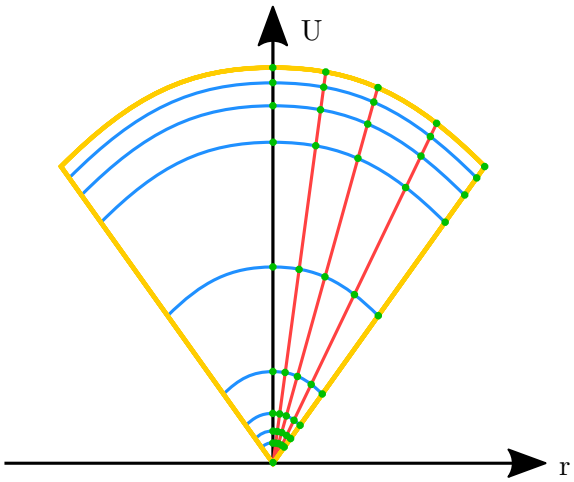

Figure 2.10: An example of how uniformly distributed step sequences might sample the state space. In this case the step lengths are $\tau_{m,\Delta} = 0.1$, each throttle step visualized as a blue line; and $\tau_{\delta,\Delta} = 0.25$, each rudder step visualized as a red line.

A model built on measurements distributed as they are in Figure 2.10 would be vulnerable to overfitting due to the long distances between measurements in the U direction in the middle of the state space. To counter this one could decrease the step size. However, this would also mean that distances between measurements in other parts of the state space become smaller. For low SOG regions this can have a negative effect on the quality of measurements. Executing a small step in this region results in a low signal-to-noise ratio, as the effects of disturbances become hard to distinguish from a step response. In Figure 2.11 two cases encountered in work with the collected data from [7] are shown. Although, these represent the worst case, similar behavior is not unexpected when operating in low speed regions. This emphasizes the fact that this modelling approach should be performed under good conditions/calm sea if a good representation of the vessel dynamics is to be obtained; particularly in this low speed region. This is also noted in [4] in the context of control applications, where it is mentioned that creation of the vessel model should be focused on capturing the vessel dynamics in nominal conditions. Then feedback terms should be used to counter discrepancies due to disturbances.

Increasing step size to reduce the impact of disturbance on step responses

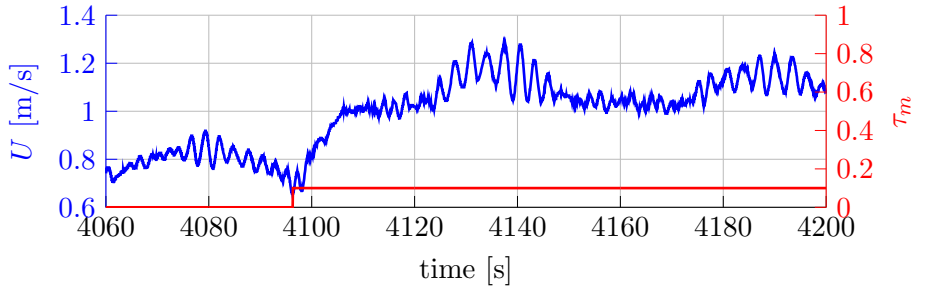

(a) Step in throttle during identification of SOG parameters.

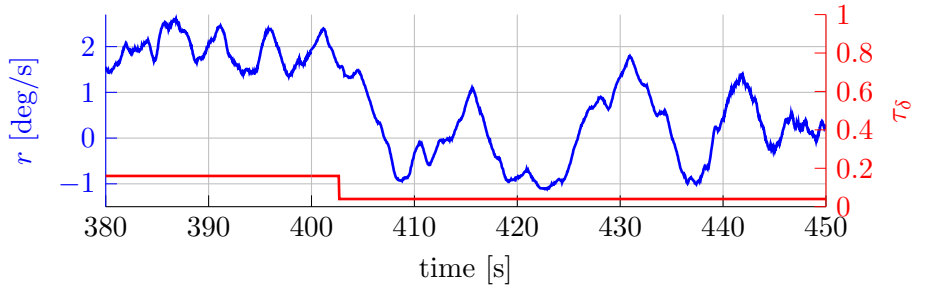

(b) Step in rudder during identification of ROT parameters.

Figure 2.11: Encounters with low signal-to-noise ratio during identification experiments done in [7].

is not necessarily a good idea either. That is because the low SOG region is also where the vessel dynamics change the most and thus sufficient sampling is required to achieve a good description. One solution would be to perform a new experiment using the same step size but sampling at an offset by setting $\tau^{new}_{m,min} = \tau^{old}_{m,min} + \frac{1}{2}\tau_{m,\Delta}$.

A better solution, and also a common approach in empirically based modelling [20], is to make the intention of the initial experiment to gather data about the system, learn from it, and then use the newly found knowledge to improve the modelling process in an iterative fashion. An illustration of this procedure, comparable to the method overview of Figure 2.7, is shown in Figure 2.12. Normally, the initial experiment is part of an extensive analysis to determine a variety of system properties. This is essentially what has been done in terms of modelling in [7]. But as suggested in the article's future work bullet list, extending the method to become iterative would likely be beneficial. Generally, every element of the procedure can be examined for improvements. But since results from [7] were satisfactory, most elements, like model structure selection, can be left out of future iterations of the method. Instead the iterative extension of the procedure should be aimed at identifying a new experiment that achieves a better sampling of the state space. Steps should be chosen to achieve a more uniform sampling of the

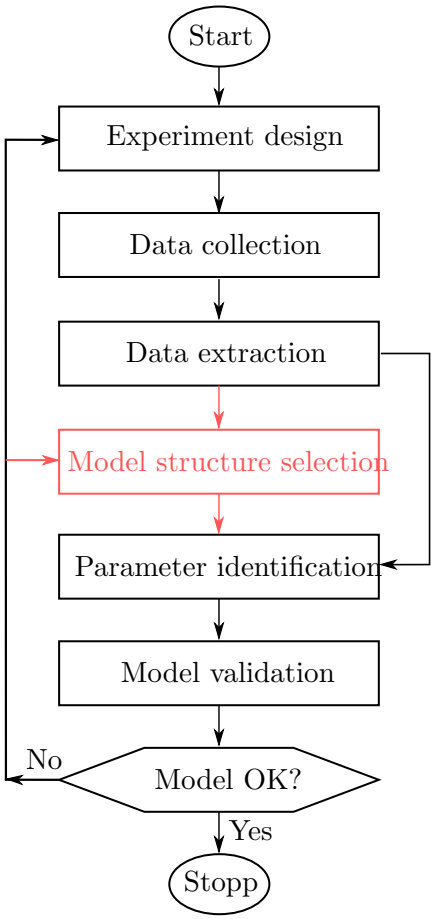

Figure 2.12: Flow of an iterative modelling procedure. Model structure selection is skipped in this method as results from [7] were satisfactory. This flow chart is an extension of the one in Figure 2.7. Figure adapted from [20].

state space. Additionally, the space between each sample should be small enough to avoid overfitting and sufficiently sample the regions of the state space hosting complex dynamics. At the same time the step size should be large enough ensure a usable signal-to-noise ratio.

2.3.2 Data extraction

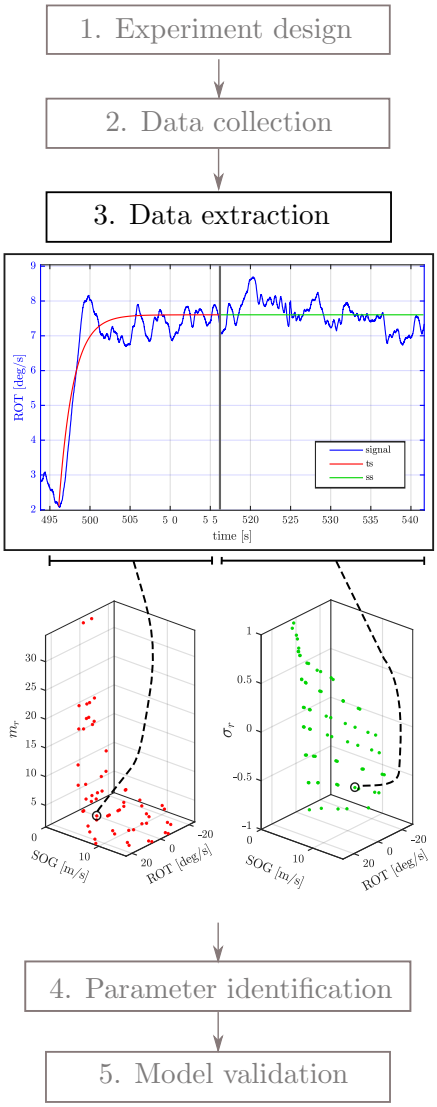

Figure 2.13: In step 3, inertia and damping data is extracted from each step response.

By performing the experimental procedure described at the start of the previous section a collection of step responses spread throughout the state space is obtained. The next step of the method described in [7] is to analyze each step response of the collection, as illustrated by Figure 2.7 in the transition from step 2 to 3. Through the analysis a measurement of damping σ, an element of $\boldsymbol{\sigma}(\boldsymbol{x})$, is extracted from the steady state region of the step response. Then a measurement of inertia m, a diagonal element of $\boldsymbol{M}(\boldsymbol{x})$, is extracted from the transient. The extraction of σ and m is illustrated in Figure 2.13. Each measurement is described by the step response's location in state space. This results in two types of data sets:

$$\mathscr{D}_\sigma = \big\{\{\boldsymbol{x}_1, \boldsymbol{x}_2, \ldots, \boldsymbol{x}_{N_\sigma}\}, \{\sigma_1, \sigma_2, \ldots, \sigma_{N_\sigma}\}\big\}, \tag{2.17a}$$

$$\mathscr{D}_m = \big\{\{\boldsymbol{x}_1, \boldsymbol{x}_2, \ldots, \boldsymbol{x}_{N_m}\}, \{m_1, m_2, \ldots, m_{N_m}\}\big\}, \tag{2.17b}$$

The data sets can be expanded by assuming that the vessel has a symmetric rudder response and therefore mirror all the measurements about the ROT axis; mirror and flip sign in the case of $\mathscr{D}_{\sigma_r}$.

Measuring damping

By evaluating the model (2.5) in steady state, that is with $\dot{\boldsymbol{x}} = 0$, it is reduced to

$$\boldsymbol{\sigma}(\boldsymbol{x}) = \boldsymbol{\tau}. \tag{2.18}$$

This means that the elements of $\boldsymbol{\sigma}(\boldsymbol{x})$ can be measured directly from input during steady state. The average of $\boldsymbol{x}$ over the whole steady state duration is used to locate the measurement in state space.

The results of applying this procedure on data from a throttle step experiment and from a rudder step experiment are the two data sets

$$\mathscr{D}_{\sigma_U} = \big\{\{\boldsymbol{x}_{U,1}, \ldots, \boldsymbol{x}_{U,N_{\sigma_U}}\}, \{\sigma_{U,1} \ldots, \sigma_{U,N_{\sigma_U}}\}\big\}, \tag{2.19a}$$

$$\mathscr{D}_{\sigma_r} = \big\{\{\boldsymbol{x}_{r,1}, \ldots, \boldsymbol{x}_{r,N_{\sigma_r}}\}, \{\sigma_{r,1}, \ldots, \sigma_{r,N_{\sigma_r}}\}\big\}, \tag{2.19b}$$

The contents of $\mathscr{D}_{\sigma_r}$ is shown as the bottom right plot in Figure 2.7.

Measuring inertia

To measure inertia a first order linear time-invariant (LTI) system is fitted to the transient part of the vessel's step response. For example, throttle transients are approximated by simulating

$$m_{U_i}\Delta\dot{U}_i + k_i\Delta U_i = \Delta\tau_{m_i}, \tag{2.20}$$

where m_{U_i} is assumed to be a constant inertia term during step i; $\Delta U_i = \hat{U} - U_i^-$, where $\hat{U}$ is the system state; $\Delta\tau_{m_i} = \tau_m - \tau_{m_i}^-$; and $k_i = \frac{\sigma_{U_i}^+ - \sigma_{U_i}^-}{U_i^+ - U_i^-}$ with $(\cdot)^-$ and $(\cdot)^+$ denoting the a priori and a posteriori steady state values respectively. Similarly, m_r is estimated from rudder steps by exchanging U for r, and τ_m for τ_δ. To select an estimate the authors of [7] suggests evaluating the root mean square error between the simulated system (2.20) and the measured vessel response for a set of inertia values. Then choose the one producing the lowest error. To locate the measurement in state space, the midrange value of the transient is calculated. It is found as $\boldsymbol{x} = (\frac{U_i^+ + U_i^-}{2}, \frac{U_i^+ + U_i^-}{2})$.

The results of applying this procedure on data from a throttle step experiment and from a rudder step experiment are the two data sets

$$\mathscr{D}_{m_U} = \big\{\{\boldsymbol{x}_{U,1}, \boldsymbol{x}_{U,2}, \ldots, \boldsymbol{x}_{U,N_{m_U}}\}, \{m_{U,1}, m_{U,2}, \ldots, m_{U,N_{m_U}}\}\big\}, \tag{2.21a}$$

$$\mathscr{D}_{m_r} = \big\{\{\boldsymbol{x}_{r,1}, \boldsymbol{x}_{r,2}, \ldots, \boldsymbol{x}_{r,N_{m_r}}\}, \{m_{r,1}, m_{r,2}, \ldots, m_{r,N_{m_r}}\}\big\}, \tag{2.21b}$$

The content of $\mathscr{D}_{m_r}$ is shown as the bottom left plot in Figure 2.13.

Measurement accuracy

There are limited ways to improve the quality of damping measurements due to the simple measurements procedure. Besides from making sure circles are completed in steady state for each step, and that the experiments are performed under good conditions, there are no obvious factors to play with that doesn't include system upgrades; i.e. sensor quality.

The accuracy of measurements in the damping data sets (2.19) affect the inertia measurements as the LTI system (2.20) depend on its values. In the low SOG region, where the signal-to-noise ratio is low, this dependency can cause quite dramatic errors in inertia measurements. An example is shown in Figure 2.14 where the vessel is left facing the current approximately head on at the end of the transient. The horizontal, red line is the measured steady state value of the step response, the r element of $\boldsymbol{x}_{r,i}$ in data set (2.19b). This value clearly deviates from where the vessel enters steady state, the value illustrated by the green line. However, this is not considered by the LTI system (2.20). Consequently, the red transient in Figure 2.14 is the simulated instance of system (2.20) that best fits the vessel response when evaluated with a least square error.

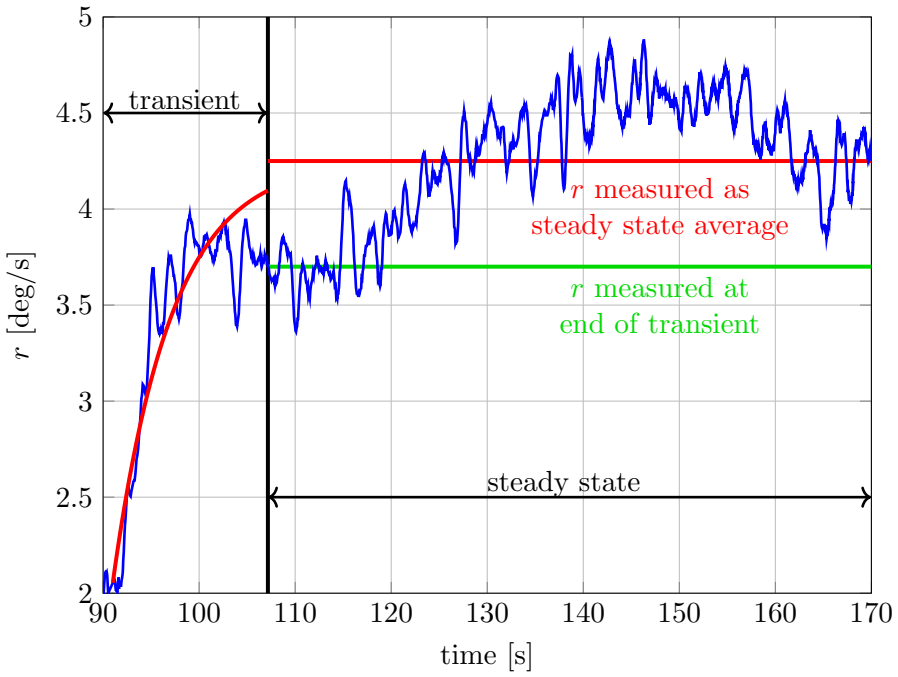

Figure 2.14: Step response with significant difference between measured steady state value and state measured at end of transient.

By studying the lower left plot of Figure 2.13 one can get an impression of how significant this error is. The measurement produced by this step is the one that is significantly higher than the rest; there are actually two because every data point is mirrored due to the symmetric rudder response assumption. As seen in the plot it has nearly double the value of any other measurement. Even though these kinds of errors only appear with significant size when the signal-to-noise ratio is low, they are a direct consequence of the method used to generate the measurements, and not caused by some

abnormality. The disturbances in steady state is purely due to current and measurements noise.

It should be mentioned that although the error appears to be very large in the data set the simulated transient in Figure 2.14 captures the vessel dynamics better than one might expect. This is due to the fact that changes in inertia do not have a linear effect on transient behavior. However, the linear regression performed later on primarily considers the size of the measurement error and not its effect. In other words it is primarily the size of the error that counts, but this will be discussed in greater detail in section 2.3.3 when it becomes more relevant.

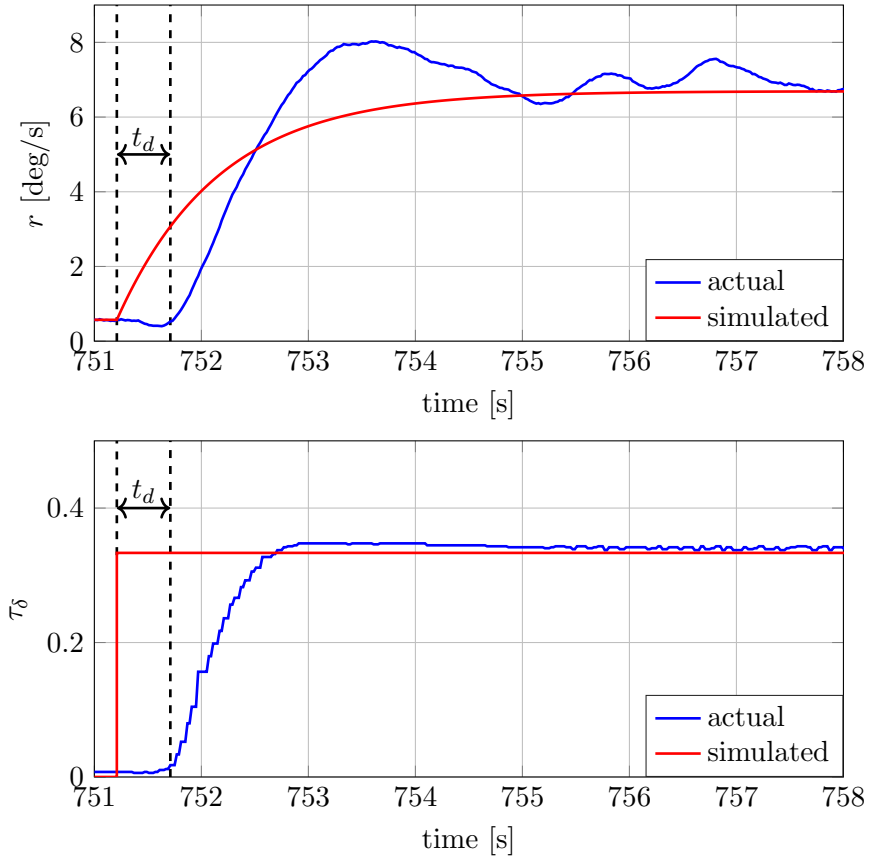

Figure 2.15: A step response from the experiment performed by the authors of [7], plotted together with a first order approximation generated by the inertia measurement technique described in [7] using equation (2.20). Below it is a plot of the input signal and the measured actuator output.

Another important source of error is propagation delay, t_d. Propagation delay comes from the time it takes the input signal to propagate through

the different parts of the system and actuate it. The delay has a consistent effect on measurements as it is a constant value that is always present. The effects of t_d can be seen in both plots of Figure 2.15. The figure shows the vessel's actual step response and actuator output in blue; in addition to the simulated response of LTI system (2.20) and the input reference signal in red. As seen in the figure, the setup used on the Telemetron for these experiments had a propagation delay of $t_d \approx 0.5s$. This constitutes a significant part of the transient in this case and results in a rather large gap between simulated and actual response. Thus propagation delay translates into the inertia models as a positive bias because the inertia measurements have to be artificially large to compensate for the gap and lower the square error.

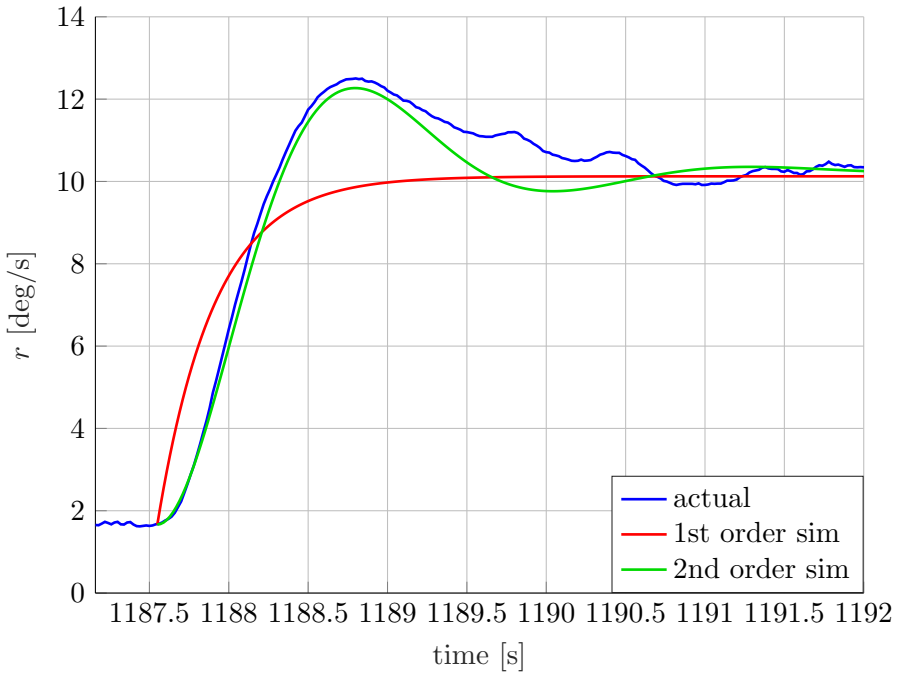

Figure 2.16: A step response from the experiment performed by the authors of [7] with propagation delay manually removed. The step is plotted together with a first order approximation generated by the inertia measurement technique described in [7] using equation (2.20). A second order approximation generated by a second order Nomoto model is included as well.

Propagation delay meant that the measured inertia became artificially high to compensate for the gap it created. By looking at Figure 2.15 one can see that there is another, relatively large, gap between simulation and reality. That would be the gap created by the overshoot. Because a first order LTI system like equation (2.20) can not emulate higher order behavior like overshoots this too means that inertia measurements have to be artifi-

cially adjusted to compensate. Figure 2.16 shows a step response where the propagation delay has been manually removed from the inertia measuring process in order to get a better look at the effect of overshoots. In the presence of overshoots the inertia value is lowered so that the transient might rise quicker and thus minimize the gap beneath the overshoot. The actual impact of this effect is most clear when the method is used in a simulation environment where propagation delay is not present and actuator dynamics have a limited effect as an integrated part of the model. Such a scenario was studied in [11] where overshoots appeared to be the major cause of measurement errors. Figure 2.17 shows the results that were obtained during the process of modelling m_r. It shows a correlation between negative measurement error and regions of the state space where overshoots occur. Note that errors seem to be smaller for measurements at high SOG, depending on perspective that is not necessarily true. The reason why is discussed in section 2.3.3.

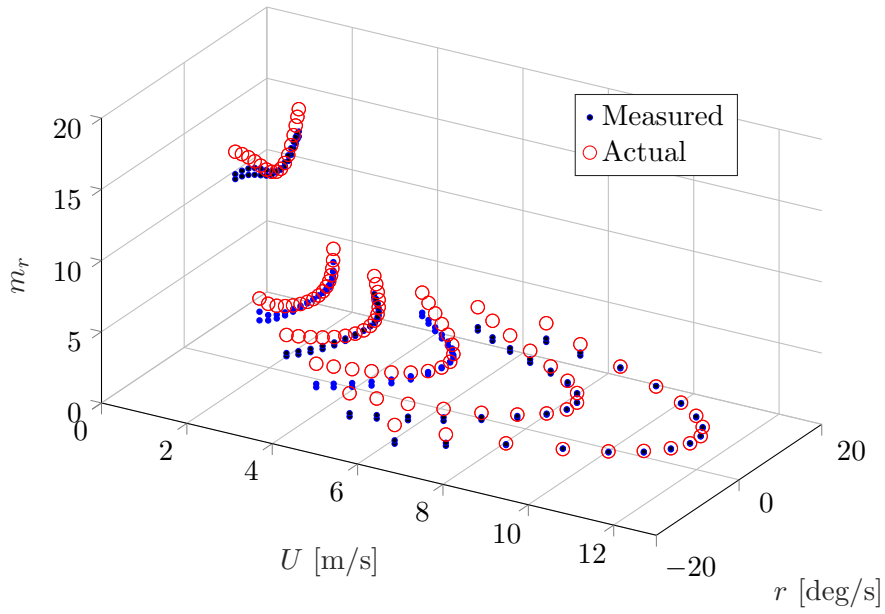

Figure 2.17: Inertia measurements obtained by applying the modelling method in a simulation environment based on the model identified in [7]. The simplicity of the simulation environment allows the consequence of the methods inability to describe overshoots to shine through. This figure is taken directly from [11].

As mentioned, the inability to capture the overshoot phenomenon is due to insufficient model order. Model order is a property that should be determined in the initial tests of an empirically based modelling process [20]. In the context of surface vessels model order is a common topic when making

heading autopilots. A well known model used in heading control applications is the Nomoto model [15][9]. Details about the Nomoto model are not relevant here but some of the considerations done when making one are. Perhaps the most common variants of the model are first order Nomoto, and second order Nomoto. When choosing between them, the question boils down to whether the model has to be able to describe overshoots or not. The overshoot in yaw rate comes from a coupling effect between sway and yaw [19]. This effect is not captured by the first order Nomoto as it is canceled out when reducing the second order version to first order. The same is true for the LTI system (2.20) as it is practically equal to a first order Nomoto model when used to identify m_r.

The coupling effect between sway and yaw becomes relevant when the vessel operates in regions of the state space where ROT is high. While the first order model is often satisfactory for larger vessels incapable of such maneuvers and vessels with limited operating space, the vessel target group of the modelling method presented in [7] are smaller and faster, like the Telemetron. That means that measurements from a significant part of the state space will be contaminated with this error as seen in Figure 2.17. Figure 2.16 provided an example of how a first order system has to deal with overshoots when fitted based on a square error. The figure also shows how a second order system might represent the step response. In this case a second order Nomoto model is used and its parameters identified manually. The complexity of the second order approximation allows it to capture the overshoot and thus more accurately describe the transient.

In Figure 2.15 one can see how the input step translates to actuator output after the propagation delay has passed. The model (2.5) also attempts to intentionally capture these actuator dynamics. As seen in Figure 2.16 the actuator dynamics are captured similarly to how propagation delay is. By creating a gap beneath the response of equation (2.20) it forces the inertia measurement to attain a higher value. Looking at the response from the second order Nomoto model one can see that the actuator dynamics are better represented. However, the actuator dynamics and the overshoot are captured by the same parameter, so in the steps where there is no overshoot the actuator dynamics wont be described properly. To do that one would have to use the measured actuator output or include nonlinearities in the system equation used to generate measurements, the equivalent of equation (2.20).

This discussion of measurement accuracy has been focused on measurement of ROT dynamics. The same themes are also relevant in the case of measuring SOG dynamics although the importance of each element might vary. Overshoots, for example, are not a big concern which means that using a first order system is more viable than in the ROT case.

2.3.3 Parameter identification

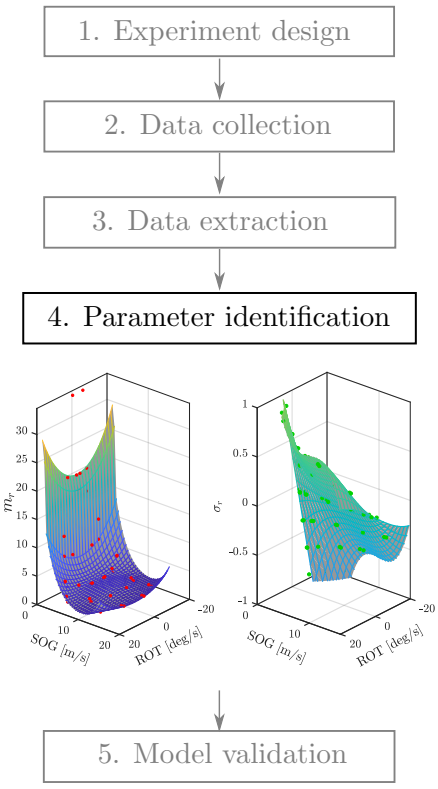

Figure 2.18: Step 4 produces a model for each extracted data set.

The data extraction step covered in section 2.3.2 produced the four data sets of equations (2.19a), (2.19b), (2.21a), and (2.21a). This section will be looking at how models of σ_U, σ_r, m_U, and m_r are obtained with the method described in [7]. A preview of the results obtained with this step is shown in Figure 2.18.

The previous section, section 2.2, describes the basics of linear regression which should be familiar before engaging the method described here. To apply linear regression in the identification of damping and inertia models, $\hat{\sigma}(\boldsymbol{x})$ and $\hat{m}(\boldsymbol{x})$, the models must be formulated as a linear combination of the parameter vector $\boldsymbol{\beta}$ and basis functions $\boldsymbol{\phi}(\boldsymbol{x})$,

$$\hat{\sigma}(\boldsymbol{x}) = \boldsymbol{\phi}_\sigma(\boldsymbol{x})^\top \boldsymbol{\beta}_{\boldsymbol{\sigma}}, \tag{2.22a}$$

$$\hat{m}(\boldsymbol{x}) = \boldsymbol{\phi}_M(\boldsymbol{x})^\top \boldsymbol{\beta}_{\boldsymbol{m}}. \tag{2.22b}$$

The main objective of the regression is to identify the $\boldsymbol{\beta}$'s that minimize the mean squared error between these models and the measurements in the corresponding data sets, $\mathscr{D}_\sigma$ and $\mathscr{D}_m$. This is achieved by minimizing the objective function of a weighted lasso, on the form

$$\varepsilon = \frac{1}{N}\sum_{i=1}^{N} w_i(y_i - \boldsymbol{\phi}(\boldsymbol{x}_i)^\top \boldsymbol{\beta})^2 + \lambda|\boldsymbol{\beta}|, \tag{2.23}$$

where N is the size of the data set being analyzed, w_i is the weight of the i'th measurement, y_i is the i'th measurement from the data set, and λ is the regularization parameter. The authors of [7] do not describe a particular weighting scheme. Weights seem to be determined through inspection as there are not many measurements that are specifically weighted. It is likely that it has been used to penalize measurements that are of an obvious low quality.

Basis functions

For the damping basis functions $\boldsymbol{\phi}_\sigma(\boldsymbol{x})$ the authors of [7] suggest using fourth order polynomials based on the structure of the data sets and the use

of polynomial damping terms in [9]. This give them the form

$$\begin{aligned}\boldsymbol{\phi}_\sigma(\boldsymbol{x}) = [&1, U, r, U^2, Ur, r^2, U^3, U^2r, Ur^2, r^3, U^4, \\ &U^3r, U^2r^2, Ur^3, r^4]^\top.\end{aligned} \tag{2.24}$$

As seen in the left plot of Figure 2.18 the structure of the inertia measurements exhibit asymptotic behavior at low SOG values. This dynamic can not be properly captured by polynomial models of reasonable order. To overcome this the authors of [7] suggests adding an asymptotic term to the polynomial basis of equation 2.24. The basis functions used in identification of inertia models becomes

$$\begin{aligned}\boldsymbol{\phi}_m(\boldsymbol{x}) = [&1, U, r, U^2, Ur, r^2, U^3, U^2r, Ur^2, r^3, U^4, \\ &U^3r, U^2r^2, Ur^3, r^4, \tanh(a(U-b)]^\top.\end{aligned} \tag{2.25}$$

Using the basis functions (2.24) and (2.25) to generate ROT damping and inertia models, equations (2.22a) and (2.22b), by minimizing the mean square error in equation (2.23) in terms of $\boldsymbol{\beta}$ results in the ROT inertia and damping models shown in Figure 2.18.

It should be noted that the basis functions suggested by the authors of [7] are not necessarily sufficient in the general case. As the model also aims to describe actuator dynamics, phenomenon like deadband could add more complex behavior. For example, a deadband in the upper range of throttle input could add asymptotic like behavior to $\boldsymbol{\sigma}_U(\boldsymbol{x})$.

Utilization of regularization

The general purpose of regularization is to reduce model complexity, often by constraining the size of the elements in the model's parameter vector. The different ways in which regularization schemes achieve this goal can be utilized by choosing a scheme that best serves the purpose of the specific problem at hand. For example, the authors of [7] have chosen to use L1-regularization, also known as lasso. As described in section 2.2, lasso has a tendency to drive parameters to zero making it suitable for overparameterized applications. As mentioned in section 2.3.1 it is assumed that the vessel has a symmetric rudder response. That implies that both inertia models and the SOG damping model are symmetric about the SOG axis; while the ROT damping model is asymmetric about the SOG axis. Considering the basis functions (2.24) and (2.25) contain both symmetric and asymmetric terms it makes sense to use lasso. It makes sense because when modelling symmetric behavior lasso should set the elements of $\boldsymbol{\beta}$ that correspond to asymmetric terms in $\boldsymbol{\phi}(\boldsymbol{x})$ equal to zero; and vice versa for an asymmetric model.

However, when modelling with regression it is common practice to use numerical solvers. This means that parameters will generally not be set equal to zero, unless specific initial conditions or termination criteria are being used. As a result the symmetric models are expected to have some asymmetric behavior due small, but nonzero, asymmetric terms. Even though the resulting error will not necessarily be impactful, it is unnecessary. Not only because it unnecessarily introduces an error but also because the characteristics of lasso are not properly utilized but still chosen over other regularization techniques with potentially beneficial characteristics. In section 3.3 we will be looking at model reduction and another regularization alternative.

Utilization of weights

Weighting is a tool that can be used to combat a multitude of error sources. However, obtaining the insight to properly do so is nontrivial in the general case. Combining the ability to visually inspect the measurements of the data, with knowledge about the expected behavior of the dynamics allows one to pick out obvious outliers in the data set and reduce their weight. As mentioned in section 2.2, it is not easy to assign weights based on statistical properties of the data becasue the data set is rather sparse. Assigning weights based on mathematical descriptions of the physical disturbances influencing the measurements is not easy either. It requires a good understanding of the physical process which is something the method presented in [7] is trying to avoid as high-speed vessels can be quite complicated systems.

Even though the system is very complicated, there is one aspect of the modelling procedure that is well understood. That is the extraction of measurements, not as in sensor data, but the procedure described in the previous section, section 2.3.2. And it just so happens that the manner in which the measurements are obtained is very impactful for how errors translate into the data set. In the discussion at the end of the previous section, four significant errors in the inertia measuring where brought up. These errors mainly affected the expected value of the measurement, as opposed to the variance, and thus can not be directly countered by weighting. As mentioned during discussion of the impact of overshoots on measurements, it seems like the error remains equal, or even gets smaller, when moving further into the state space where SOG is high. This can be seen in Figure 2.17. From what was said about the occurrence of overshoots this seems a bit peculiar. Overshoots are something that occur with increasing magnitude when operation take place in regions of the state space with high ROT values. Clearly, errors are not linearly transformed into the inertia data set.

This nonlinear transformation also makes sense when looking at the error visualized in Figure 2.14. The figure showed how a high signal-to-noise ratio

meant that the measured steady state value was unfit for use in the inertia measuring process. The phenomenon lead to an outlier in the data set with an error of about $\varepsilon_{m_r} = 20$. Although the outlier seems to have a quite dramatic value, the simulated transient does better at describing the real transient than one might expect. A similar case is shown in Figure 2.19a. If an error of this size appeared in a region of the state space where inertia values are lower the effect would be much more dramatic as seen in Figure 2.19b. This means that even though an error of $\varepsilon_{m_r} = 1$ could be acceptable in some parts of the state space, it could be unacceptable in other parts.

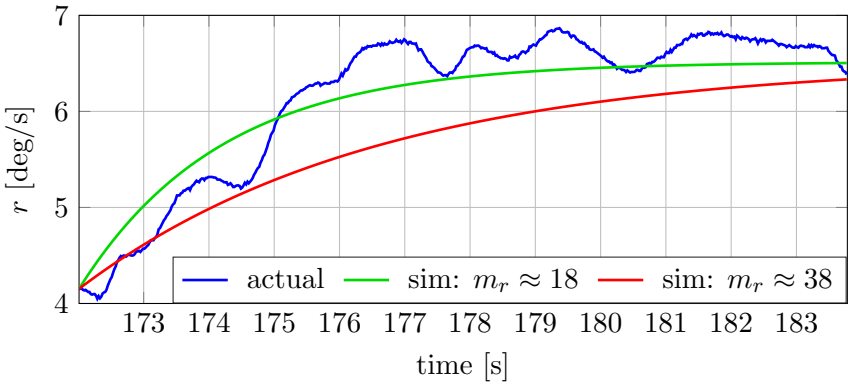

(a) Step in throttle during identification of SOG parameters.

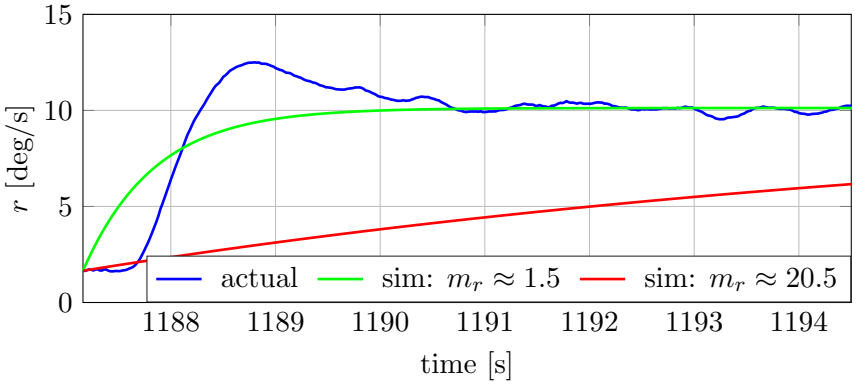

(b) Step in rudder during identification of ROT parameters.

Figure 2.19: Encounters with low signal-to-noise ratio during identification experiments done in [7].

Unfortunately, the linear regression does not consider this. It merely evaluates the squared distance from the model to each measurement. Thus if it evaluates a model during the regression process that describes the low inertia region fairly well, but there is a relatively large error in the high inertia region, the parameter vector will be adjusted to reduce the total error which

might mean that significant errors will occur in the low inertia region. This is an effect that influences the variance of measurements across the whole state space and should be dealt with. The use of weights to counter the effect is investigated in section 3.3, but it is also important to be aware of this during the measurement extraction step.

2.3.4 Model validation

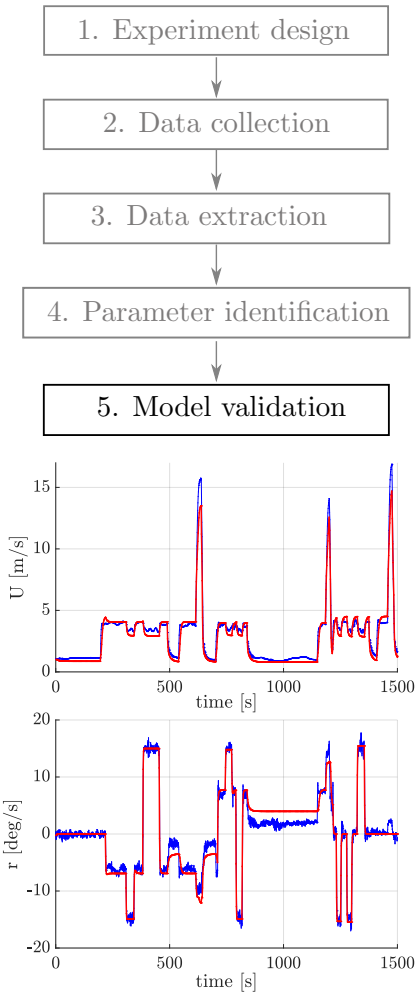

Figure 2.20: The model is validated in step 5.

The last step of the model identification procedure suggested in [7] is to validate the identified vessel model. Figure 2.20 shows an overview of the validation results presented in the article. The validation experiment shown in the figure does a decent job of exploring the modes of the ROT dynamics. It is however somewhat lacking in its investigation of SOG dynamics. Additionally, the experiment only consists of step responses so including various oscillatory inputs as well would be a good start. When validating it is generally a good idea to use rich signals that are a good representation of what will be encountered in actual applications.

A closer look at the results is not important at this point. Although validation is an essential part of any modelling procedure it has not been given enough attention during the work with this thesis to receive discussion beyond this section. This means that even though results from, and execution of, each step of the modelling procedure presented in Chapter 3 are compared to the method in [7], a comparison of the methods' overall performance will not be done. The results should therefore be analyzed with some skepticism.

Chapter 3

A method for automatic model identification

In this chapter an automatic method for model identification based on the method suggested in [7] is described. An attempt at automating the procedure was made the autumn of 2017 and is described in [11]. The project work described in [11] successfully developed an automated procedure in a simulation environment where the model identified in [7] was simulated. The last piece of work done in [11] was applying the method on actual vessel data gathered by the authors of [7]. Although the application of the automated method on actual data was not entirely successful, each step of the method showed potential. A fully functional automated modelling procedure is what is presented in this chapter.

The method presented in this chapter is mainly an automated extension of the method presented in [7]. In Chapter 2 some weaknesses and potential improvements of the method were discussed. Most of these will not be adressed and/or implemented in this chapter as the focus will be on the challenges of automating the method. Instead, a description of strategies for general improvement can be found in section 3.4. Some of the challenges that arise when attempting to automate the procedure are as follows:

1. First of all the experiment performed in the data collection step must be carried out automatically. With no human operator in the loop a method for SSID is needed to identify the transition between transient and steady state such that inertia and damping measurements can be obtained, and to progress the experimental procedure by initiating new input steps.

2. Although the procedure for obtaining damping measurements is fully automatic, the current brute force solution for measuring inertia translates poorly to an automatic solution capable of handling the general

case as both search boundaries and resolution must be set, and the resulting set sizes could be come quite large. It also extends poorly to the multivariate case which will likely be relevant when looking to improve the model.

3. At its core linear regression is an automatic process. The challenges of automation faced in the parameter identification step are identification of an automatic weighting scheme.

From the challenges listed above it is clear that the focus of this chapter will be on step 2 "Data collection," step 3 "Data extraction," and step 4 "Parameter identification." Step 1 "Experiment design" will be left as it is in [7]. In fact this chapter will use the same experiment data used in the model identification performed in [7], and thus the same experiment. There are some consequences of doing this as the SSID technique suggested in this chapter obviously will not match the exact choices made by the human operator who performed the experiments in [7]. These consequences will be made clear as they become relevant, and their impact on the result will be discussed as well.

3.1 Data collection

This section will look at how the experiment can be executed automatically. The experimental procedure remains the same as the one described in section 2.3.1 with the parameters used in [7] which are listed in Table 3.1. Algorithm 1 shows an algorithmic representation of the experimental procedure for a throttle experiment. The main challenge of the algorithm is the SSID in line 11, and the rest of this section is dedicated to answering the challenge it poses. Figure 3.1 and Figure 3.2 show the data collected in the throttle experiment and rudder experiment.

Table 3.1: Parameters of experimental procedure used in [7].

Input	τ_{min}	τ_{max}	τ_{Δ}
τ_m	0	0.6	0.1
τ_δ	0	1	0.333

3.1.1 The steady state identification problem

The purpose of SSID in this method is to determine a point in time t_{ss} when the vessel has reached steady state so that measurements of inertia and damping can be extracted from their respective regions. That is, inertia measurements can be extracted from the data sampled before t_{ss}, and

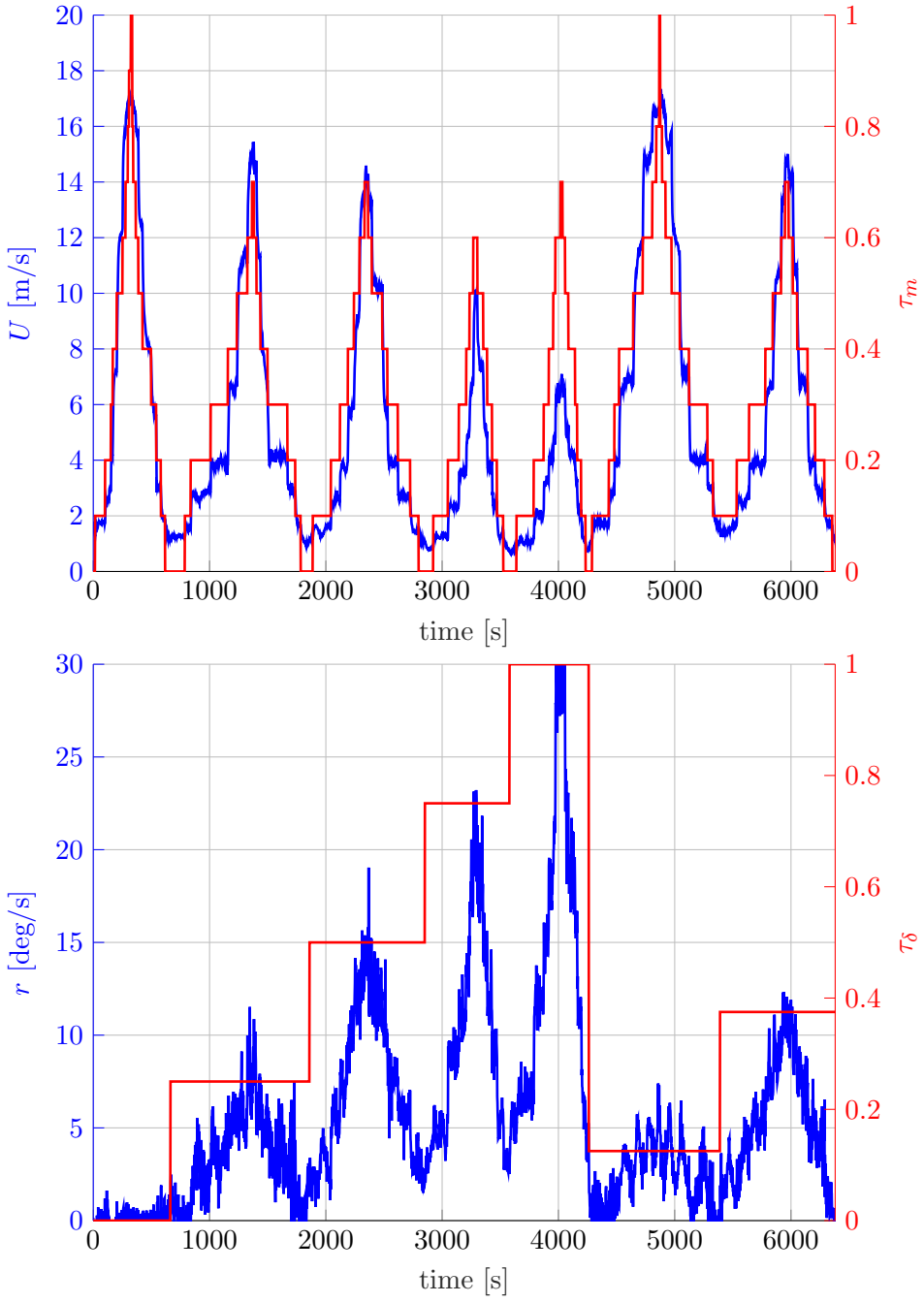

Figure 3.1: Throttle experiment performed by the authors of [7]. The parameters used can be found in Table 3.1.

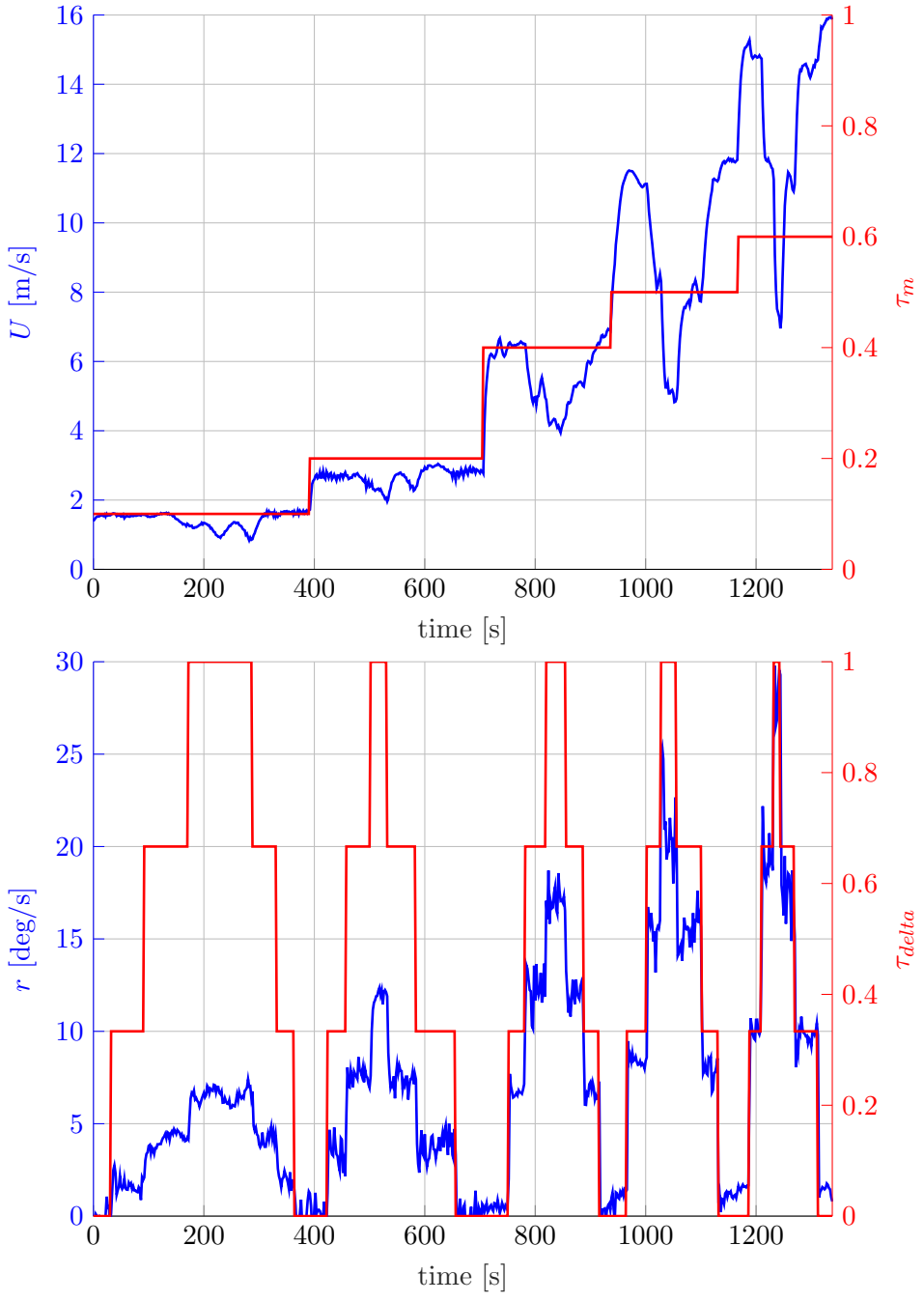

Figure 3.2: Rudder experiment performed by the authors of [7]. The parameters used can be found in Table 3.1.

Algorithm 1 Experimental procedure (throttle case)

```
1: procedure EXPERIMENT(τ_min, τ_max, τ_Δ)
2:     for τ_δ = τ_δ,min to τ_δ,max step τ_δ,Δ do
3:         EXECUTESTEPSEQUENCE(τ_δ, τ_m,min, τ_m,max, τ_m,Δ)
4:         EXECUTESTEPSEQUENCE(τ_δ, τ_m,max, τ_m,min, −τ_m,Δ)
5:     end for
6: end procedure
7:
8: procedure EXECUTESTEPSEQUENCE(τ_δ, τ_m,min, τ_m,max, τ_m,Δ)
9:     for τ_m = τ_m,min to τ_m,max step τ_m,Δ do
10:        Apply step input to actuators.
11:        Let U and r reach steady state.
12:        Let the vessel do at least on full turn after reaching steady state.
13:    end for
14: end procedure
```

measurements of damping can be extracted from the data following t_{ss}. It is not crucial that t_{ss} is a high quality estimate of the time of actual transition between transient and steady state t^*_{ss}. Rather, it should be a point in time after the transition is completed. Whether it is $t^*_{ss} + 1$ second or $t^*_{ss} + 10$ seconds is not important, as will be demonstrated now.

First, given that the results of the SSID can be described as

$$t_{ss} = t^*_{ss} + \Delta t, \tag{3.1}$$

where Δt is an arbitrary length of time; how would the size of Δt influence the damping measurements? From section 2.3.2 the damping measurement was read directly from the input value, $\sigma_r = \tau_\delta$ in the ROT case. Its location in state space $\boldsymbol{x}_{\sigma_r}$ was found by letting the vessel complete a turn after steady state had been identified and then average the state value during the turn. Clearly, as long as $\Delta t \geq 0$ the damping measurements are not influenced by the value of Δt. If $\Delta t < 0$ the measurement of $\boldsymbol{x}_{\sigma_r}$ would suffer as data points from the non zero mean transient would impact the average.

Second, how will the size of Δt influence the inertia measurements? The answer to that can be seen in Figure 3.3. In the description of the inertia measurement process described in 2.3.2 it is mentioned that the simulated step response of a first order LTI system is curve fitted to the vessel's step response to measure inertia. The results from six such simulations, performed with different values of t_{ss}, is shown in the figure. As seen in the figure the first order responses hold a constant value once the transient is over. This constant value is determined by the already obtained damping measurement which means that the only degree of freedom left in the simulated system is

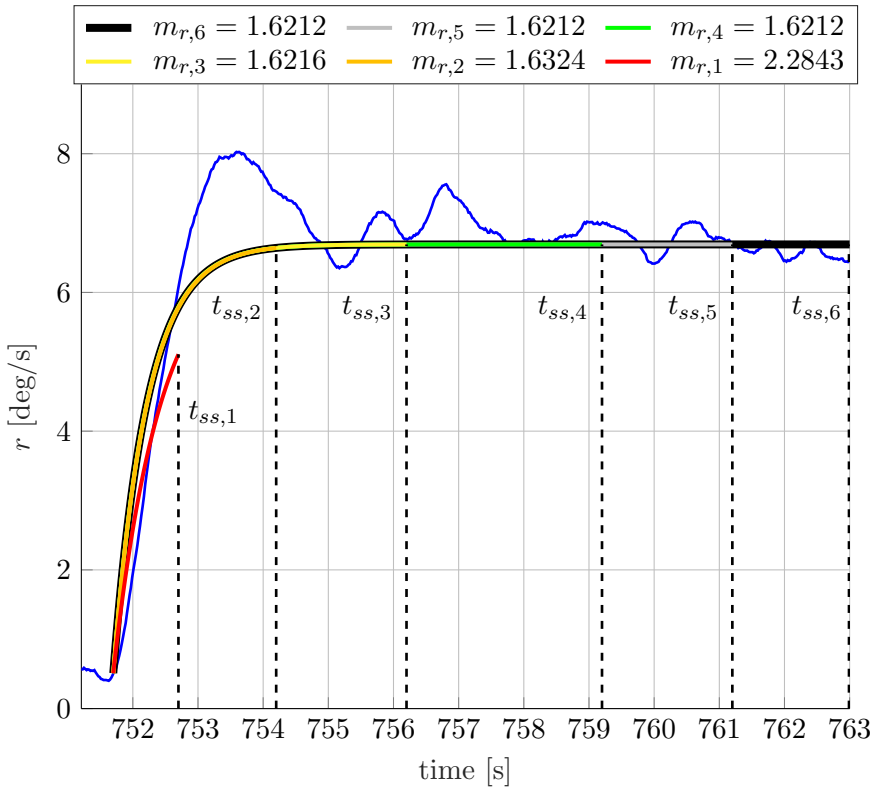

Figure 3.3: The effects of premature steady state identification versus overdue identification on the inertia measurement.

the inertia parameter. Because the inertia parameter is unable to influence the simulated system's steady state behavior it does not matter what size Δt has. Even if there was a relatively large disturbance affecting the signal at some point after t^*_{ss} the system has no practical way to describe it.

Looking at Figure 3.3 one can see that after a certain point the value of t_{ss} has negligible effect on the inertia measurements. Judging by the values of m_r shown in the legend of the figure, this point is somewhere close to $t_{ss,3}$. Any value $t_{ss} < t_{ss,3}$ would have to be considered a premature SSID as the value of the measurement start to change. Premature SSID would also affect the inertia measurement indirectly as $\boldsymbol{x}_{m_r}$ is dependent on $\boldsymbol{x}_{\sigma_r}$. Although delayed identification is favourable, there are some situations where accurate identification of the transition between transient and steady state is important. Figure 2.14 showed an example of such a situation. When the signal-to-noise ratio is low scenarios can occur where it becomes hard to distinguish the effects of current from the step response transient. These situations are already troublesome and increased accuracy of the SSID will not have a significant effect (positive) unless other aspects of the method

are improved as well.

In conclusion, the focus of the SSID method should be on certainty rather than accuracy. In general, this reduces the difficulty of the problem as the method will be allowed to take a passive approach, waiting out disturbances that result in ambiguous behavior.

3.1.2 A method for steady state identification

The method that is going to be used for SSID in this thesis is one suggested in [5] and more recently discussed and described in [16]. A very approachable introduction to SSID and a relatively expansive overview of its use in various fields is given in [5], and it is therefore a highly recommended starting point for further investigation of the subject.

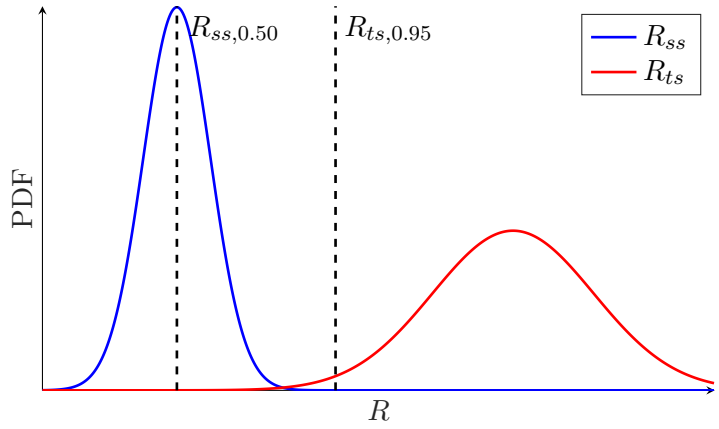

Figure 3.4: Hypothetical probability density function of R during steady state and transient state.

A common approach to SSID is statistical hypothesis testing where a null hypothesis, H_0, is formulated and a suitable test statistic, R, is defined. For SSID the H_0 should be formulated as a condition that when satisfied by R implies that "the system is probably in steady state." Similarly an alternate hypothesis/condition, H_1, must be formulated such that when satisfied rejects H_0, implying that "the system is probably in transient state." Figure 3.4 shows the probability density function (PDF) of R in two hypothetical scenarios and will be used to define H_0 and H_1. More specifically it shows the PDF of R when the system operates in steady state, labeled R_{ss}; and the PDF of R when the system is in transient state, R_{ts}. Looking at the figure one could argue that a reasonable formulation of H_0 and H_1 could be

$$H_0 \ : \ R \leq R_{lb}, \text{ and} \tag{3.2a}$$
$$H_1 \ : \ R \geq R_{ub}, \tag{3.2b}$$

where R_{lb} is a lower bound, and R_{ub} is an upper bound. Furthermore R_{lb} and R_{ub} should be well separated to minimize the likelihood of R fluctuating between the two conditions. For example, assume a vessel is in steady state when a step in input is initiated. The vessel transitions into to transient state and H_0 is rejected (H_1 is accepted). Shortly thereafter a disturbance affects the vessel state causing R to drop for a moment. If R_{lb} and R_{ub} are too close R might drop below R_{lb} causing H_0 to be accepted and a false, premature identification of steady state occurs.

As stated in the previous section being certain that steady state is correctly identified is a priority. This means that R_{lb} should have a value that is characteristic of steady state behavior. For the scenario presented in Figure 3.4, one could consider setting $R_{lb} = R_{ss,0.50}$ or even lower. Setting the boundary even lower means that the certainty of steady state is higher, but if R_{lb} is set too low steady state might not be identified for a considerable amount of time after it occurs as values of R satisfying H_0 in this case only occurs as fluctuations due to disturbances.

Although the PDF of R_{ts} is depicted as belonging to a normal distribution in Figure 3.4 the case is quite different when working with surface vessel step responses. There will not be any characteristic values of R during the transient, nor a well defined range of values, that provide a good choice for R_{ub}. Another way in which the application covered in this thesis differ from the general application is that identification of transient state is purely need to avoid premature identification of steady state. This is because the system already knows when the transient/step response starts; it starts when the step input is applied. That is not entirely true as dead time delays the transient but there are better option for correcting for dead time, some are discussed in 3.4. How does this affect the choice of R_{ub}? It means that R_{ub} should be set to a value that is comfortably reached by R during all step responses, while maximizing the distance to R_{lb}. The issue should become clearer later on once the behavior of R is introduced.

Defining the R statistic

The R statistic should be a defined as a value that has a distinctly different behavior in steady state when compared to its behavior in transient state. The authors of [5] suggest an R statistic based on the ratio between two measurements of variance. The two variance measurements are based on the distances d_1 and d_2 visualized in Figure 3.5. The figure shows a plot of

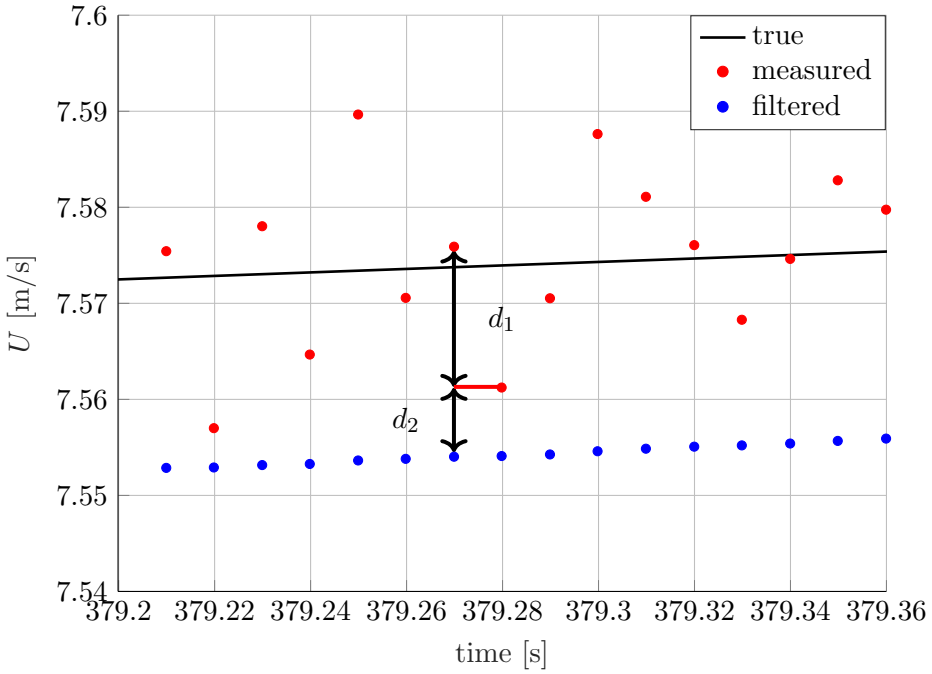

Figure 3.5: Figure showing the deviations used to measure variance. The deviation d_1 being the distance between current measurement of the state variable U_i and the filtered measurement of U at the previous time step, $U_{f,i-1}$. And d_2 being the deviation between U_i, and the measurement of U at the previous time step, U_{i-1}. The data seen in the figure is from a simulated transient response.

the vessel state U during a transient. The black line in the figure represents the true value of U, U_{true}; the red marks are the sensor measurements, U; and the blue marks are generated by filtering the measurements, and are given the notation U_f. To describe the general case the notation x_{true}, x, and x_f will be used. As seen in the figure the distances can be defined as

$$d_1 = x_i - x_{i-1}, \text{ and} \tag{3.3}$$
$$d_2 = x_i - x_{f,i-1}, \tag{3.4}$$

where x_i denotes the i'th measurement of x. The idea is that when the system reaches steady state the filtered value x_f will be centered in the measurements x, approximating the true value x_{true}. If measurements from an interval of steady state are examined one should be able to see that the variance estimated by d_2, $\sigma^2_{d_2}$, is approximately equal to the variance estimated by d_1, $\sigma^2_{d_2}$. When the system enters transient state x_f will start to lag behind x_{true}, creating a gap between the two signals such as the one seen in Figure 3.5. When this gap grows in size so does d_2 which means

that the ratio between the two variance estimates, $r_{\sigma^2} = \frac{\sigma^2_{d_2}}{\sigma^2_{d_1}}$, quickly grows. This means that the ratio between d_2 and d_1 can serve as a good foundation for making a distinction between transient and steady state as the two cases can be described by

$$r_{\sigma^2} \approx 1 \text{ in steady state, and}$$
$$r_{\sigma^2} \gg 1 \text{ in transient state.}$$

Based on the discussion above an R statistic can be formulated. First of, the authors of [5] defines the filtered state value x_f as x run through an exponential filter,

$$x_{f,i} = \lambda_1 x_i + (1 - \lambda_1) x_{f,i-1}, \tag{3.5}$$

where $\lambda_1 > 0$ is a constant filter coefficient. Second, the two variance estimates d_2 and d_1 are measured by the two exponentially filtered values

$$\nu^2_{f,i} = \lambda_2 (x_i - x_{f,i-1})^2 + (1 - \lambda_2)\nu^2_{f,i-1}, \text{ and} \tag{3.6}$$
$$\delta^2_{f,i} = \lambda_3 (x_i - x_{i-1})^2 \quad + (1 - \lambda_3)\delta^2_{f,i-1}, \tag{3.7}$$

where $\lambda_2 > 0$ and $\lambda_3 > 0$ are constant filter coefficients, similar to λ_1. Finally, the R statistic is defined as

$$R = \frac{(2 - \lambda_1)\nu^2_{f,i}}{\delta^2_{f,i}}. \tag{3.8}$$

The derivation of the equation for the R-statistic (3.8) is described in [5].

3.1.3 Application of method to surface vessel step responses

Figure 3.6 shows the results of applying the method to the rudder experiment. As seen in the figure, R has a distinct, spiking behavior during the transients, and in steady state R falls down to a lower value which seems to be in roughly the same range for all the steady state regions. This behavior goes well with the hypotheses of equations (3.2a) and (3.2b) that were formulated to determine if the system is in steady or transient state. Before the results are analyzed further a closer look will be taken at how the R statistic functions.

As described by equation (3.8), R is determined by the two variance measurements ν^2_f and δ^2_f. The behavior of these two values is shown in Figure 3.7a and 3.7b. Starting with Figure 3.7a one can see that ν^2_f is responsible for the spiking behavior in R. This makes sense as equation 3.6 defines ν^2_f as the difference between the measured and the filtered signal. When a transient occurs the filtered signal lags behind the measurements causing ν^2_f

to generate the spikes seen in the figure. However, these spikes alone are not well suited for SSID. As seen in the figure, the height of the spikes is correlated to the vessel's SOG as rudder steps at high SOG are larger and steeper; remember that each pair of ascending and descending transients is performed with a constant throttle input and thus at roughly the same SOG.

To balance the height of each spike one can make use of the fact that the variance measured by δ_f^2 is measured as the difference in state value between each sample. During a transient this difference is primarily a measure of the vessel state's acceleration caused by input change. Therefore, δ_f^2 is also going to spike during transients, and can be used to scale the spike in R. Note these spikes are not the large spikes seen in Figure 3.7.

Although hard to see in Figure 3.7a, the steady state value of ν_f^2 is also correlated with SOG. This is because disturbances become more violent when the vessel operates at high speed. Again, this affects δ_f^2 in a similar fashion, and so δ_f^2 can also be used to scale the steady state value of R. Figure 3.11 shows a δ_f^2 during an interval from a throttle step experiment where the effect can be seen much clearer; observe how δ_f^2 increases as SOG increases. To summarize, the behavior of R is caused by ν_f^2 spiking due to lag between measured and filtered state, and made independent of noise level, and transient characteristics, through δ_f^2.

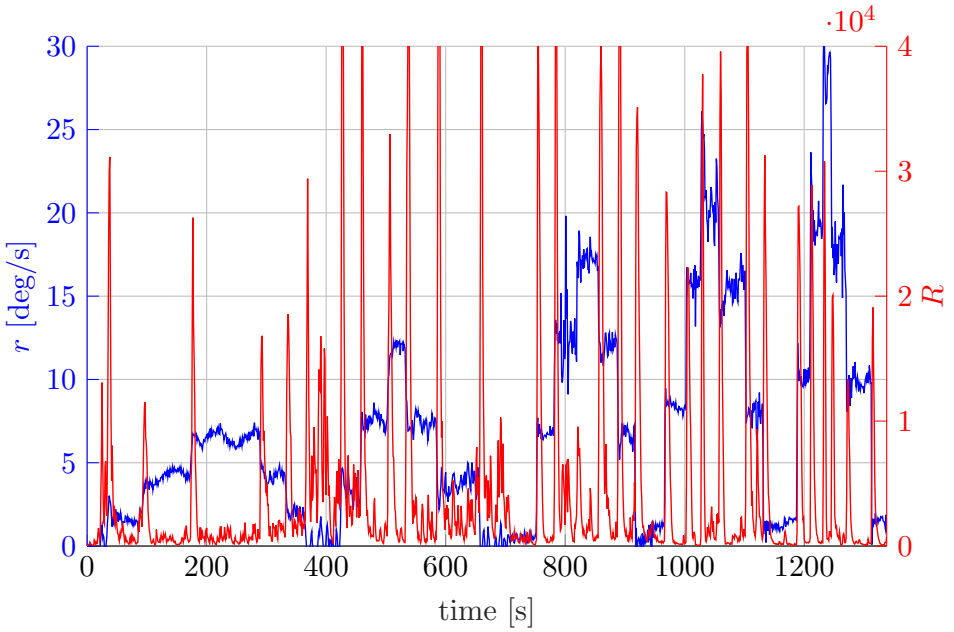

Figure 3.6: Application of the method described in [5] for steady state identification in a rudder experiment performed by the authors of [7]. The parameters used can be found in Table 3.2.

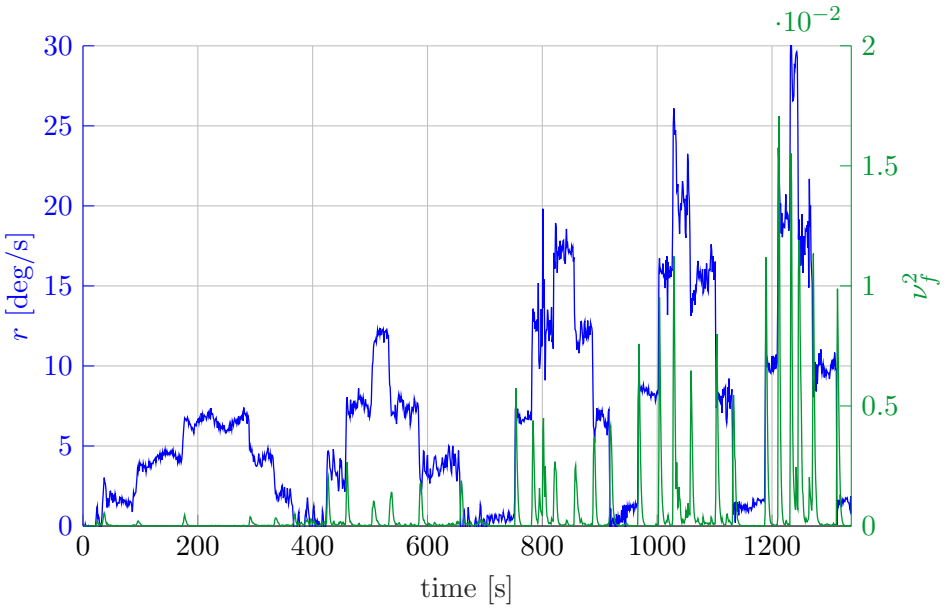

(a) Variance measurement ν_f^2.

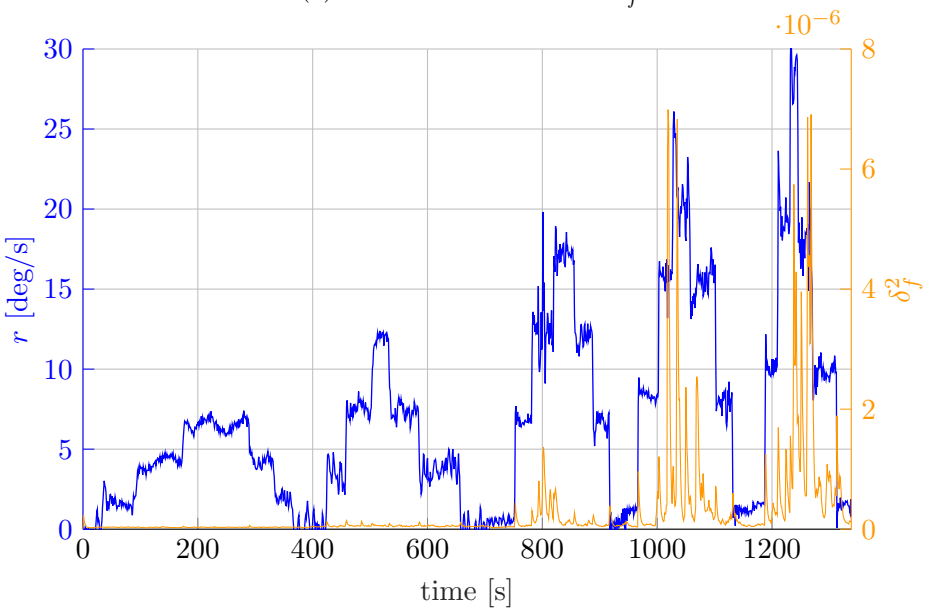

(b) Variance measurement δ_f^2.

Figure 3.7: Plots of the two variance measurements defining R through equation (3.8). The parameters used can be found in Table 3.2.

Figure 3.8a and Figure 3.8b shows a portion of the results from application of the SSID method to the rudder and throttle experiments. As seen in the figures the SSID seems to be pretty accurate; although, as mentioned in section 3.1.1 it is preferable with a reasonably delayed identification. In general, this could be achieved by increasing the λ_1, the filtering coefficient of the state. But, because the method is applied to previously recorded data, as opposed to on-line with live data, its parameters have to be overfitted to deal with certain scenarios that other wise could have been either waited out or called for a redo of the step (if framework for redos were in place). A couple of restricting scenarios will be discussed later but first a case that could not be solved with realistic application of SSID method.

Of the two experiments examined, the motor experiment was the hardest to obtain proper results from. This is partially because SSID performed by a human operator can vary in consistency. In experiments like the throttle experiment, which contained 146 step responses and lasted nearly 2 hours, it is hard for a person to stay focused. This is a typical reason and important motivator for pushing for automated solutions. In this case, the most relevant consequence was the fact that completing a circle in steady state, line 12 of Algorithm 1, was sometimes skipped, and the cases where there was significant premature identification. These consequences have in common that they reduce the duration of steady state and thus it becomes difficult to apply a method that should play on certainty. An example of where the SSID method was unable to settle in time is shown in Figure 3.9. As seen in the figure the value of the R statistic has yet to settle when a new step is applied at roughly $t = 4160$ seconds. It is clear that if the vessel had been given a few more seconds in steady state the identification would have been successful as the value of R is very close to R_{lb} and thus accepting H_0. One could argue that R_{lb} could be raised to allow it to happen, but this was not done as the parameters of the method are already fairly overfitted at this point and error is in the data and not the method in this context.

There are a couple more of these cases in the motor experiment meaning some datapoints are left out. Because of this, the models of σ_U and m_U obtained in the later stages of the modelling procedure are not considered valid and fit for comparison to the manual case. The data will still be used in the analysis, but should be analyzed with this in mind. Another important factor that impacts both the SOG and ROT models obtained later is the methods inability to properly describe the inconsistency of human operators. This means that the steady state interval will differ from the ones found in [7] and thus the effects of disturbances, especially current, will be different. This does not directly affect damping measurements, but measurements of inertia and particularly the vessel state measurements used to locate damping and inertia measurements in the state space. This should also be kept in mind

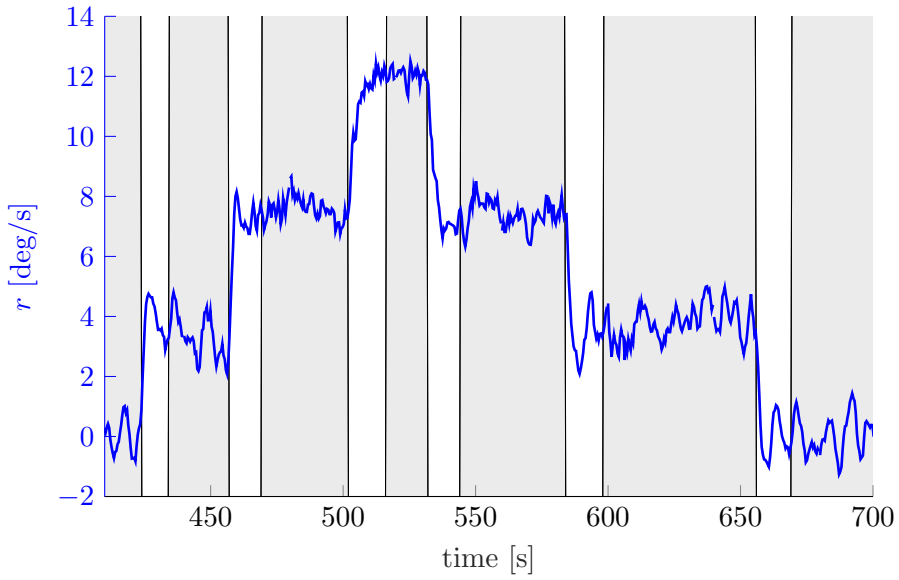

(a) Results from rudder experiment.

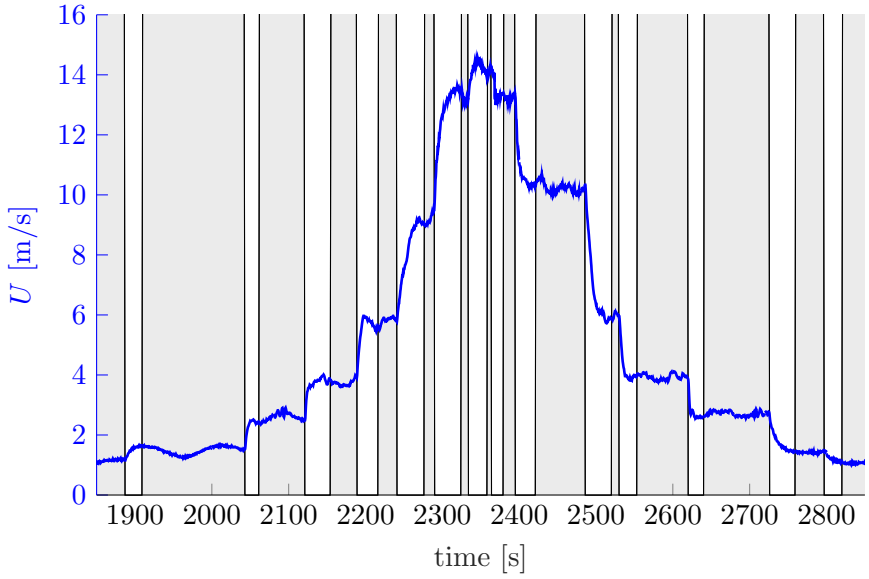

(b) Results from throttle experiment.

Figure 3.8: Parts of the results from applications of the SSID method. 3.1. Grey areas represent steady state regions and white regions are transients. The parameters used can be found in Table 3.2.

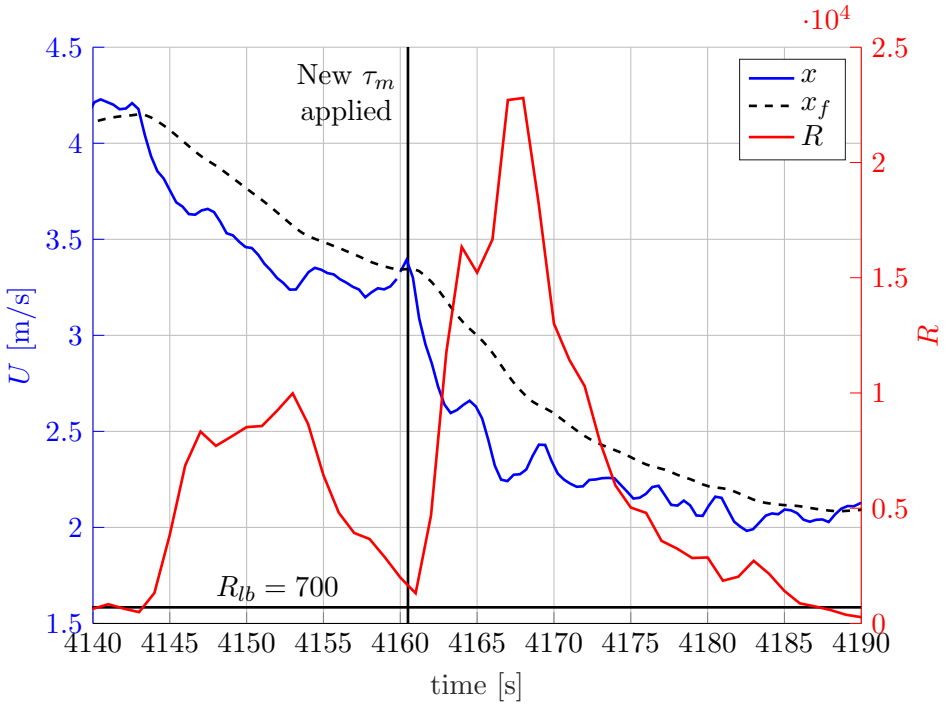

Figure 3.9: The method is unable to identify steady state before the next step is applied. The parameters used can be found in Table 3.2.

when evaluating future results.

Filter coefficient values λ_1, λ_2, and λ_3, and bounds R_{lb} and R_{lu}

Although the SSID method can be considered automatic in operation, it is not without parameters. As of now, the parameter values can not be found automatically. That means the model identification method presented in this chapter can not be considered fully automatic. However, finding suitable values for the parameters of the SSID method is an intuitive procedure which will be described here. Results from applying following the procedure using data from [7] are shown in Table 3.2.

Table 3.2: Filter coefficients and R boundaries used throughout this chapter, where h is the time step.

Experiment	λ_1	λ_2	λ_1	R_{lb}	R_{ub}
SOG	$0.2h$	$0.5h$	$0.075h$	700	2000
ROT	$0.3h$	$0.75h$	$0.5h$	2000	6000

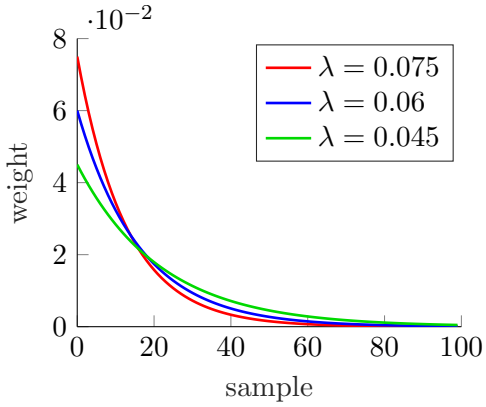

Figure 3.10: Exponential smoothing.

The filter coefficient values λ_1, λ_2, and λ_3 should be determined first. To calculate R the method uses the two variance measurements ν_f^2 and δ_f^2, as well as a filtered state x_f. These three measurements are all obtained through exponential filtering as seen equations (3.6), (3.7) and (3.5). The value of the filter coefficient determines how the weight of a sample decays as new samples arrive, the decays is illustrated in Figure 3.10. As seen in the figure, increasing the value of λ essentially means measurements are forgotten quicker. In our application it makes more sense to consider the past n seconds than the past n samples to avoid a solution that depends on sensor sampling rate. Therefore the value of the filter coefficient will always be multiplied with the sampling step size h.

When looking for a good set of filter coefficients one can start by either studying ν_f^2 which is dependent on λ_2, and λ_1 through its dependency of x_f; or δ_f^2 which is controlled by λ_3. In this case ν_f^2 will be studied first and when doing so one should start with x_f and λ_1.

Coefficient λ_1 is the most intuitive of the three. It restricts the filtered state's ability to describe rapid change, and thus is responsible for creating the gap between measured and filtered state. The value of λ_1 should be low enough so that the gap remains for the duration of the transient. As a slightly delayed identification is preferred, see start of the section, λ_1 should be chosen such that x_f catches up to x a short period after x reaches steady state. Decreasing λ_1 too much is not advisable as x_f should still be able to follow oscillations due to the vessel rotating in current. Because the steps of the experiments are spread throughout the state space the generated transients vary in behavior but checking x_f against all of them is not desirable. Instead it should be enough to use data from the slowest step that will be performed during the experiment. This means the step starting with the lowest throttle input and the largest rudder angle.

With λ_1 in place λ_2 can be chosen to achieve satisfactory behavior of ν_f^2. Coefficient λ_2 determines how sensitive ν_f^2 is to the gap formed between x_f and x. A high λ_2 means that the height of the spike in ν_f^2 will be tall, but it also starts to describe noise and disturbances instead of the trend. The value of ν_f^2 should therefore be chosen so that ν_f^2 spikes distinctly during the transient and decays quickly after, but it should also be a relatively smooth signal. As δ_f^2 primarily scales the R statistic, ν_f^2 can be an good representation of how R will behave.

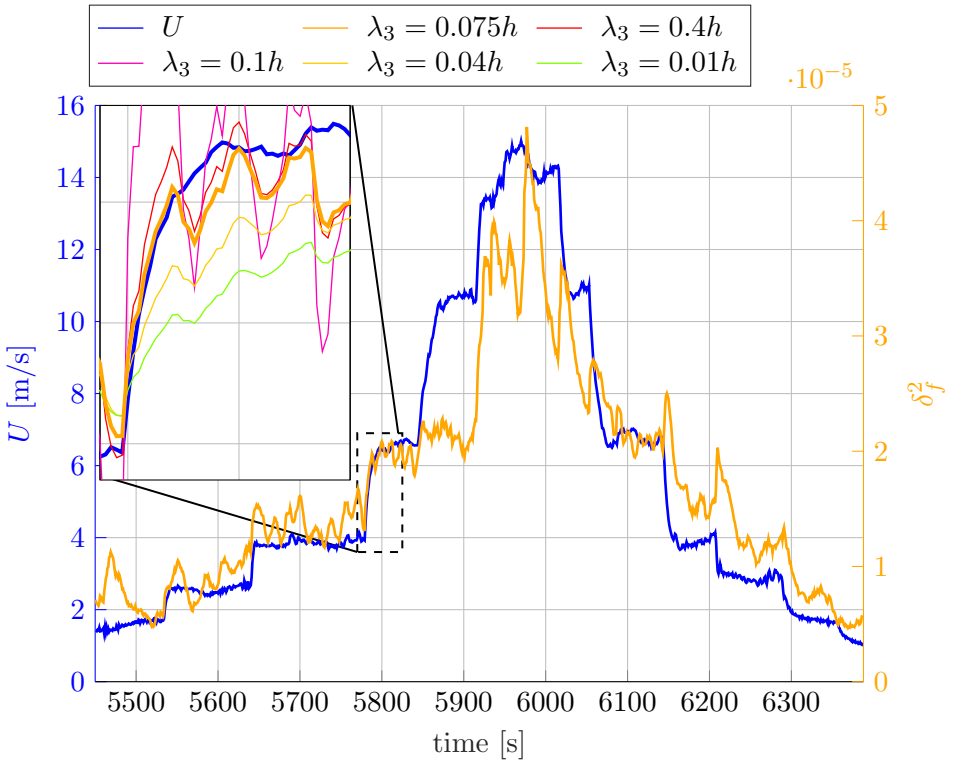

Figure 3.11: Desired behavior of δ_f^2 in a throttle step sequence.

To determine λ_3 the behavior of δ_f^2 must be examined. As mentioned earlier the intensity of noise and disturbances increases with SOG and this is what δ_f^2 is supposed to capture. Therefore λ_3 should be chosen such that the value of δ_f^2 increases with steps in throttle. The desired behavior can be seen in Figure 3.11. The figure also shows the behavior of δ_f^2 for different values of λ_3. If λ_3 is too large the value of δ_f^2 fluctuates significantly and these fluctuations will be transferred to R. If λ_3 is too low δ_f^2 will lag behind the state and R will be scaled poorly. Rudder steps should not affect δ_f^2. Except for spiking during the transient the value of δ_f^2 should be approximately the same before and after the step.

Having lots of data available is generally beneficial in an identification process, but spending a lot of time on gathering data defeats the purpose of the automated procedure that follows. From the description of filter coefficient identification described above a minimum of needed data can be determined. To choose λ_1 and λ_2 data from the slowest transient is needed. Thus two steps are required, one throttle step for $\lambda_{1,U}$ and $\lambda_{2,U}$, and one rudder step for $\lambda_{1,r}$ and $\lambda_{2,r}$. To choose $\lambda_{3,U}$ and $\lambda_{3,r}$ its recommended to perform a couple of consecutive throttle steps and a couple of consecutive rudder steps as using single steps could be challenging.

With values for the filter coefficients in place, and thus the R statistic, R can be used to determine a good set of values for the boundaries R_{lb} and R_{lb} which define H_0 and H_1. The boundaries were to be chosen such that:

1) R_{lb} and R_{ub} are well separated, and

2) during any transient R should comfortably be able to reach R_{ub}.

It was also suggested that R_{lb} should be chosen as a characteristic steady state value. However, this suggestion should be relaxed as sea conditions can be unpredictable and to some extent challenge the concept of steady state. Instead, the criteria is reformulated as:

3) R_{lb} should be high enough so that R dips comfortably below during the noisiest forms of steady state.

Based on the three criteria presented above R_{ub} should be determined using data from the slowest transient as it should have the lowest spike, thus the data used to identify λ_1 and λ_2 should be sufficient. To find a value for R_{lb} data from steps at high speed should be used.

Even though the necessity of this identification process implies that the SSID is not fully automatic, it has been reduced from a typical dull, dirty, dangerous task in the manual case to an automatic process preceded by a one time parameter identification. Furthermore, the identification process can be considered easily accessible as it is of a visual nature and very little theoretical insight is required to obtain satisfactory results. It is also possible that automation of the parameter identification is feasible, especially if framework for redos of poorly executed steps is in place.

3.2 Data extraction

This section describes the automation of the data extraction procedure suggested in [7] and discussed in section 2.3.2. As described in section 2.3.2 damping measurements can be taken directly as the input during steady

state using equation (2.18), and are therefore already obtained automatically. Therefore, this section will be centered around the method for extraction of inertia measurements. An automatic method for extracting inertia measurements was suggested during work leading up to this thesis, performed in the autumn of 2017 [11]. The automated method was successfully applied on the SSID results obtained at that time and has remained largely unchanged.

The main ideas of the original method described in section 2.3.2 are restated here to give a more complete picture of the method. Inertia measurements are obtained by fitting the step response of a first order LTI system to the recorded step response of the vessel. The first order LTI system can be formulated as follows when measuring ROT inertia;

$$m_{r_i}\dot{\Delta r}_i + k_i \Delta r_i = \Delta\tau_{\delta_i}, \tag{3.9}$$

where i means the i'th transient of the experiment is under examination, and m_{r_i} is assumed to be a constant inertia term during step i, $\Delta r_i = \hat{r} - r_i^-$, $\Delta\tau_{\delta_i} = \tau_\delta - \tau_{\delta_i}^-$ and $k_i = \frac{\sigma_{r_i}^+ - \sigma_{r_i}^-}{r_i^+ - r_i^-}$ with $(\cdot)^-$ and $(\cdot)^+$ denoting the a priori and a posteriori steady state values respectively.

The authors of [7] suggested that a set of possible inertia values could be used to evaluate the root mean square error between the simulated response of system (3.9) and the inertia value producing the lowest error is chosen as the inertia measurement. To avoid depending on a priori knowledge to identify a suitable range of values and choose a satisfactory resolution, and to generally improve performance, the application of numerical optimization algorithms was suggested during the work with [11].

The mean square error ε_i between the simulated step response of system (3.9) and the recorded vessel response from the i'th rudder step is formulated as

$$\varepsilon_{r_i} = \frac{1}{N_{r_i}} \sum_{j=1}^{N_{r_i}} (r_{i,j} - \hat{r}_{i,j}(m_{r_i}))^2, \tag{3.10}$$

where $r_{i,j}$ and $\hat{r}_{i,j}$ are the j'th data points of the recorded vessel step response and the simulated step response of system (3.9). Figure 3.12 shows a plot of ε_{r_i} evaluated for a range of inertia values. The figure reveals that the ε_{r_i} has a strictly quasiconvex form, and this is noted to be true for all other recorded steps, both from the throttle experiment and the rudder experiment. During the work described in [11] the inertia extraction was formulated as a one dimensional optimization problem where the mean square error (3.10) serves as the objective function and m_{r_i} as the optimization variable.

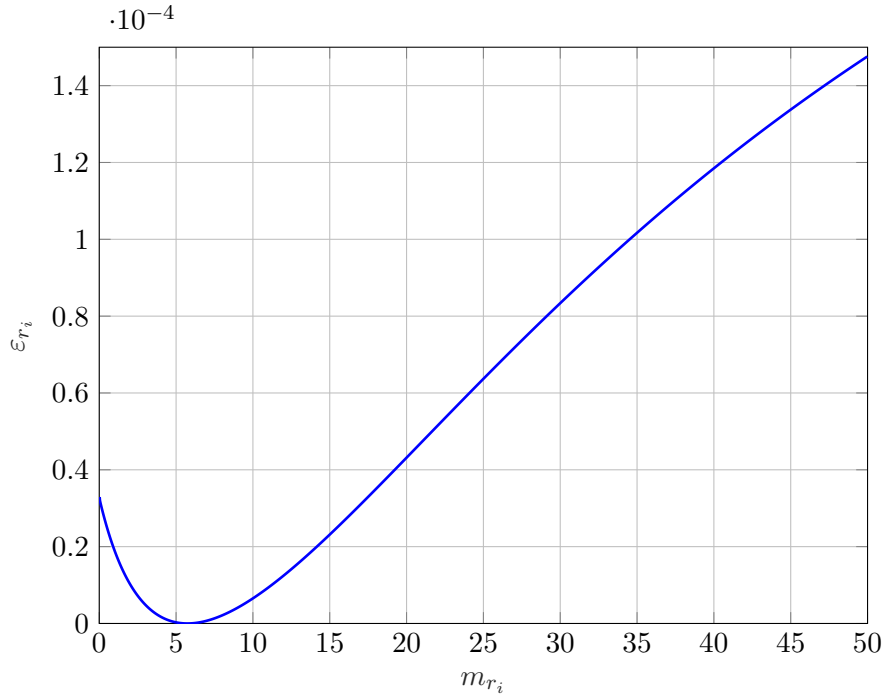

Figure 3.12: Mean square error between simulated and actual step response for a set of inertia values. Figure taken from [11].

3.2.1 Numerical optimization

This section will cover how numerical optimization tools can be utilized to obtain inertia measurements. For a good introduction on numerical optimization the book [14] is highly recommended. The discussion that follows in this section is based on that book and it provides a good starting point if further details or alternative methods are wanted.

Properties of the objective function

To start off, some properties of the optimization problem should be made clear. As noted earlier, the objective function (3.10) seems to be strictly quasiconvex. A strictly quasiconvex function is defined as follows [6].

Definition 3.1. A function $\varepsilon : S \to \mathbb{R}$ defined on a convex subset S of a real vector space is quasiconvex if and only if for every $m_1, m_2 \in S$ and $\lambda \in [0, 1]$ the inequality $\varepsilon(\lambda m_1 + (1 - \lambda)m_2) < \max\{\varepsilon(m_1), \varepsilon(m_2)\}$ holds.

This is important as it means that the objective function only has one minimum; given that the quasiconvex assumption is right. Because one of the elements in the objective function (3.10), $r_{i,j}$, is a signal from the real world,

and thus has few limits in terms of complexity, it is not unthinkable that multiple minima can appear in the objective. However, considering that the optimization variable m_{r_i} is very limited in its ability to affect the behavior of the system (3.9), essentially only increasing or decreasing the time constant of the step response, it is considered highly unlikely that multiple minima appear in the objective. The cases where this could happen would likely be the effect of a very dramatic disturbance, for example a collision, and can assumed to be dealt with before the data is used in the data extraction step, by requiring a redo of the step for example.

The gradient is an important concept in optimization. In order to obtain an analytical gradient of the objective function (3.10) the system (3.9) would have to be discretized, increasing the complexity of the optimization problem. Instead derivative free optimization will be considered. There are multiple approaches to derivative free optimization, see [14], but in this case finite differences will be used to estimate the gradient which means that methods requiring the gradient to be calculated can be used. More specifically the gradient will be estimated as a forward finite difference,

$$\nabla_{m_{r_i}} \varepsilon_{r_i} = \frac{\varepsilon_{r_i}(m_{r_i} + \Delta m_{r_i}) - \varepsilon(m_{r_i})}{\Delta m_{r_i}}, \tag{3.11}$$

where Δm_{r_i} is a small step. Finite differences are vulnerable to objective functions that can not be accurately evaluated, for example nosiy objective functions. Even though $r_{i,j}$ in the objective (3.10) comes from a very noisy signal, the objective function is smooth because the derivative of the area between a smooth line and a non-smooth line is the derivative of an area between two smooth lines plus a constant term.

BFGS, a quasi-Newton method

As mentioned earlier the book [14] describes a good selection of approaches to numerical optimization. One of the more popular methods is the Broyden, Fletcher, Goldfarb, and Shanno's method (BFGS) method, the most commonly used variation of the quasi-Newton algorithm. It can be found in most optimization libraries.

As a quasi-Newton method, BFGS works by approximating the objective function, (3.10) in this case, by a quadratic model at each iteration k of the algorithm. The solution to the quadratic model is found as

$$m_{r_i,k+1}(p) = \varepsilon_{r_i,k} + \nabla \varepsilon_{r_i,k} p + \frac{1}{2} p B_k p, \tag{3.12}$$

where $p \in \mathbb{R}$ is the search direction; $\varepsilon_{r_i,k}$ is the objective (3.10) evaluated at the current step $m_{r_i,k}$; and B_k is an approximation of the Hessian, or the

second order derivative of (3.10) in this one dimensional case. The search direction that minimizes this quadratic approximation is calculated as

$$p_k = -H_k \nabla \varepsilon_{r_i,k}, \tag{3.13}$$

where $H_k = B_k^{-1}$. With the new search direction p_k, the solution at the current step and next iterate of the algorithm will be

$$m_{r_i,k+1} = m_{r_i,k} + \alpha_k p_k, \tag{3.14}$$

where $\alpha_k > 0$ is a currently unknown step length. A line search method for finding a satisfactory α_k is described in the next section. Given a step length α_k, the Hessian approximation can be updated for the next iteration at $m_{r_i,k+1}$ as

$$H_{k+1} = \frac{m_{r_i,k+1} - m_{r_i,k}}{\nabla \varepsilon_{k+1} - \nabla \varepsilon_k}, \tag{3.15}$$

and a new search direction and step length can be found using equation (3.13) and the line search described in the next section. The algorithm continues until the current solution $m_{r_i,k}$ satisfies a set of termination criteria.

Line search based on Wolfe conditions

As mentioned above, the objective function is approximated by a quadratic function at each step $m_{r_i,k}$ of the BFGS. If $\alpha_k = 1$, the solution of the current step $m_{r_i,k+1}$ will be the solution of the quadratic approximation. It is unlikely that this also is the actual solution of the objective function (3.10) as the objective is not a quadratic function, and both the gradient (3.11) and Hessian (3.15) are estimates. However, the closer the algorithms gets to the actual solution of the objective (3.10), the better the quadratic approximation will be; given that B_k becomes an increasingly accurate approximation [14]. A solid set of conditions should be used to determine whether or not the current solution $m_{r_i,k+1}$ brings the algorithm sufficiently close to the solution such that it is beneficial to calculate a new quadratic approximation. And, an efficient line search method is needed to suggest new step lengths in case the current is rejected.

The conditions used to evaluate the step of a quasi-Newton method such as this one should be formulated such that $\alpha_k = 1$ is the optimal initial guess. Because, as mentioned earlier, when the algorithm approaches the solution of the objective, the quadratic approximation becomes better. And therefore, at some iterate $k = k^*$ the step length $\alpha_k = 1$ should be admissible for all iterates after k^* which gives the algorithm a superlinear convergence [14].

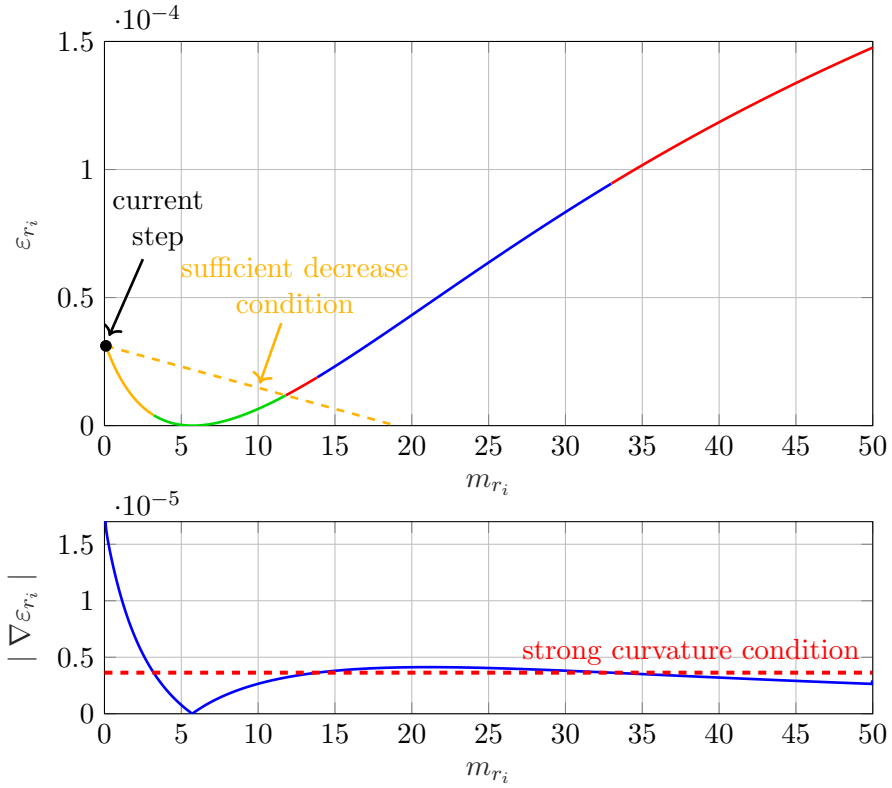

Figure 3.13: A visualization of the Wolfe conditions. Figure adapted from [11].

A set of conditions that have seen wide use are the Wolfe conditions which are formulated as

$$\varepsilon_{r_i,j} \leq \varepsilon_{r_i,k} + c_1 \alpha_j \nabla \varepsilon_{r_i,k} p_k, \tag{3.16a}$$

$$\left|\nabla \varepsilon_{r_i,j} p_k\right| \leq c_2 \left|\nabla \varepsilon_{r_i,k} p_k\right|, \tag{3.16b}$$

where $\varepsilon_{r_i,j}$ is the objective function evaluated at iteration j of the line search, α_j is the suggested step length, and $0 < c_1 < c_2 < 1$ are constant design parameters. Figure 3.13 shows a visualization of the Wolfe conditions (3.16). Condition (3.16a) is known as the sufficient decrease condition and ε_{r_i} values satisfying it are colored orange in the figure. It accepts any step length that gives a reduction in the objective function large enough to satisfy expectations based on knowledge of the current value and gradient estimate. Condition (3.16b) is called the strong curvature condition and ε_{r_i} values satisfying it are colored red in the figure. It requires the gradient in the new point to be smaller than the current gradient because a high gradient value suggests there is still much to be gained by moving in the current direction p_k. Values satisfying both condition are colored green in the figure.

If the the next step $m_{r_i,k}$, found with equation (3.14) using initial step length α_k, fails to satisfy the Wolfe conditions (3.16), a method for selecting a new step length must be in place. The line search described in [14] is taken to use. When a step length is suggested, one of four cases can occur.

Case 1: The step fails to satisfy the sufficient decrease condition (3.16a). This is exemplified by a step landing to the right of the intersection between the objective function and the line of sufficient decrease in Figure 3.13. In this case the sufficient decrease condition is implying that a larger objective reduction was expected based on the length of the step and the derivative at the current position. It is therefore likely that a better solution can be found closer to the current step, and an interpolation is performed.

Case 2: The step fails to satisfy the strong curvature condition, and has a negative gradient in the direction of the step. This is exemplified by a step landing in the orange interval of the objective function in Figure 3.13. In this case the curvature condition is implying that substantial gains can be achieved by stepping further in the current direction, and an extrapolation is performed.

Case 3: The step fails to satisfy the strong curvature condition, and has a positive gradient in the direction of the step. This is not possible in the case illustrated by Figure 3.13, but would have appeared as a orange interval between the green interval and line of sufficient decrease. In this case the curvature condition is implying that substantial gains can be achieved by reducing the step length, and an interpolation is performed.

Case 4: The step satisfies both Wolfe conditions. The current step length is considered satisfactory and a new iteration of the BFGS can be started.

Further details about the line search are not considered important for the intuition of the algorithm. Instead, [14] is referred to as the line search, interpolation, and extrapolation described there match what was implemented and used in this chapter.

3.2.2 Data sets obtained from extraction

Figure 3.14a and 3.14b show the data sets $\mathscr{D}_{m_U}$ and $\mathscr{D}_{m_r}$, equivalent of the inertia sets described in section 2.3.2, that were obtained when extracting inertia measurements from the transients identified in section 3.1.3. Comparing the general data structures shown in the figures to the ones obtained with the manual method in [7], there are strong similarities. This is not unexpected when considering that practically the same evaluation criteria

were used; a root mean square error in [7], and the mean square error objective (3.10) used here. If anything one would expect the inertia values, m_U and m_r, to be more precisely determined using the numerical optimization technique as adjusting the termination criteria adds little to an already low computation time, while in the manual case the problem scales poorly with precision as a predetermined set of inertia values was used and iterated through.

Although the inertia values m are expected to be very similar to what was obtained in [7], there are some noticeable differences, especially in $\mathscr{D}_{m_U}$ which was generated from the throttle experiment. The biggest source of the inertia errors is believed to be due to the results of the SSID described in section 3.1.3. As mentioned during the discussion of the SSID results it was necessary to overfit the SSID parameters in order to minimize the consequences of the incompatibility between human SSID and the result of the applied method. However, there were still some invalid results produced from the throttle experiment, and while the majority were valid, the quality of the state measurements varied as a significant portion of the SSID intervals ended up too short, and thus susceptible to disturbances. These inaccuracies transfer into the inertia measurement m. The effect is similar to the case illustrated by Figure 2.14 in section 2.3.1, but generally has a lower impact.

The steady state intervals obtained from the rudder experiment were more consistent and the results in Figure 3.14b do not seem to be significantly impacted by the overfitted SSID parameters. The biggest difference from the m_r data set $\mathscr{D}_{m_r}$ obtained in [7] is the value of the outlier. In Figure 3.14b it is shown to have a value of about $m_r \approx 40$, while in [7] it is approximately doubled. This is probably due to the authors of [7] having manually set the time of steady state t_{ss} to be later than what was found in section 3.1. For example, looking at the figure, if $t_s s$ was chosen to be $t_s s \geq 110s$ there would be a significant gap between the current simulated transient and the actual signal. In order to reduce the gap and decrease the mean square error of the objective (3.10) the inertia value m_r of the simulated transient (3.9) would have to increase significantly.

As just mentioned, there is some variance in the quality of the state measurement. Besides from affecting the measured inertia, low quality state measurements also mean that the measurements' placement in the state space will be inaccurate. The effect is easily seen in Figure 3.14a where the measurements are supposed to form arcs for each throttle step, similar to the pattern seen in Figure 3.14a.

Figure 3.14c and 3.14d show the data sets $\mathscr{D}_{\sigma_U}$ and $\mathscr{D}_{\sigma_r}$. Because damping measurements are read directly of the control input as described in section

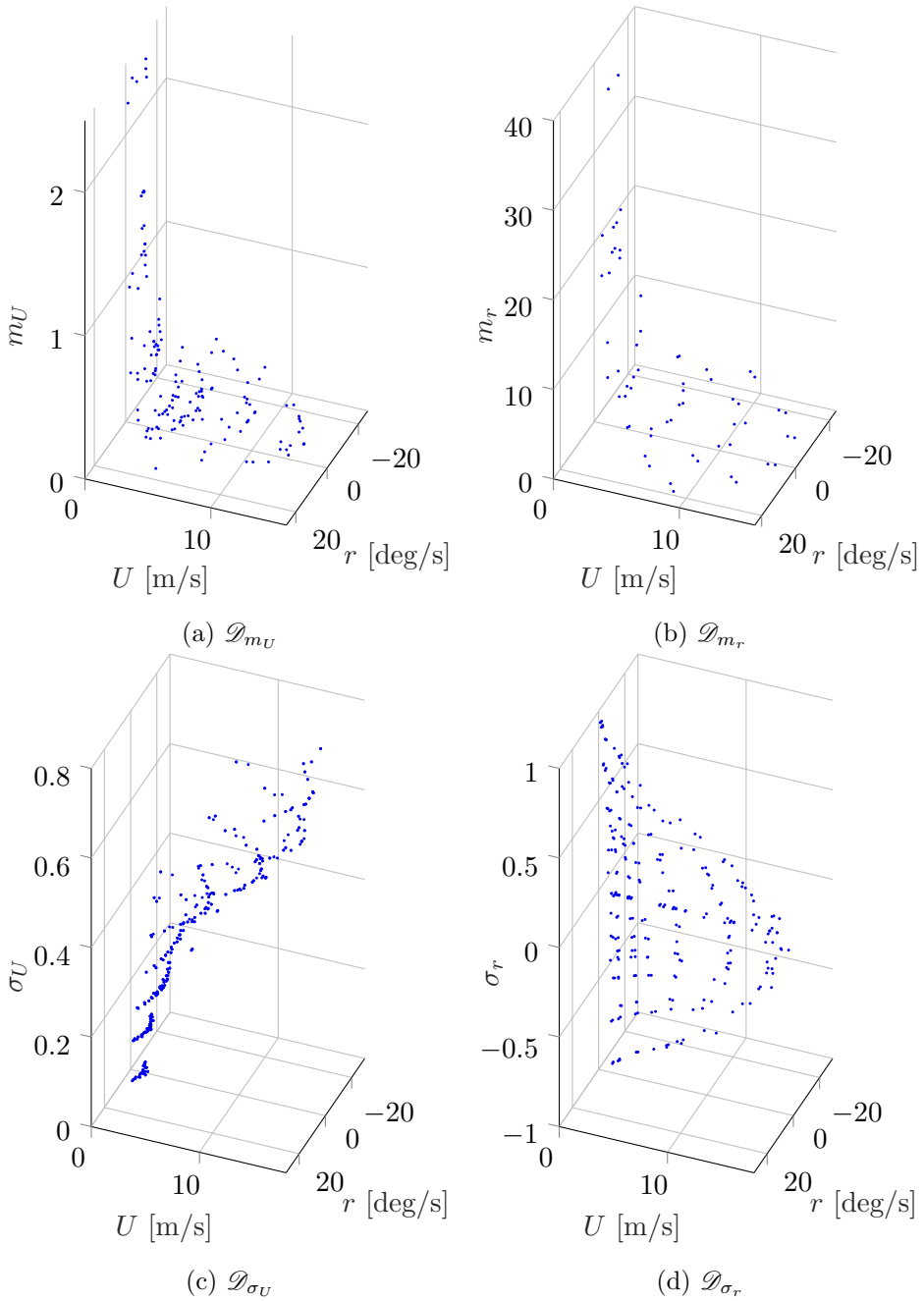

(a) $\mathscr{D}_{m_U}$ (b) $\mathscr{D}_{m_r}$

(c) $\mathscr{D}_{\sigma_U}$ (d) $\mathscr{D}_{\sigma_r}$

Figure 3.14: Data sets with measurements extracted from experiments performed in [7].

2.3.2, the values of σ_U and σ_r should be identical to what was found in [7]. However, the measurements' placement in state space is subject to the same errors that affected the inertia data sets. Because damping data can be obtained from both experiments, measurements of σ_r extracted from the throttle experiments are included in $\mathscr{D}_{\sigma_r}$; the same applies in the SOG case. It might be better to leave them out as they are of a lower quality than the ones obtained from the rudder experiment, as mentioned earlier. However, they will be included as excluding them halves the size of the data set, making it quite sparse.

3.3 Parameter identification

Because the parameter identification step is done using linear regression it is automatic at its core. When used as described in [7], and covered in section 2.3.3, the only aspect that is considered manual is the weighting scheme. When the step was examined with the intention of automation and improvement during project work done in the autumn of 2017 [11], the examination was based on application of the method in a simulation environment. The simulation environment did not produce data with enough complexity for the purpose of techniques like regularization and weighting to be of importance. As the data from [7] was available it was decided that the examination of weighting and regularization should be saved for future work, the work done in this thesis, were the method was applied to the experimental data. This section will cover new suggestions for use of regularization and weighting. Some background for the utilization of regularization and weighting has already been covered in the discussion at the end of section 2.3.3.

3.3.1 Model reduction

As discussed in section 2.3.3 the basis functions $\boldsymbol{\phi}_\sigma(\boldsymbol{x})$ and $\boldsymbol{\phi}_m(\boldsymbol{x})$ are both based on fourth order polynomials and were formulated as

$$\begin{aligned}\boldsymbol{\phi}_\sigma(\boldsymbol{x}) = [&1, U, r, U^2, Ur, r^2, U^3, U^2r, Ur^2, r^3, U^4,\\ &U^3r, U^2r^2, Ur^3, r^4]^\top, \text{ and}\end{aligned} \tag{3.17a}$$

$$\begin{aligned}\boldsymbol{\phi}_m(\boldsymbol{x}) = [&1, U, r, U^2, Ur, r^2, U^3, U^2r, Ur^2, r^3, U^4,\\ &U^3r, U^2r^2, Ur^3, r^4, \tanh(a(U-b)]^\top.\end{aligned} \tag{3.17b}$$

The two basis functions contain both even and odd functions. Due to the assumption of symmetric rudder response, all models are assumed to be

either even or odd about the zy-plane in a coordinate system where x, y, z correspond to r, U, σ (or m). This can be seen in Figure 3.14 where the models m_U, and m_r are even about the (m, U)-plane; while σ_U and σ_r are respectively even and odd about the (σ, U)-plane.

When $\phi_\sigma(\boldsymbol{x})$ and $\phi_m(\boldsymbol{x})$ are used to describe an even model, all elements of the corresponding parameter vector $\boldsymbol{\beta}$ describing odd terms should be set to zero; opposite in the case of an odd model. To do this the authors of [7] utilized the regularized linear regression technique known as lasso. Lasso was described in section 2.2 and has the property of feature selection as it drives a selection of values in $\boldsymbol{\beta}$ to zero. However, lasso is generally implemented as a numerical solver and therefore it is unlikely that any of the elements in $\boldsymbol{\beta}$ actually receive the value zero, and instead are left as small but nonzero values. The resulting error can easily be avoided by removing redundant terms. The new reduced models are formulated as

$$\boldsymbol{\phi}_{\sigma_r}(\boldsymbol{x}) = [1, U, r, U^2, Ur, U^3, U^2r, r^3, U^4, U^3r, Ur^3]^\top, \tag{3.18a}$$

$$\boldsymbol{\phi}_{\sigma_U}(\boldsymbol{x}) = [1, U, U^2, r^2, U^3, Ur^2, U^4, U^2r^2, r^4]^\top, \tag{3.18b}$$

$$\boldsymbol{\phi}_{m_r}(\boldsymbol{x}) = [1, U, U^2, r^2, U^3, Ur^2, U^4, U^2r^2, r^4, \tanh(a_r(U - b_r)]^\top. \tag{3.18c}$$

$$\boldsymbol{\phi}_{m_U}(\boldsymbol{x}) = [1, U, U^2, r^2, U^3, Ur^2, U^4, U^2r^2, r^4, \tanh(a_U(U - b_U)]^\top. \tag{3.18d}$$

3.3.2 Regularization

Because the basis models of equation (3.18) no longer contain redundant terms, the use of lasso for regularization should be reconsidered. Perhaps the most commonly applied regularization technique in linear regression when looking to minimize prediction errors is ridge regression [10]. A comparison and interpretation of the workings of lasso and ridge is given in section 2.2. Now that more context is given to the regularization issue, the description of how ridge and lasso effectively influence the elements of the parameter vector $\boldsymbol{\beta}$ can be continued.

Section 2.2 described a group of penalty functions used in regularization that were formulated as

$$R(\boldsymbol{\beta}) = \sum_{j=1}^{M} |\beta_j|^q, \tag{3.19}$$

where M is the number of model parameters in $\boldsymbol{\beta}$, and $q \in \mathbb{R}_{>0}$. Figure 3.15 shows how three different variations of the penalty (3.19) might affect the elements of the parameter vector $\boldsymbol{\beta}$ in a two dimensional case. When $q = 0$ the linear regression applying the penalty (3.19) is called best subset regression. Best subset regression essentially works by picking out the least

descriptive elements of the parameter vector $\boldsymbol{\beta}$, removing them by assign a value of zero, and then utilize the remaining elements to form the model. Using the identification of m_U as an example, best subset regression would zero the elements of $\boldsymbol{\beta}_U$ corresponding to odd basis functions in $\boldsymbol{\phi}_m(\boldsymbol{x})$ of equation (3.17b) as the model is even and there is no need for the odd elements. When $q = 2$ the linear regression applying the penalty (3.19) is called ridge. Ridge essentially works by reducing the values of the parameter vector $\boldsymbol{\beta}$ according to the explained variance of the corresponding elements in $\boldsymbol{\phi}(\boldsymbol{x})$. More specifically, the coefficient β_i of an element $\phi_i(\boldsymbol{x})$ with low explained variance is reduced heavily, while elements with high explained values are only slightly reduced as these are considered critical in capturing the model dynamics. Lasso lies between best subset regression and ridge at $q = 1$, which means that its properties are a balance of feature selection and favouring elements that have a high explained variance. However, since feature selection is no longer as important and ridge's ability to favour high explained variance is better, ridge should be the preferred option.

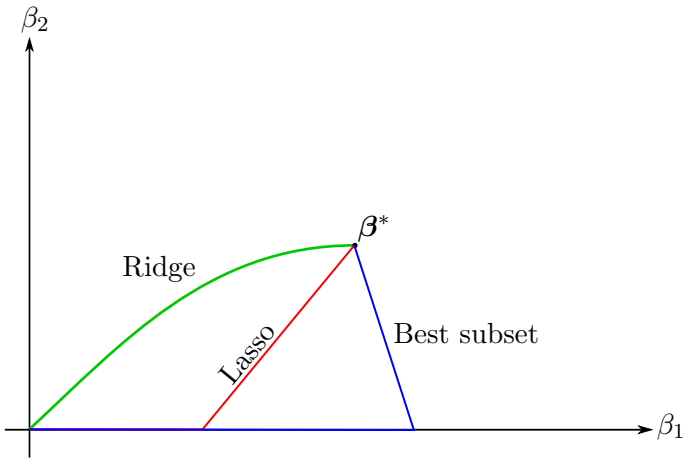

Figure 3.15: Illustration of how different regularization penalties might affect the parameter vector with increasing regularization weight λ. $\boldsymbol{\beta}^*$ denotes the solution of the regression without regularization. Note lasso and ridge shrink continuously while best subset regression makes two discrete steps. Figure adapted from [10].

3.3.3 Weighting scheme

The weighting scheme described here is motivated by the discussion of utilization of weights in section 2.3.3. Weighting will be applied to combat the effects the inertia measuring process has on the variance of inertia values. It is not intended to account for variance in the state measurements as this

has been considered a complex issue so far. This means that weighting will not be considered in identification of damping models as disturbances only affect the state measurements in the damping data set. Leaving out weighting from the damping model identification is justified by the fact that the damping data sets contain approximately twice as many data points as the inertia sets, and the complexities of the models are lower than in the inertia case.

From the discussion of weighting in section 2.3.3 it was concluded that errors in the inertia value caused by disturbances and noise were not linearly transformed into the data set through the measurement method. The implication of an error of $\varepsilon_m = 1$ varies based on the true inertia value m^*. For example a measurement of $m = m^* + \varepsilon_m$ where $m* = 20$ and $\varepsilon_m = 1$ could be considered fairly accurate. On the other hand, a measurement where $m^* = 1$ and $\varepsilon_m = 1$ would be considered an outlier and should be removed. This effect is not considered by the linear regression as it only aims to minimize the mean square error and thus an error of $\varepsilon_m = 1$ is considered to be equally bad independently of the true value m^*. The weighting scheme described below is aimed at assigning weights based on inertia value.

Inertia measurements are obtained by simulating the step response of a first order LTI system on the form

$$m\dot{x} + kx = \tau, \tag{3.20}$$

as described in sections 2.3.2 and 3.2. Then, the value of m that minimizes the mean square error between simulated and actual step response is chosen as the measurement. One interpretation of this process is that the measurement is chosen by matching the derivative of the state through the simulated transient, $\dot{x}$, with the derivative of the state through the actual transient, $\dot{x}$. The sensitivity of $\dot{x}$ with respect to m at a given point in the step x_c can be measured as

$$\frac{\partial \dot{x}|_{x=x_c}}{\partial m} = -m^{-2}(\tau - kx_c), \tag{3.21}$$

which for any point x_c during the transient becomes some constant multiplied by m^{-2}. Based on this a weighting scheme is suggested, formulated as

$$w_i = (\frac{m_{up} + m_{down}}{2})^{-2}, \tag{3.22}$$

where m_{up} and m_{down} forms the measurement pair generated by the same step in opposite directions.

The scheme gives a low weight to measurements with a high value as errors will be larger in these measurements. If a measurement has a negative error, lowering its value, the measurements receives a higher weight. This is not

considered a problem as disturbances causing the vessel to accelerate faster, and thus lowering the measured inertia, are believed to be rare and usually of an insignificant size.

When combining regularization and weighting it is important to remember that the regularization coefficient λ determines the weight of the regularization penalty relative to the weight of the mean square error. Therefore the mean of the weights should be kept at a value near 1 so as not to disturb this balance. To do this the weights are linearly transformed to be in the interval $w_i \in (w_{min}, w_{max}) = (0.5, 1.5)$. The resulting weighting scheme becomes

$$w_i = a(\frac{m_{up} + m_{down}}{2})^{-2} + b, \tag{3.23}$$

where

$$a = \frac{w_{min} - w_{max}}{m_{max}^{-2} - m_{min}^{-2}}, \text{ and}$$
$$b = w_{max} - a m_{min}^{-2},$$

and m_{min} and m_{min} are the minimum and maximum inertia values in the data set. Results from application of the weighting scheme to data from the ROT data set are shown in Figure 3.16.

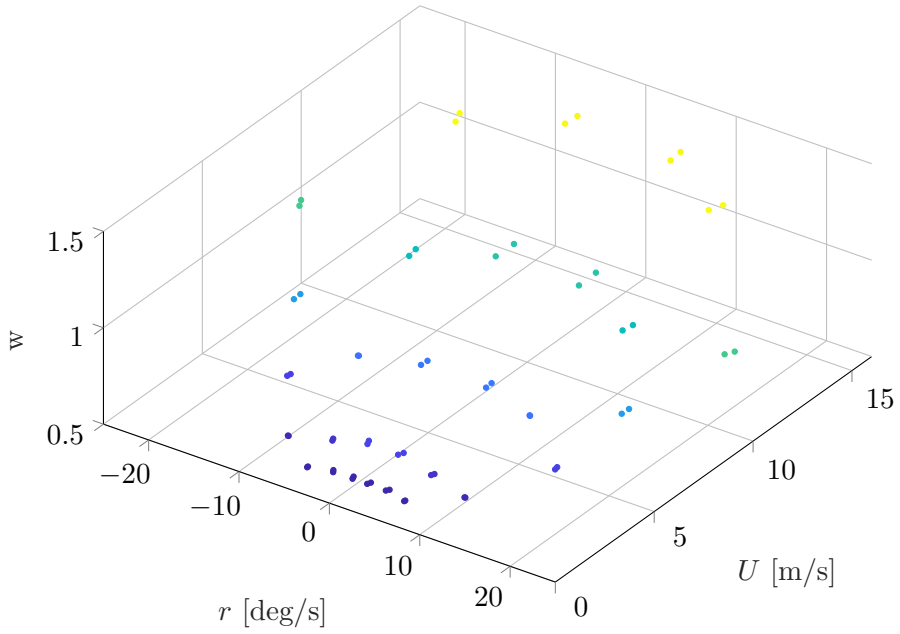

Figure 3.16: Weighting scheme applied to $\mathscr{D}_{m_r}$.

Outlier detection

Outliers pose a significant threat in applications of linear regression. Weighting as it was used by the authors of [7] played an important role in combating outlier. Through manual inspection outlier could be selected visually and assigned a weight depending on how dramatic they were. As a more generalized weighting scheme has been suggested here there is no effective weight to deal with outliers.

An effort was made to apply the standard score technique for outlier detection [13]. It works by assigning a score to each value in a data set where the score indicates how many standard deviations the value deviates from the mean of the set. The technique was applied by considering measurements generated with the same throttle input as a data set because these measurements generally have inertia values in the same range. However, the data sets were to small for the method to be effective. Twelve measurements are generated for each throttle input in an rudder step experiment, but there is effectively only six as they are mirrored about the ROT axis. Even in the set associated with the lowest throttle input, which contains an outlier with $m_r \approx 40$ and the other measurements all being $m_r \approx 20$, the outlier only received a standard score of $z = 1.97$; recommended z-score thresholds typically do not go lower than $z = 2.5$.

Not having a proper solution for outliers is likely to have a significant impact on the regression results as the outlier in the m_r data set mentioned earlier is very large. Furthermore, since this particular outlier is not caused by unexpected behavior or any abnormal disturbance as discussed in section 2.3.3, outliers like it are expected to happen. Finding a proper method for handling outliers is therefore an import task for future work, unless the inertia measurement process is to be modified.

3.3.4 Identified models

Figure 3.17 shows the identified models. Unfortunately, weighting was not successfully combined with ridge regression, and due to time constraints the reason was not identified. Because the weighting scheme is essential for identification of the m_r model as there is no outlier detection in place, the inertia models are identified using lasso combined with the weighting scheme. No weighting scheme was formulated for use on the damping data sets, so these are found using ridge. Successfully combining the weighting scheme and ridge regression is not believed to be a particularly difficult task and is left for future work.

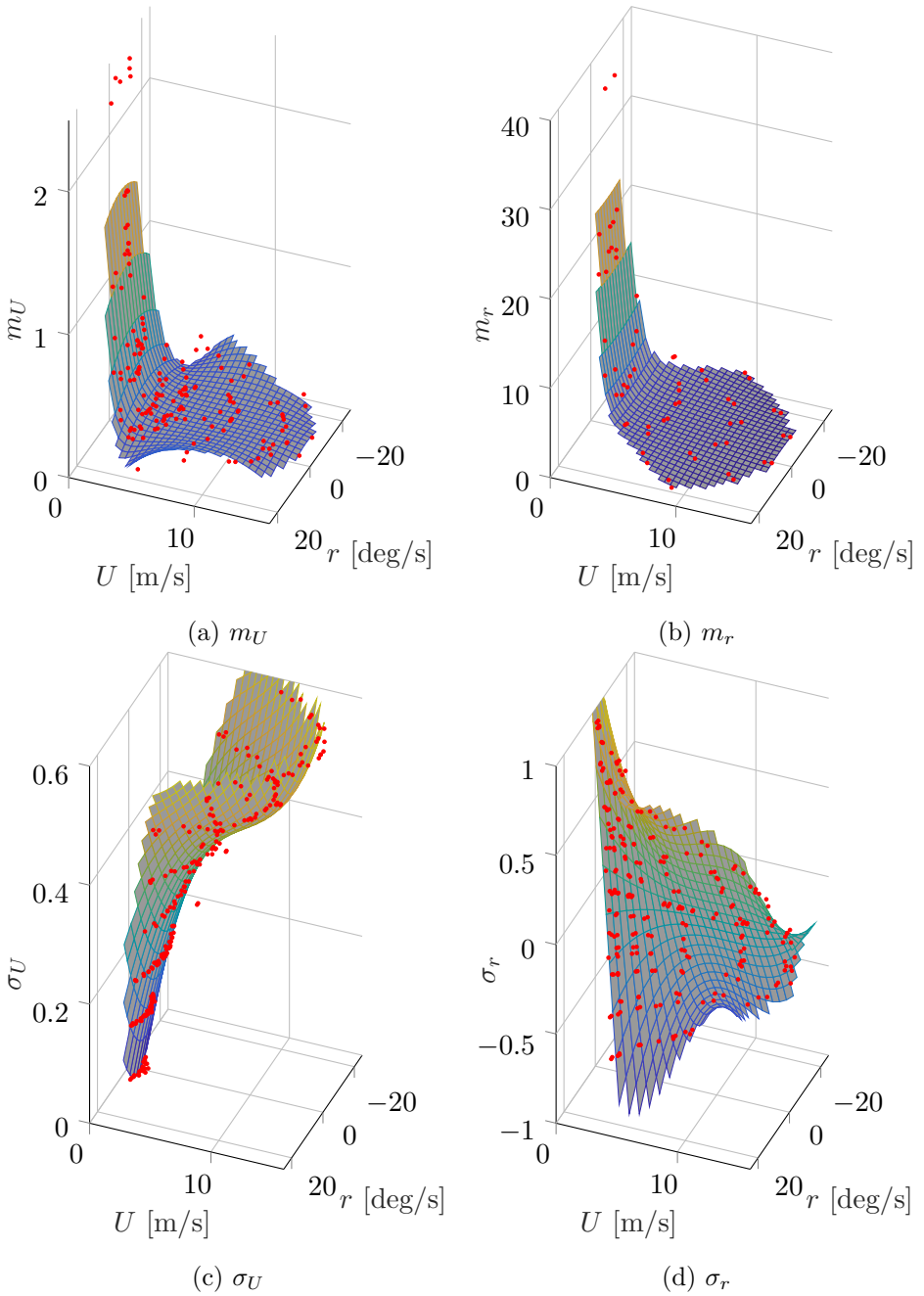

(a) m_U (b) m_r

(c) σ_U (d) σ_r

Figure 3.17: Models identified using data sets from Figure 3.14.

The model surfaces are nicely centered in the measurements for the most part; although this might be difficult to see without 3D inspection capabilities. They seem to be structurally very similar to the models obtained in [7]. However, no quantitative comparison will be given here. Because the data gathered from the throttle experiment has considerable errors as it was the hardest to obtain proper measurements from, explained in section 3.1.3, its difficult to say how well the m_U model captures the data structure. The model of m_r does a captures the dynamics of the data well, considering the presence of the outliers. Removing the outliers does allow the model to better capture the transition at the end of the asymptotic behavior, but the results are satisfactory with outlier present. The model of σ_U is also affected by outliers, although they only cause a slight change in curvature. These outliers come from the problematic application of SSID on the throttle experiment discussed in section 3.1.3 and are not expected to be a problem in a real application. The model of σ_r generally seems to be a good fit, but it somewhat struggles to properly capture the damping dynamics at very high throttle input and very high rudder angle. Insufficient model complexity and a low amount of samples could be the cause.

3.4 Proposed model and identification extensions

This section will cover some suggestions for extension of the model and of the model identification method. These suggestions were not investigated enough to be included in the implementation, but they are believed to offer significant improvement if proven to be feasible. Therefore, the proposed extensions are highly relevant for future work.

3.4.1 Propagation delay

Propagation delay was identified as a significant source of error in the discussion presented in section 2.3.2. It meant that all inertia measurements received artificially high values. Propagation delay is generally a constant value, although it might differ depending on the destination of the delayed signal. This means that in the general case propagation delay is a vector $\boldsymbol{t}_d = [t_{d,m}, t_{d,\delta}]$, where $t_{d,m}$ and $t_{d,\delta}$ are the delays associated with the motor and rudder actuators. Extending the vessel model to include t_d could be done by formulating the model equation (2.5) as

$$\boldsymbol{M}(\boldsymbol{x})\dot{\boldsymbol{x}} + \boldsymbol{\sigma}(\boldsymbol{x}) = \boldsymbol{\tau}(\boldsymbol{t} - \boldsymbol{t}_d), \tag{3.24}$$

where $\boldsymbol{t}$ is a vector with duplicate entries of the current time.

There are various ways to get an estimate of $\boldsymbol{t}_d$. If measurements of the true actuator output are available $\boldsymbol{t}_d$ could be obtained by for example applying a SSID technique to the true actuator output signals. Then $\boldsymbol{t}_d$ could be obtained as the time between applied reference input and time of detected transient.

If measurements of true actuator output are unavailable $\boldsymbol{t}_d$ can be found using numerical optimization. The objective function (3.10) used in section 3.2 for curve fitting of step responses can be extended to include a term describing the delay. Using identification of m_r and $t_{d,\delta}$ as an example, the new objective could be formulated as

$$\begin{aligned}\varepsilon_{r_i} = \frac{1}{N_{r_i} - t_{d,\delta}h^{-1}} \sum_{j=t_{d,\delta}h^{-1}}^{N_{r_i}} (r_{i,j} - \hat{r}_{i,j}(m_{r_i}))^2 \\ + \frac{1}{t_{d,\delta}h^{-1}} \sum_{j=1}^{t_{d,\delta}h^{-1}} (r_{i,j} - r_i^-)^2,\end{aligned} \tag{3.25}$$

where h is the sampling rate, and r_i^- is the state measurement from the previous steady state interval. In this objective function there are two optimization variables m_r and t_d. Although this increases the complexity of the problem, it is unlikely that the likelihood of multiple minima in the objective increases; given no abnormal scenarios as described in section 3.2.1. That is because the simulated delay plus transient is still very limited in its ability to describe vessel dynamics.

Figure 3.18 illustrates how the objective function would work. The first term of the function is similar to the original objective. It evaluates the mean square error between simulated and actual step; the simulated step being the green line in the figure. But there is a slight change; the simulated step starts at some time $t_{d,\delta}$ in the actual transient. The second term is an extension of the preceding steady state by some time $t_{d,\delta}$. This extended steady state is visualized as a red line in the figure and has the constant value r_i^-.

3.4.2 Second order model

The motivation for increasing the model order is described in the discussion of measurement accuracy in section 2.3.2. It is mentioned that since high speed surface vessels are expected to operate in regions of the state space where rudder steps cause overshoots in ROT, a first order model will not accurately capture the dynamics of the step responses. This means that the inertia measurements become artificially low.

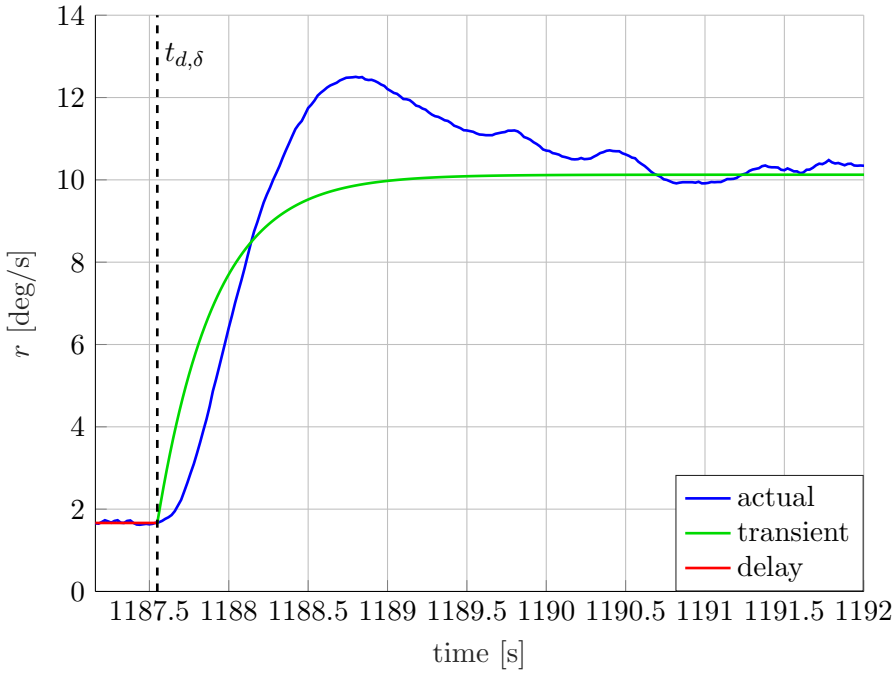

Figure 3.18: How results from identification of $t_{d,\delta}$ and m_r would look like. An input step was applied at $t \approx 1187.0$.

To improve the inertia measurement process it is proposed to apply a second order LTI system in the curve fitting process. Using measuring of m_r as an example, the new system could be formulated as

$$n_{r_i}\ddot{\Delta r}_i + m_{r_i}\dot{\Delta r}_i + k_i \Delta r_i = \Delta\tau_{\delta_i}, \tag{3.26}$$

where n_{r_i} is the jerk coefficient. Note that inertia is not a well defined concept in a second order system and the validity of interpreting m_{r_i} as inertia should be investigated further. By adding the second order term, n_{r_i} enters the numerical optimization objective as a second optimization variable. The new second order extension of the previous objective function (3.10) has the form

$$\varepsilon_{r_i} = \frac{1}{N_{r_i}} \sum_{j=1}^{N_{r_i}} (r_{i,j} - \hat{r}_{i,j}(m_{r_i}, n_{r_i}))^2, \tag{3.27}$$

where $\hat{r}_{i,j}(m_{r_i}, n_{r_i})$ is the step response generated by simulating system (3.26).

As more complex representations of the vessel's step response can be obtained by increasing the model order, it is very likely that the objective

function contains multiple minima. This means that the optimization problem becomes significantly harder to solve. Fortunately the desired minimum should have a decent physical interpretation. By considering the physical properties of the system, constraints can be formulated to restrict the valid region of the objective function. The physical properties should also allow for good estimates of the optimization variable which could be used as the initial point of the search. With a good set of constraints and a good estimate it should be possible to isolate the desired minimum and formulate a feasible measuring strategy.

First off, estimation strategies will be suggested. To estimate inertia m_r one could simply solve the old optimization problem. The solution should be a very good inertia measurement as it is the one inertia models are based on in the current model identification method. To estimate a value for the jerk coefficient n_r the concept of damping ratio could be used. The damping ratio of system (3.26) is given as

$$\zeta_i = \frac{m_{r_i}}{2\sqrt{k_i n_{r_i}}}. \tag{3.28}$$

When $\zeta = 1.0$ the system is critically damped, and so has no overshoot. A critically damped system should be a good initial estimate. By solving the damping ratio (3.28) for n_{r_i} and using the previously calculated value of k_i and the estimated m_{r_i} the jerk coefficient could be estimated as

$$\hat{n}_{r_i} = \frac{m_{r_i}^2}{4k_i\zeta_i^2}. \tag{3.29}$$

With estimations in place, boundaries can be formulated. Overshoots are one of few phenomena that cause a negative error in the inertia measurement found with the original method. This means that the lower boundary could be set as the value of the inertia estimate; or at least close to it. The upper boundary could for example be set as the inertia estimate plus a certain percentage of the estimated value. Boundaries for the jerk coefficient can be formulated based on the damping ratio ζ. As mentioned earlier, $\zeta = 1.0$ implies the system is critically damped. An underdamped system, capable of producing overshoots, has a $\zeta > 1.0$; and the system is overdamped when $\zeta < 1.0$. The boundaries can therefore be formulated as $\zeta_{lo} \leq \zeta \leq \zeta_{hi}$ where the values for ζ_{lo} and ζ_{hi} are set so that the overshoot is within reason; for example $0.9 \leq \zeta \leq 1.25$.

The strategy described above could be used to expand the model (2.5) to the second order, and then use linear regression to find model parameters for the jerk coefficient n, as is done for inertia and damping. Or, it could solely be used to increase the accuracy of the inertia measurements, and leave the model as it is; however the validity of this must be investigated further.

Chapter 4

Results from full-scale experiments

4.1 Experiments

Figure 4.1 and Figure 4.2 show the full-scale experiments performed using a ROS implementation of the automatic model identification method. The implementation is not covered in this thesis. The parameters of the experiment can be found in Table 4.1. Additionally the following boundary is used

$$\tau_{\delta,max} = \begin{cases} 0.4, \text{ if } \tau_m > \tau_{m,max} - \tau_{m,\Delta} \\ 1.0, \text{ else.} \end{cases} \tag{4.1}$$

The reason for using $\tau_{\Delta,\delta} = 0.2$, instead of 0.33 as in [7], is because the rudder was capped at $\tau_\delta = 0.8$, unlike at $\tau_\delta = 1$ as it was earlier. This means signal-to-noise ratio will be a bigger threat this time around.

Table 4.1: Parameters of experimental procedure used in [7].

Input	τ_{min}	τ_{max}	τ_Δ
τ_m	0	0.6	0.1
τ_δ	0	0.8	0.2

It should be noted that intervals of the experiment where a manual takeover was necessary to avoid collisions have been removed. Collision avoidance is something that should be added to the implemented system using its existing framework for user interaction where the user is replaced with a collision avoidance system. This is a necessity for the feasibility of the identification method as it is unlikely that the vessel will not cause danger if left running on its own for one hour at a time. It should also be noted that

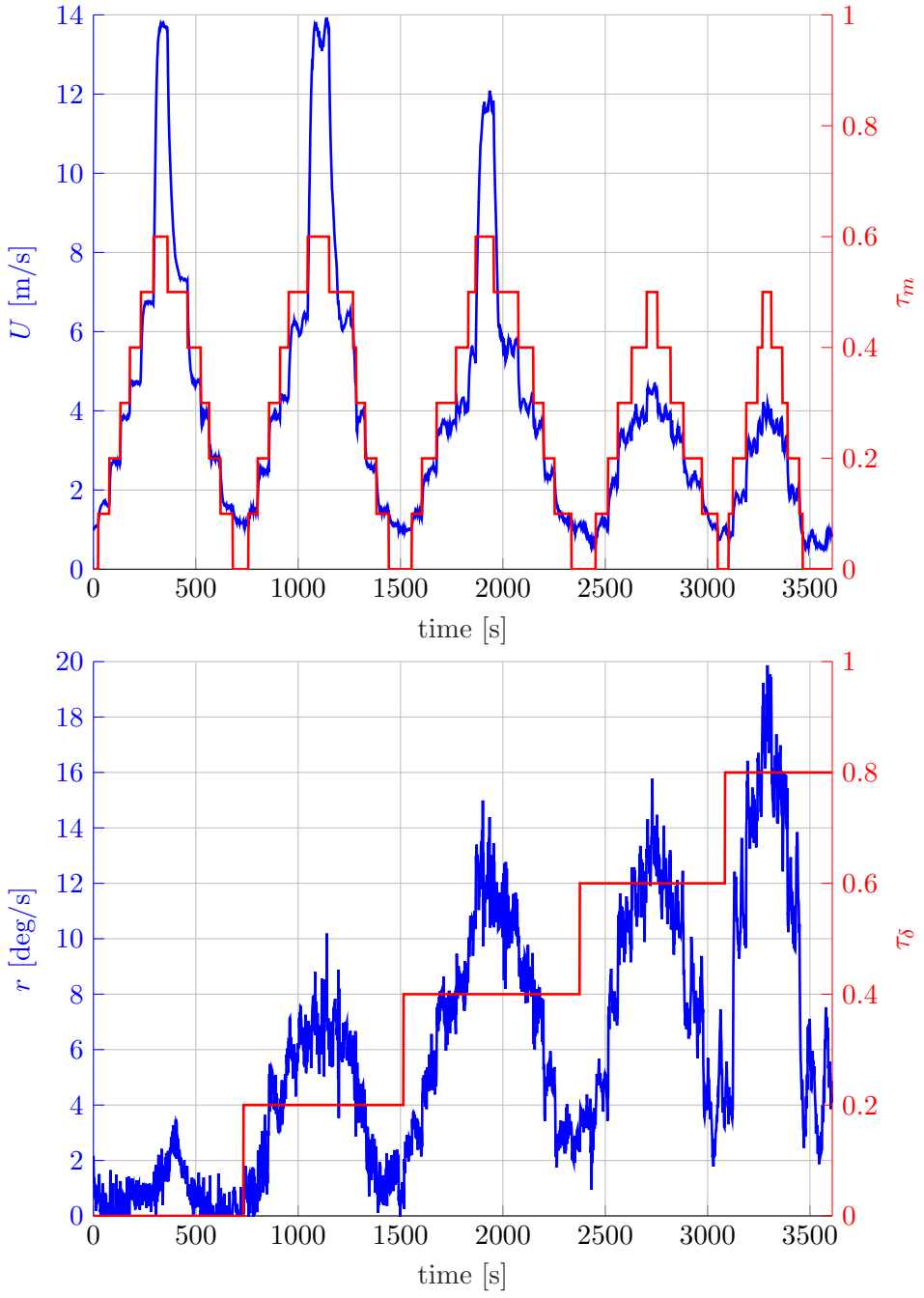

Figure 4.1: Throttle experiment performed using the ROS implementation of the method developed in Chapter 3. The parameters of the experiment can be found in Table 4.1.

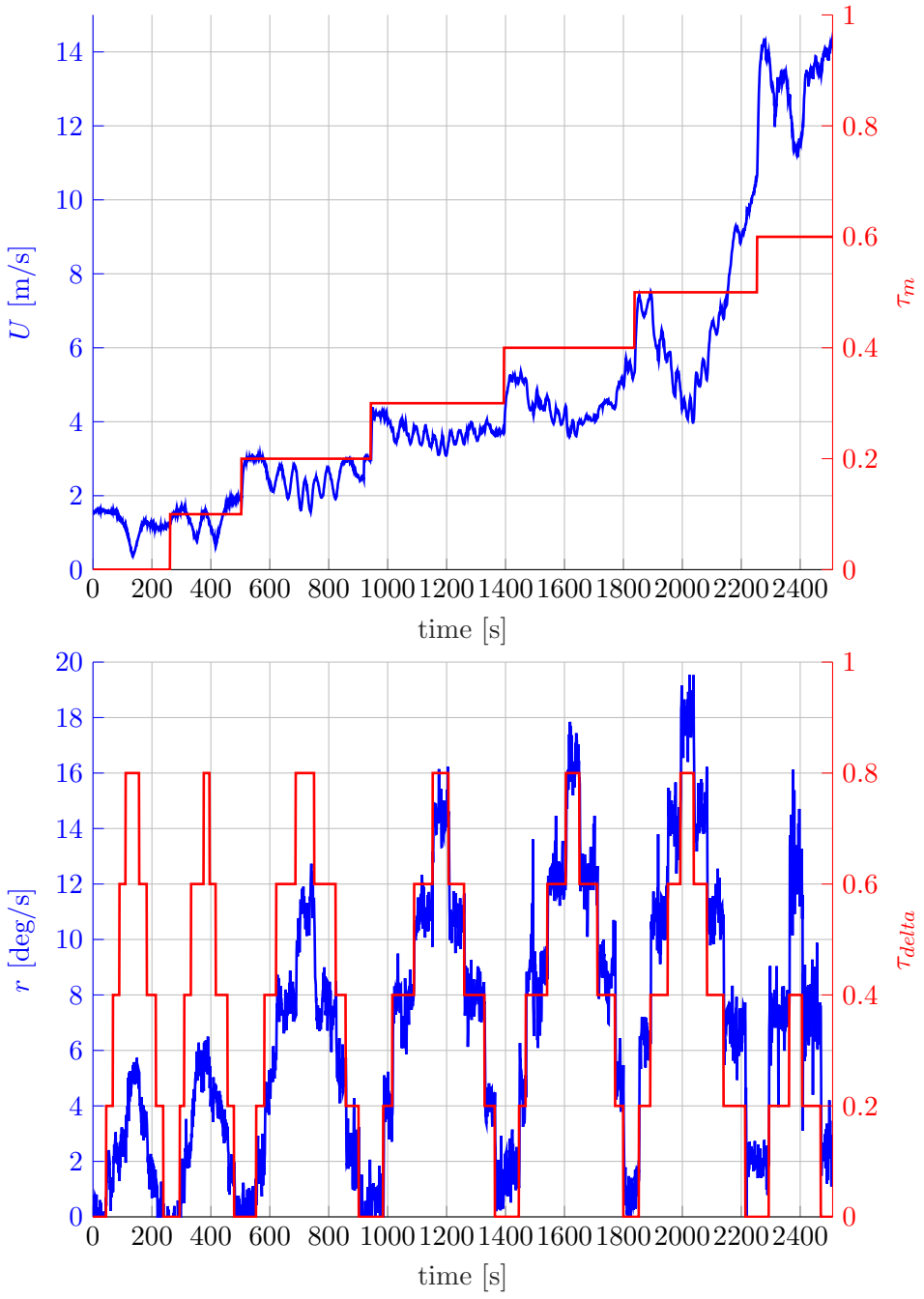

Figure 4.2: Rudder experiment performed using the ROS implementation of the method developed in Chapter 3. The parameters of the experiment can be found in Table 4.1.

a bug in the implementation caused premature SSID in a couple of some steps; intervals of manual takeover in an attempt to repeat these steps have been removed from the data. Neither the bug or its consequences will be discussed further as there are more important factors to cover. A third note is that due to time constraint circles in steady state were only completed if the r indicated that the turn would take less than one minute to complete. If the vessel was turning to slowly the next step was applied after ten seconds. One last note; the rudder experiment was performed with low fuel while the throttle experiment was performed with a full tank. This affects the identified models and should be kept in mind throughout the chapter, that being said it will not be addressed in the discussion as it will be focused on the general structures of the results.

Comparing the experiments of figures 4.1 and 4.1 to the experiments done in [7] and shown in figures 3.1 and 3.2, it is clear that the motor dynamics are quite different. This can easily be seen by observing the effect of stepping the throttle from $\tau_m = 0.5$ to $\tau_m = 0.6$. In the experiments presented here this step approximately doubles the steady state value of U, causing changes up to 8 meters per second. In the experiments shown in Chapter 3 the preceding step from $\tau_m = 0.4$ to $\tau_m = 0.5$ is larger and the step only causes a change in U of about 3 meters per second. This is concerning as signal-to-noise ratio will likely become a bigger problem, and the measurements will be less uniformly spread throughout the state space as there will be a large gap between the ones extracted from operations at max throttle and the rest. At the same time this increases the motivation behind development of an automatic model identification procedure. This is because it proves that the vessel dynamics can change significantly over time and thus the model parameters need to be re-identified relatively often to guarantee satisfactory performance of which ever system utilizes it. The changing actuator dynamics also emphasizes the need for a better approach to experiment design so that experiments may be formulated such that measurements can be well placed in the state space. A small discussion of this is given at the end of section 2.3.1, but this is important for future work.

Some of the steps that were performed were of a very low quality due to significant disturbances although this is somewhat hard to see in the figures due to the time scale, the two first step sequences of the rudder experiment include visible examples. In some cases the disturbances were so bad that the step did not characterize the vessel dynamics at all, Figure 4.3 provides two examples. As seen in Figure 4.3a at $t \approx 3100$, the effects of the throttle step barely affect SOG. Figure 4.3b shows a case where the step is dragged out over a longer interval. Neither of these two steps are fit for use in an parameter identification procedure and calls for the need of method for detecting and repeating uncharacteristic steps. This also emphasizes the

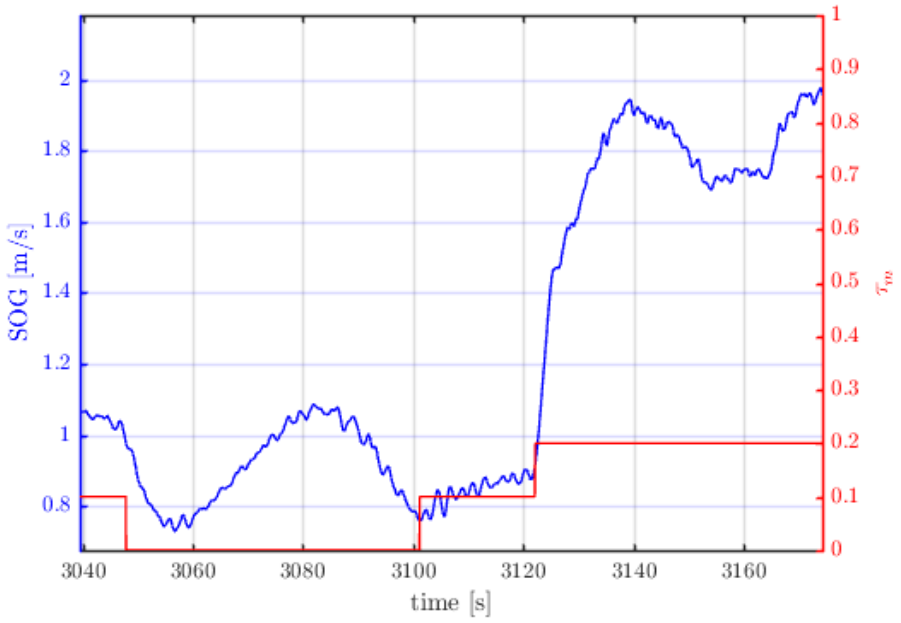

(a) Disturbances dominating throttle step.

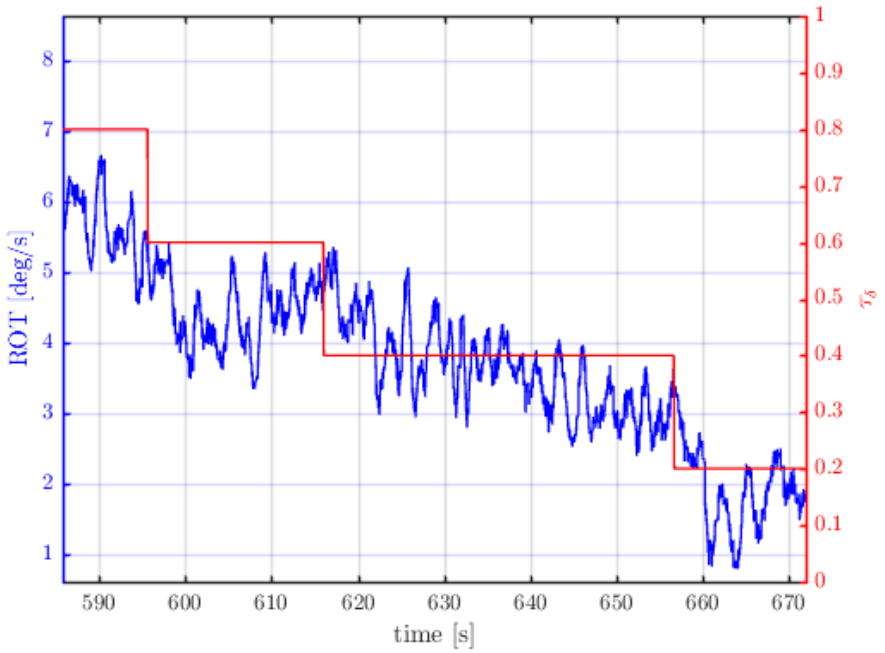

(b) Disturbances dominating rudder step.

Figure 4.3: Examples of step responses that are unfit for using in identification and should be repeated.

fact that experiments should be performed in ideal sea conditions.

4.2 Steady state identification

Results of the SSID are shown in Figure 4.4. The parameters of the SSID are listed in Table 4.2. For the most part the SSID method was well behaved, but as some steps were dominated by disturbances as shown in Figure 4.3 some identifications were premature. An example of premature identification is shown in Figure 4.5. The root of the problem lies in the experiment and will translate through all the following steps. Unfortunately, other challenges with use of the SSID will not be discussed here, but a good portion was covered in section 3.1.

Table 4.2: Filter coefficients and R boundaries used throughout this chapter, where h is the time step.

Experiment	λ_1	λ_2	λ_1	R_{lb}	R_{ub}
SOG	$0.1h$	$0.5h$	$1.0h$	1500	6200
ROT	$0.075h$	$0.75h$	$0.5h$	40	95

4.3 Data extraction

Results of the data extraction procedures are shown in Figure 4.6. As can be seen in all data sets there is a large gap between the measurements generated with max throttle input and the rest. This is especially clear in the SOG data sets and will likely cause overfitting in the during the parameter identification. Although the spread should be equally large in the $\mathscr{D}_{m_r}$ set, hysteresis has had significant impact on the measurements generated with $\tau_m = 0.5$ causing the gap to be filled by a line of measurements. There is also quite a lot of noise in the inertia data sets. Most of it is explained by how the signal-to-noise ratio affected the transients, and the fact that full turns in steady state were only completed for a relatively small percentage of the steps. Not completing turns affect the steady state measurements, especially when there are significant disturbances present, and this facilitates poor inertia measurements. A closer look at the concerns of the data extraction raised in sections 3.2 and 2.3.2 will not be taken here, but they are assumed to be equally relevant.

4.4 Parameter identification

The identified models are shown in Figure 4.7. Starting with the model of m_U one can see significant overfitting in the large gap behind measurements

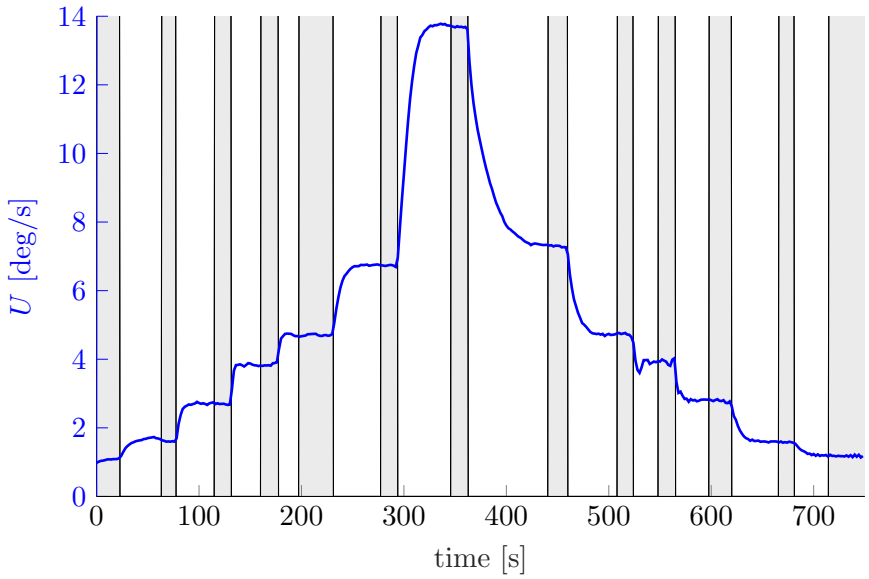

(a) Results from rudder experiment.

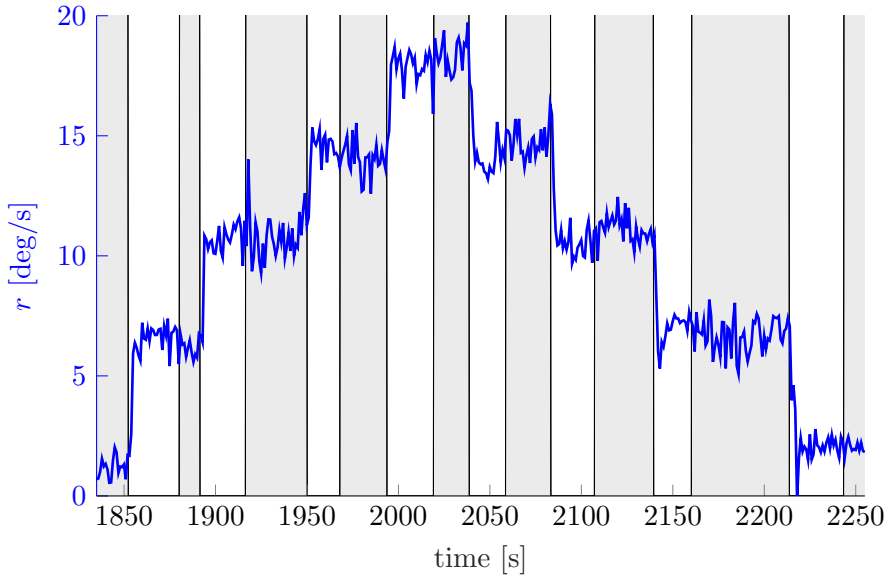

(b) Results from throttle experiment.

Figure 4.4: Parts of the results from applications of the SSID method in full-scale experiment. Grey areas represent steady state regions and white regions are transients. Parameters of the SSID method are listed in Table 4.2.

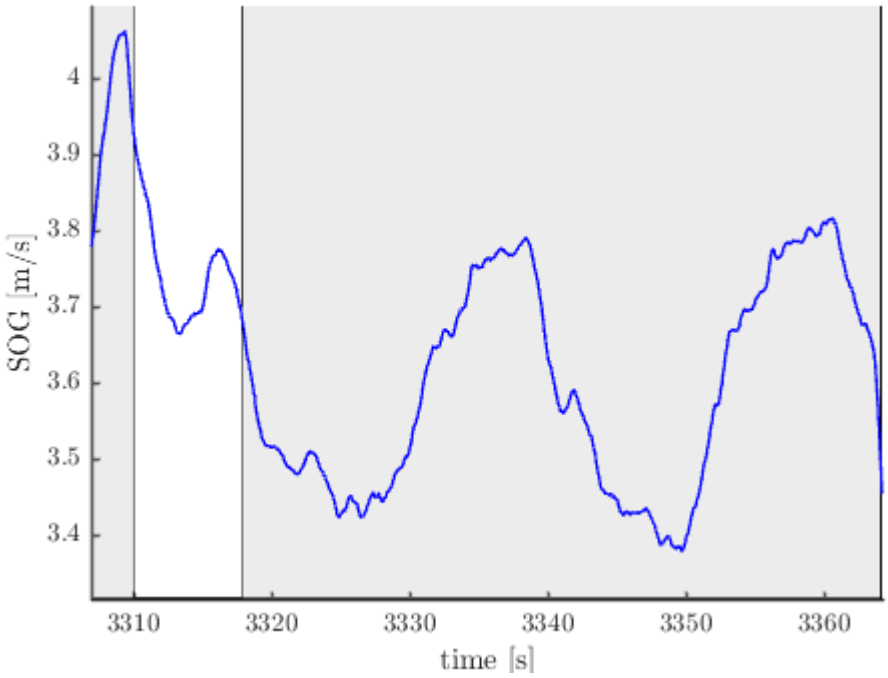

Figure 4.5: The transient, white region, shows an example of premature SSID.

generated with max throttle input. This was expected and although regularization provides a counter measure, it can only do so much. The proper solution is to formulate the experiment such that measurements are evenly spread throughout the state space. There are also a couple of outliers which are extra influential as they are located next to the large gap and thus there are not enough measurements nearby for the weighting scheme to sufficiently deal with them. The model of m_r is somewhat better as the gap is filled due to hysteresis as mentioned earlier. Looking at the model for σ_U the new actuator dynamics cause a plateau like structure to form in the gap. Looking at this new structure it might be necessary to add an asymptotic term to the basis function of σ_U, similarly to what is done for the inertia models. However, the model identified in Figure 4.7c does a surprisingly good job. The model for σ_r is a fairly good representation of the structure of the data set, no obvious shortcomings can be seen.

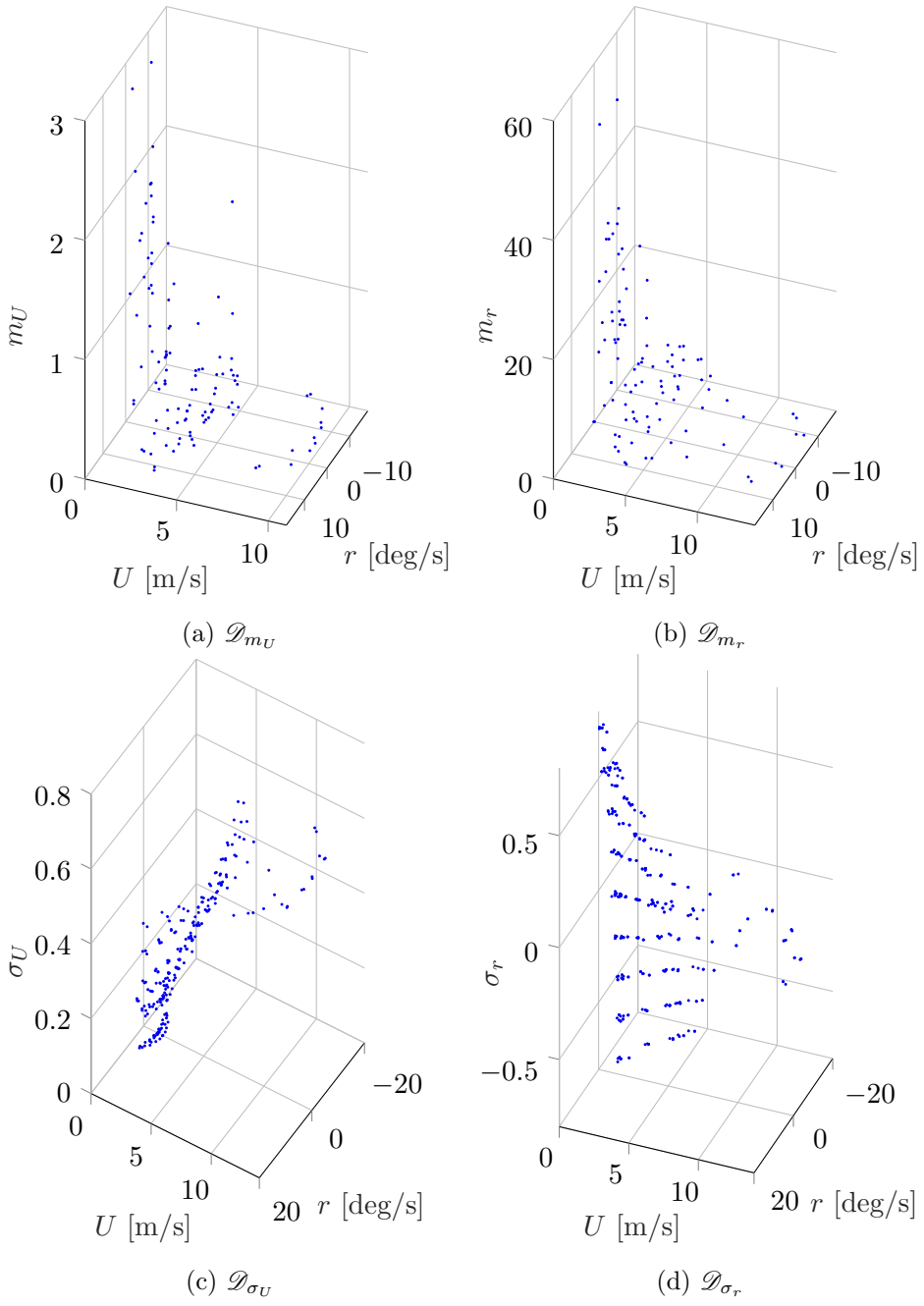

(a) $\mathscr{D}_{m_U}$ (b) $\mathscr{D}_{m_r}$

(c) $\mathscr{D}_{\sigma_U}$ (d) $\mathscr{D}_{\sigma_r}$

Figure 4.6: Data sets with measurements extracted from full-scale experiments.

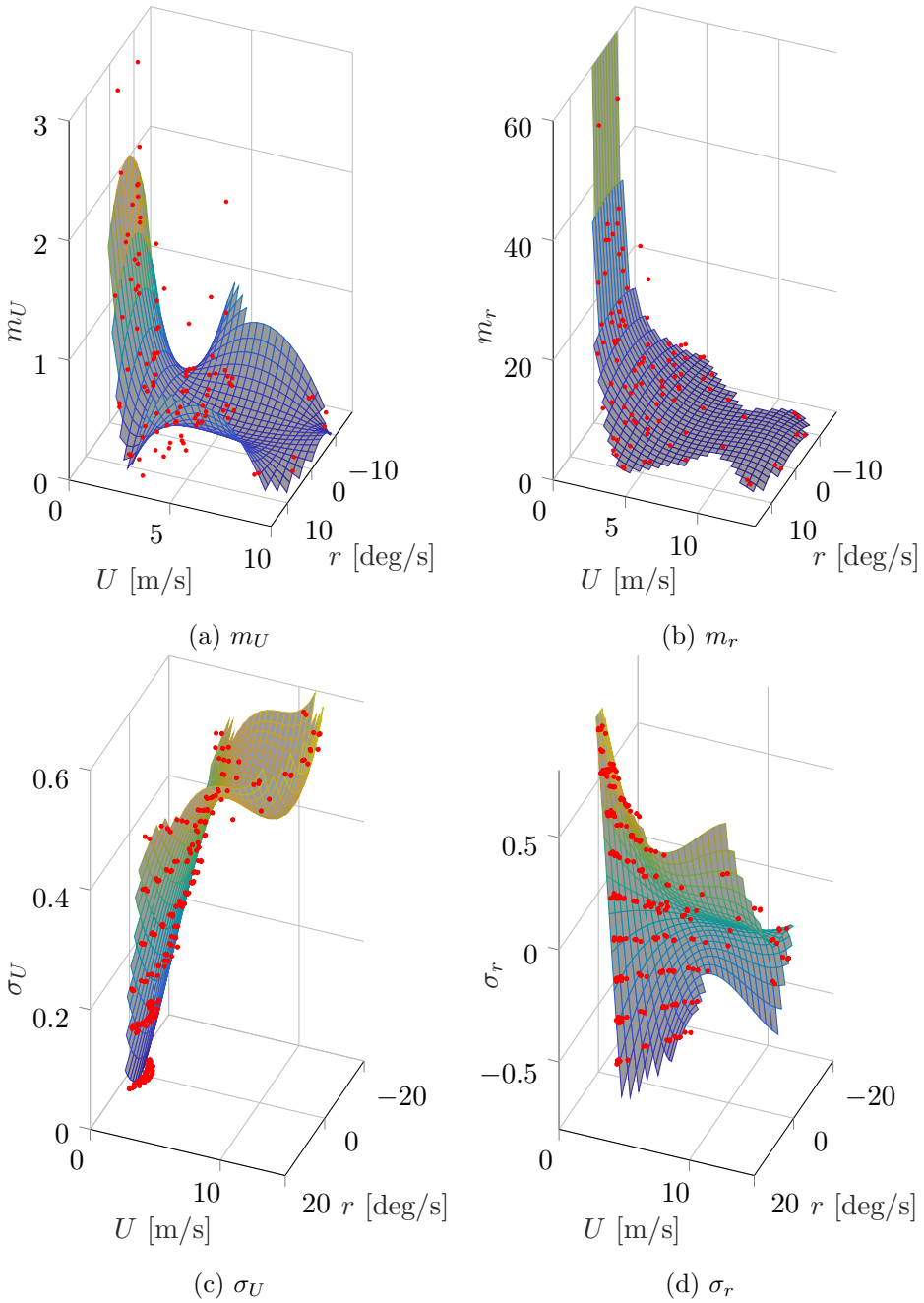

(a) m_U (b) m_r

(c) σ_U (d) σ_r

Figure 4.7: Models identified using data sets from Figure 4.6.

Chapter 5

Conclusions and future work

The purpose of the work described in this thesis was to analyze and automate the model identification procedure suggested in [7]. Through the analysis of the original manual method room for improvement was highlighted in the different steps of the method. To start the development of an automatic replacement three steps of the method where focused on. These steps were data collection, data extraction and parameter identification. Automatic solutions for each step were formulated and some of the weaknesses of the new solutions were discussed based on results obtained from application of the method on real data gathered by the authors of [7].

To further assess the steps of the automated method it was implemented as a real time system using ROS. Full scale experiments were performed using an ASV provided by Maritime Robotics. A rather brief discussion of the results from the experiments suggested that there is a need for better experiment design and a framework for detecting, rejecting and repeating poorly executed steps.

5.1 Future work

A list of suggestions for future work is provided:

- Extend the model identification procedure to be iterative as described at the end of section 2.3.1. This way experiments can be formulated that cover the state space better.
- Look into methods for detecting and repeating input steps that produce step response not suited for measurement extraction. The proposed SSID method could maybe used for this.
- Include outlier detection in the identification procedure. See discussion in section 3.3.3.

- Extend the model to include propagation delay as described in section 3.4.
- Look into increasing the model order as described in section 3.4 to better capture the dynamics at high speeds.

Bibliography

[1] Beck, J. A. and Cord, T. (1995). A framework for analysis of aircraft maneuverability. In *Proceedings of the AIAA Atmospheric Flight Mechanics Conference*, Baltimore, Maryland, USA.

[2] Bertram, V. (2008). Unmanned surface vehicles–a survey.

[3] Breivik, M. (2010). *Topics in guided motion control of marine vehicles*. PhD thesis, Norwegian University of Science and Technology, Trondheim, Norway.

[4] Breivik, M., Hovstein, V. E., and Fossen, T. I. (2008). Straight-Line Target Tracking for Unmanned Surface Vehicles. *Modeling, Identification and Control (MIC)*, 29(4):131 – 149.

[5] Cao, S. and Rhinehart, R. (1995). An efficient method for on-line identification of steady state. *Journal of Process Control*, 5(6):363 – 374.

[6] dos Santos Gromicho, J. A. (1998). *Quasiconvex Optimization and Location Theory*. Kluwer Academic Publishers, Gouda, The Netherlands, 1st edition.

[7] Eriksen, B.-O. H. and Breivik, M. (2017). Modeling, Identification and Control of High-Speed ASVs: Theory and Experiments. In Fossen, T. I., Pettersen, K. Y., and Nijmeijer, H., editors, *Sensing and Control for Autonomous Vehicles: Applications to Land, Water and Air Vehicles*, pages 407–431. Springer International Publishing, Cham.

[8] Faltinsen, O. M. (2005). *Hydrodynamics of High-Speed Marine Vehicles*. Cambridge University Press.

[9] Fossen, T. I. (2011). *Handbook of Marine Craft Hydrodynamics and Motion Control*. John Wiley & Sons, Ltd.

[10] Hastie, T., Tibshirani, R., and Friedman, J. (2009). *The elements of statistical learning*. Springer, New York.

[11] Kvalvaag, T. M. (2017). Automatic model identification of high-speed autonomous surface vehicles. Unpublished report.

[12] Liu, Z., Zhang, Y., Yu, X., and Yuan, C. (2016). Unmanned surface vehicles: An overview of developments and challenges. *Annual Reviews in Control*, 41(Supplement C):71 – 93.

[13] NIST/SEMATECH (2013). e-Handbook of Statistical Methods. `https://www.itl.nist.gov/div898/handbook/`. Accessed: 2018-04-20.

[14] Nocedal, J. and Wright, S. J. (2006). *Numerical Optimization*. Springer, New York, 2nd edition.

[15] Nomoto, K., Taguchi, K., Honda, K., and Hirano, S. (1957). On the steering quality of ships. *International Shipbuilding Progress*, 4:354–370.

[16] Rhinehart, R. R. (2013). Automated steady and transient state identification in noisy processes. In *Proceedings of the American Control Conference*, pages 4477–4493, Washington, DC, USA.

[17] Sonnenburg, C. R., Gadre, A., Horner, D., Kragelund, S., Marcus, A., Stilwell, D. J., and Woolsey, C. A. (2010). Control-oriented planar motion modeling of unmanned surface vehicles. *Proc. of OCEANS 2010*.

[18] Sonnenburg, C. R. and Woolsey, C. A. (2013). Modeling, identification, and control of an unmanned surface vehicle. *Journal of Field Robotics*, 30(3):371–398.

[19] Tzeng, C.-Y. and Chen, J.-F. (1999). Fundamental properties of linear ship steering dynamic models. *Journal of Marine Science and Technology*, 7(2):79–88.

[20] Witrant, E. (2014). Control-oriented modeling and system identification. `http://www.gipsa-lab.grenoble-inp.fr/~e.witrant/classes/`. Accessed: 2018-05-01.